united nations
educational, scientific
and cultural
organization

international atomic
energy agency

the
abdus salam
international centre for theoretical physics

ICTP 40th Anniversary

SCHOOL ON SYNCHROTRON RADIATION AND APPLICATIONS
In memory of J.C. Fuggle & L. Fonda

19 April - 21 May 2004

Miramare - Trieste, Italy

1561/31

Nanocrystals and nanoclusters

embedded in glass matrices

A. Craievich

Nanocristals and nanoclusters embedded in glass matrices

Outline

- **Formation and growth of liquid Bi droplets**
  Phys. Rev. B. 67, 085405 (2003)

- **Melting of Bi nanocrystals**
  Phys. Rev. B 65, 134204 (2002)

- **Formation of Ag nanocrystals. Evidence of strain effects.**
  Phys. Rev. B, Submitted (2004)

In situ SAXS study in real time of the growth of Bi liquid nanodroplets embedded in a borate glass

G. Kellermann and A.F. Craievich. Phys. Rev. B 67, 085405 (2003)

- Nanostructured materials are macroscopic objects composed of nanometric building blocks

- They are supported by substrates

or

- embedded in a volume matrix

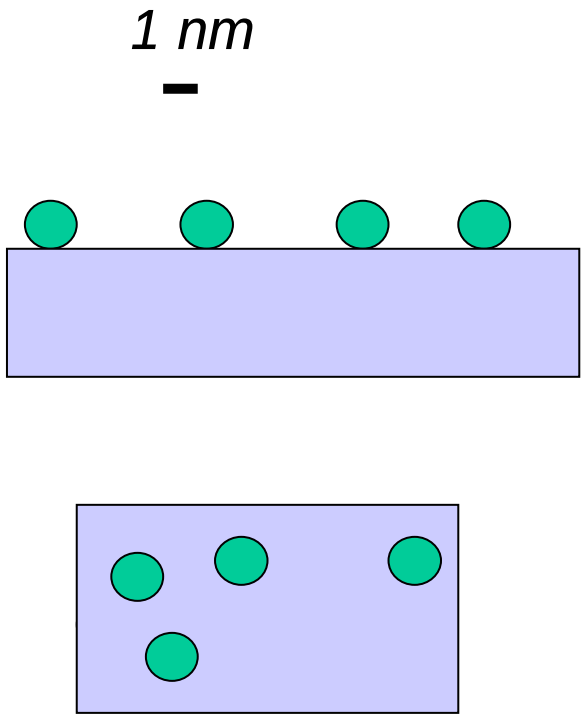

- Nanostructured materials are macroscopic objects composed of nanometric building blocks

- They are supported by substrates

or

- embedded in a volume matrix

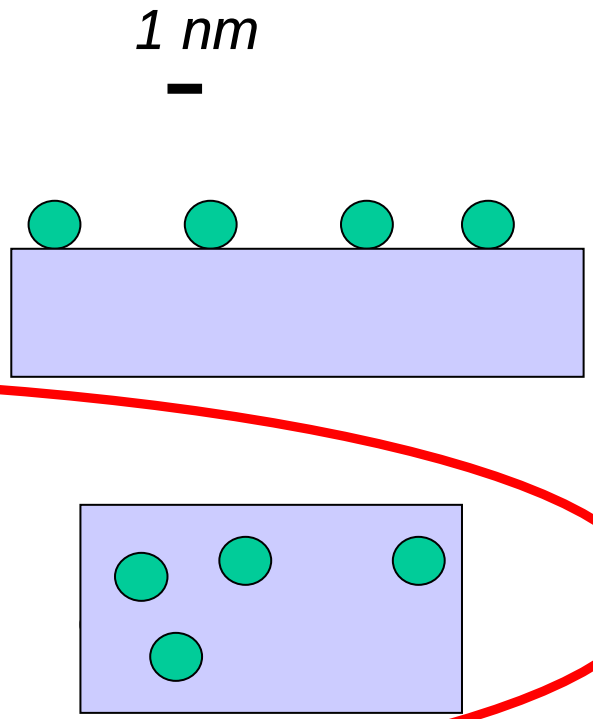

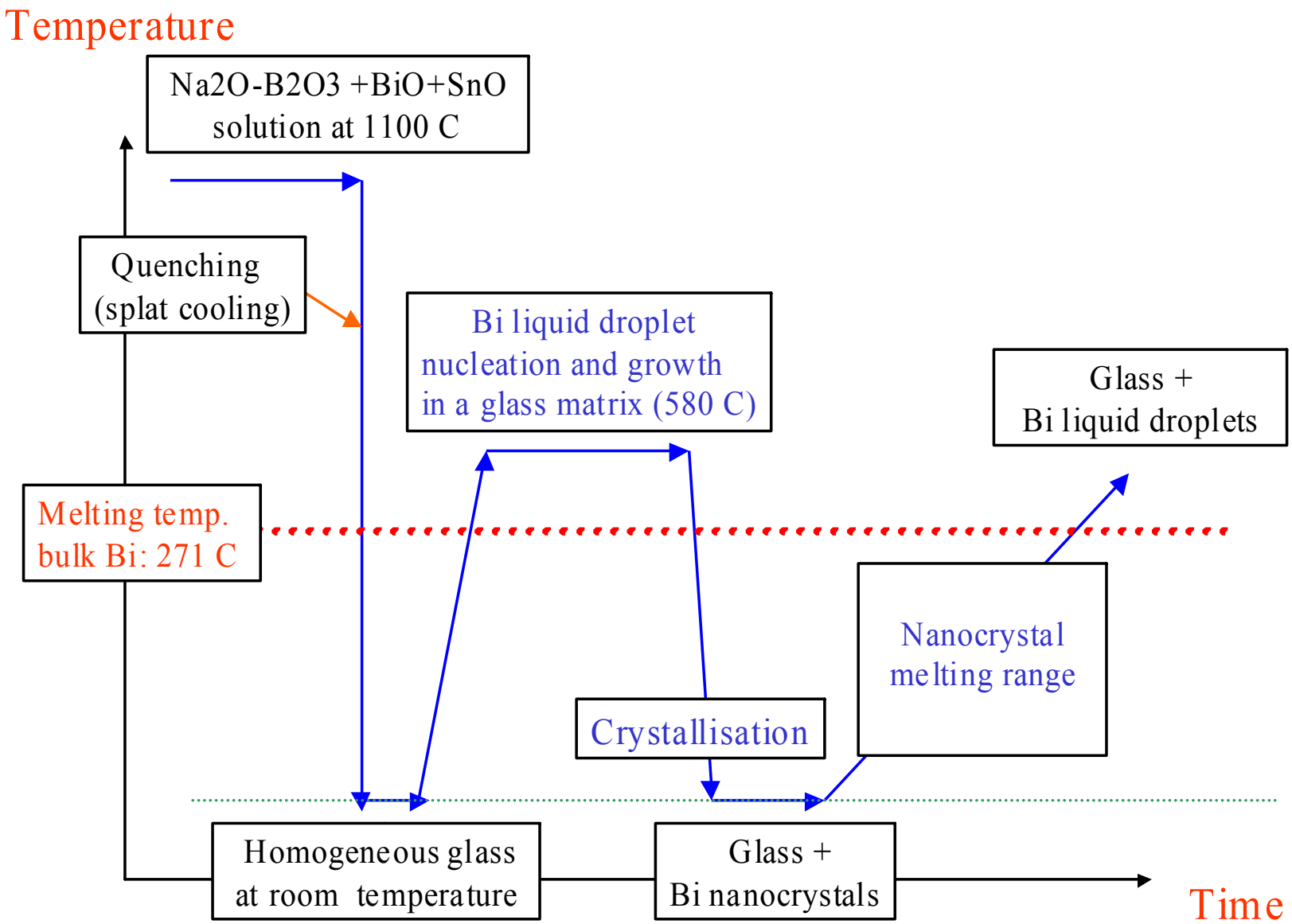
Temperature
Na2O-B2O3 +BiO+SnO
solution at 1100 C
Quenching
(splat cooling)
Bi liquid droplet
nucleation and growth
in a glass matrix (580 C)
Glass +
Bi liquid droplets
Melting temp.
bulk Bi: 271 C
Nanocrystal
melting range
Crystallisation
Homogeneous glass
at room temperature
Glass +
Bi nanocrystals
Time

Materials and transformations: Formation and growth Bi nanoclusters (quantum dots) embedded in a glass matrix

~1 nm

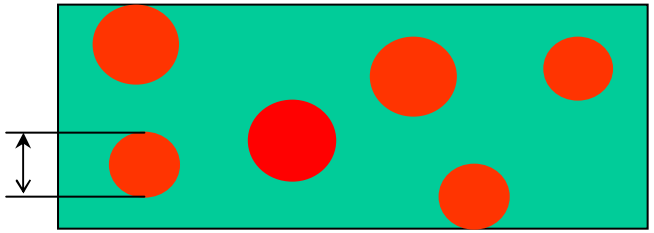

T=1100C

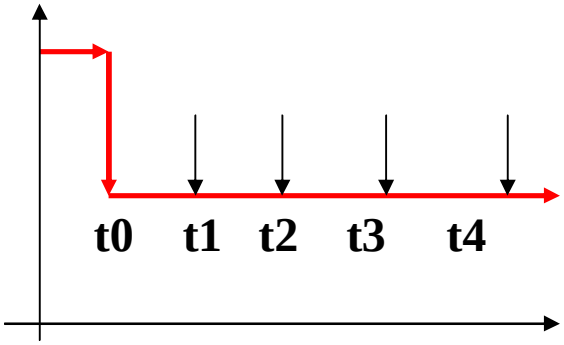

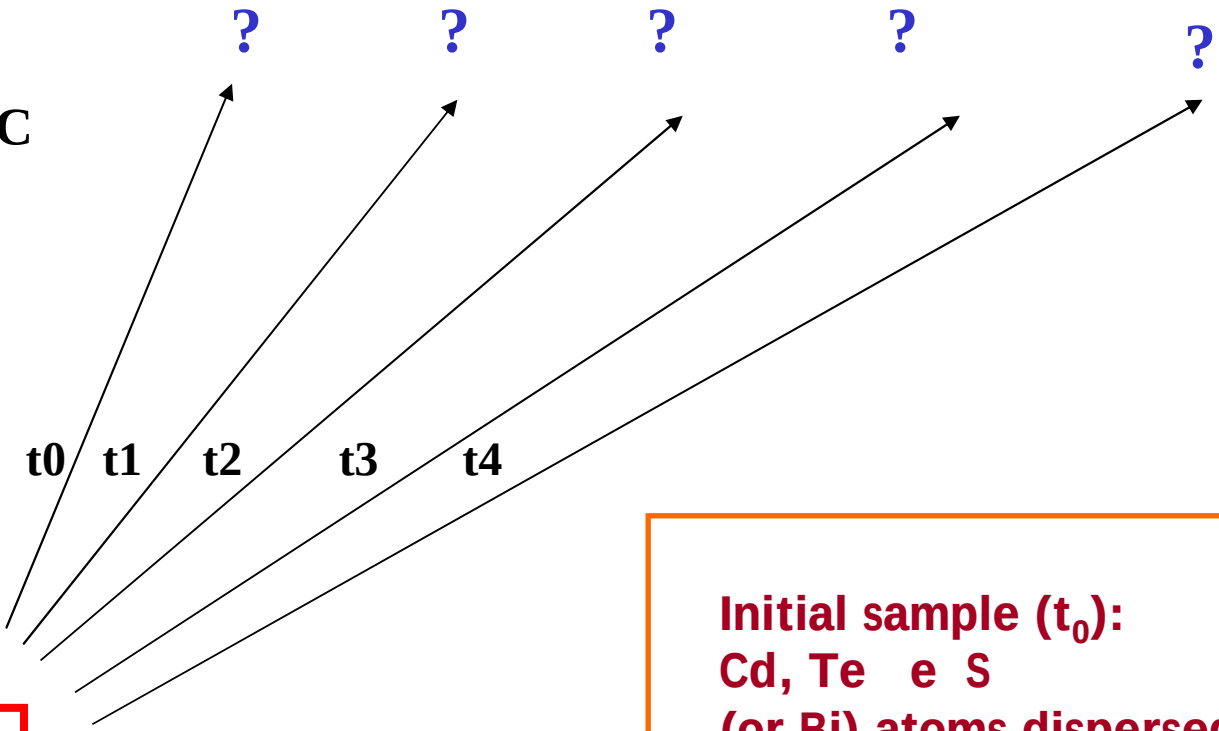

1100C (melt)

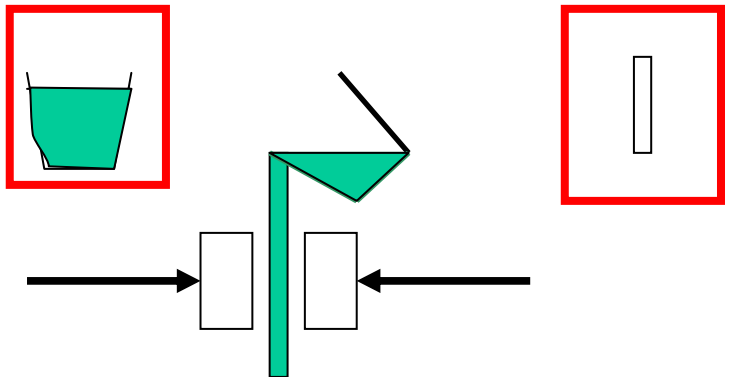

T = 560 C: t1, t2, t3, t4

Initial sample (t_0):
Cd, Te e S
(or Bi) atoms dispersed
in a glass matrix

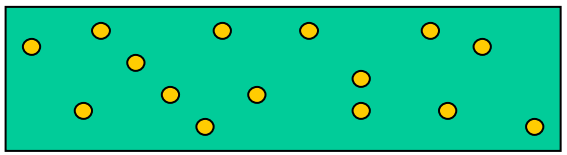

Nanoclusters embedded in a glass matrix
Preparation and optical properties

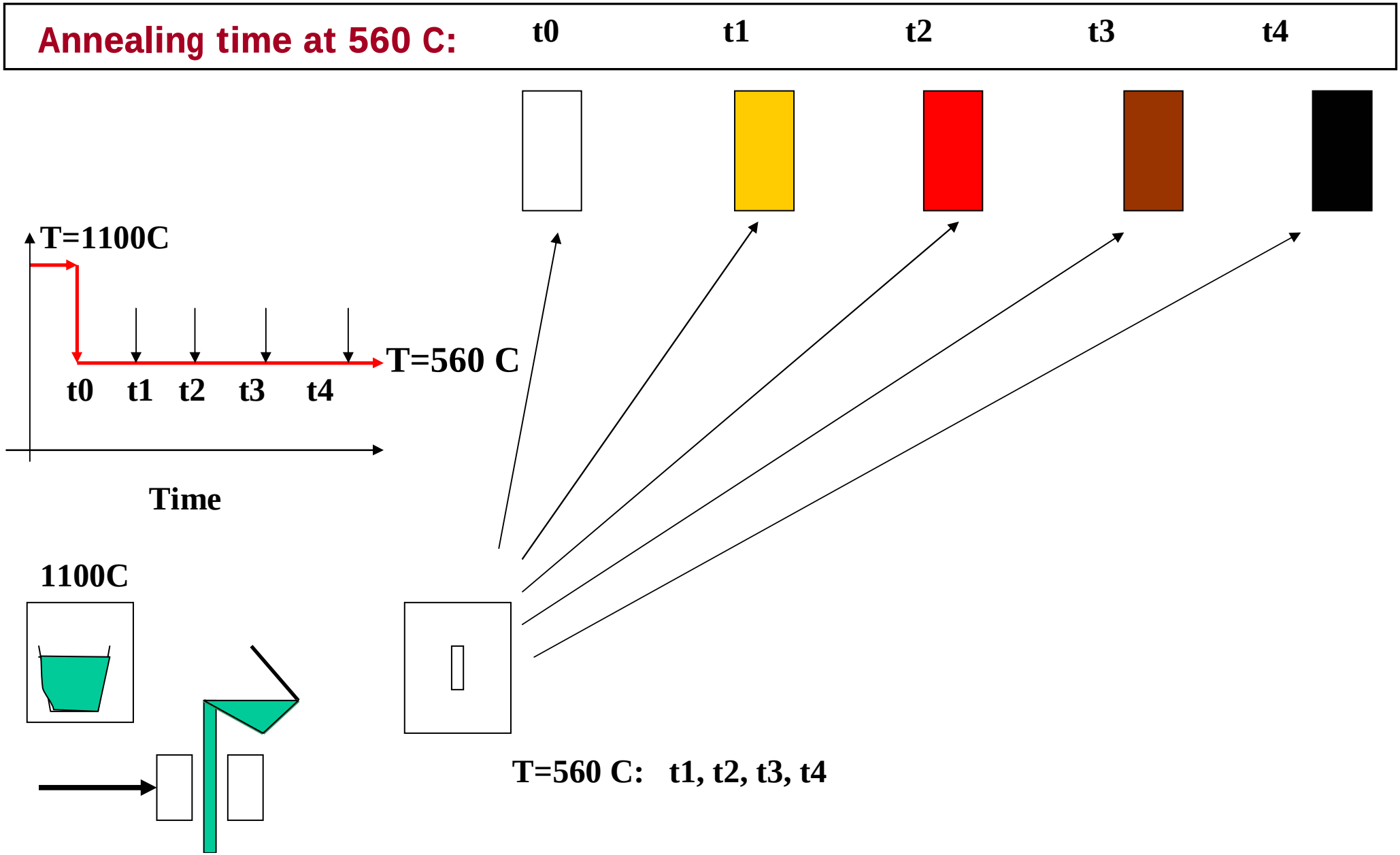

- The kinetics of formation and growth of liquid Bi nanodroplets embedded in a $28Na_2O$-$72B_2O_3$ glass was studied by small-angle X-ray scattering (SAXS).

- A Bi doped borate glass melted at 1300K was quenched down to room temperature by splat-cooling and then subjected to isothermal annealings at different temperatures ranging from 803 up to 843 K.

- These temperatures are close to the borate glass transition and well above the melting temperature of bulk Bi crystals (T_m=544 K).

- The isothermal annealing of the material promoted the nucleation, growth and coarsening of Bi *liquid* nanodroplets.

- The coarsening process was analysed within the frame of the Landau-Slyozov-Wagner theory.

- Using exclusively small-angle X-ray scattering data, the diffusion coefficient of Bi at several tempartures and the activation energy were determined.

-The properties of nanostructured materials depend strongly on the shape and size of the nanometric building blocks.

-The properties of nanostructured materials are functions of the process of preparation.

SHAPE

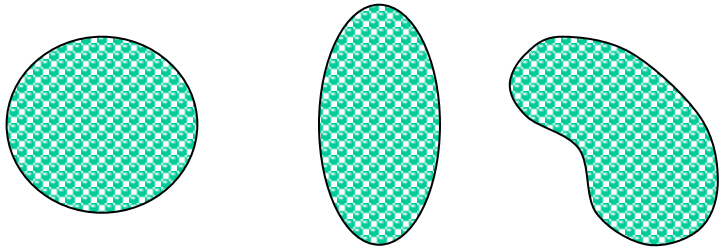

and

SIZE

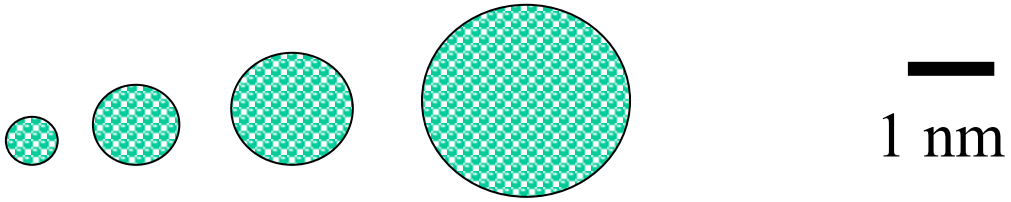

... are relevant structural characteristics of nanometric materials.

Direct space:

HRTEM

Reciprocal space:

-Small-angle X-ray (neutron) scattering

(Low resolution Fourier transfom providing low resolution structural features)

High resolution structure

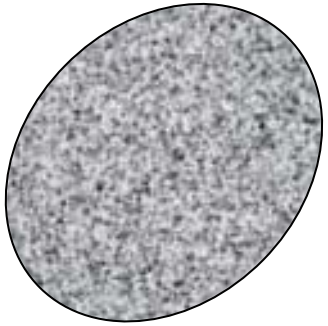

Low resolution structure shape, size

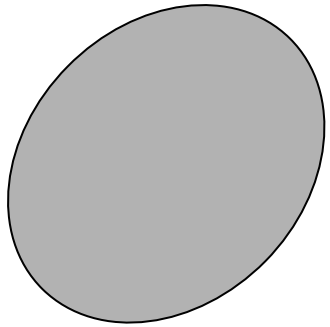

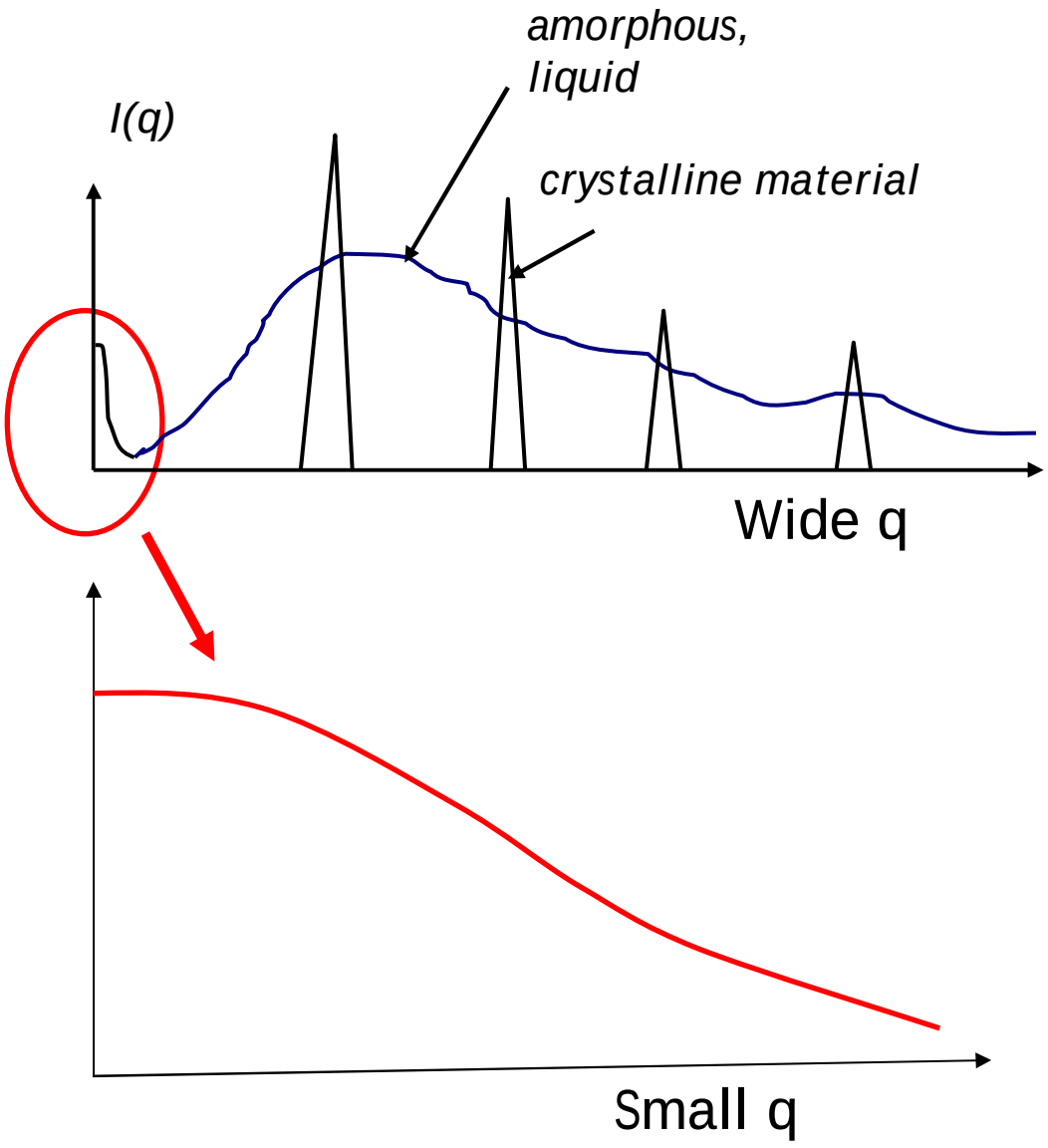

Direct space

Reciprocal or Fourier space

Synchrotron SAS beamline

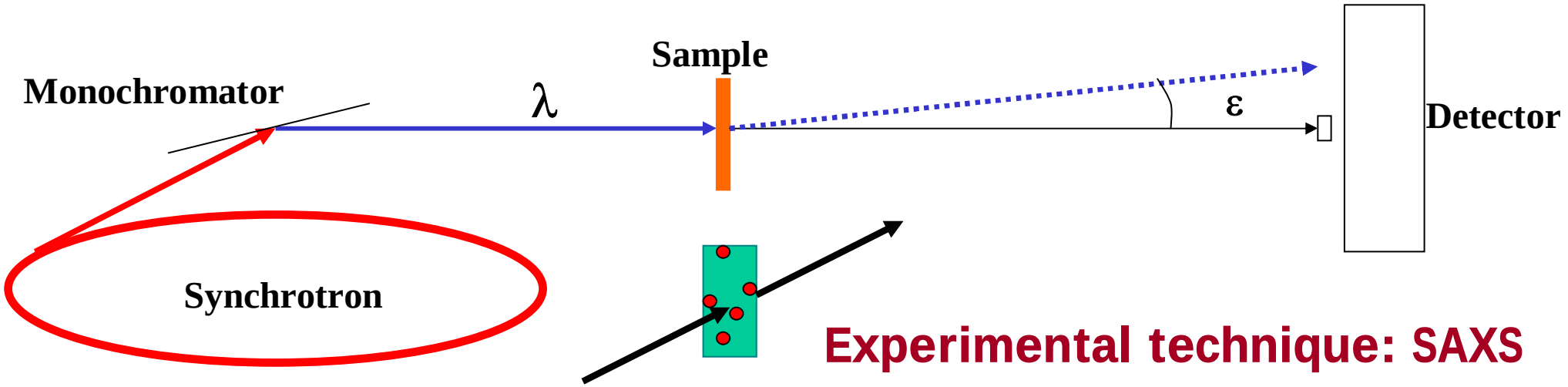

Experimental technique: SAXS

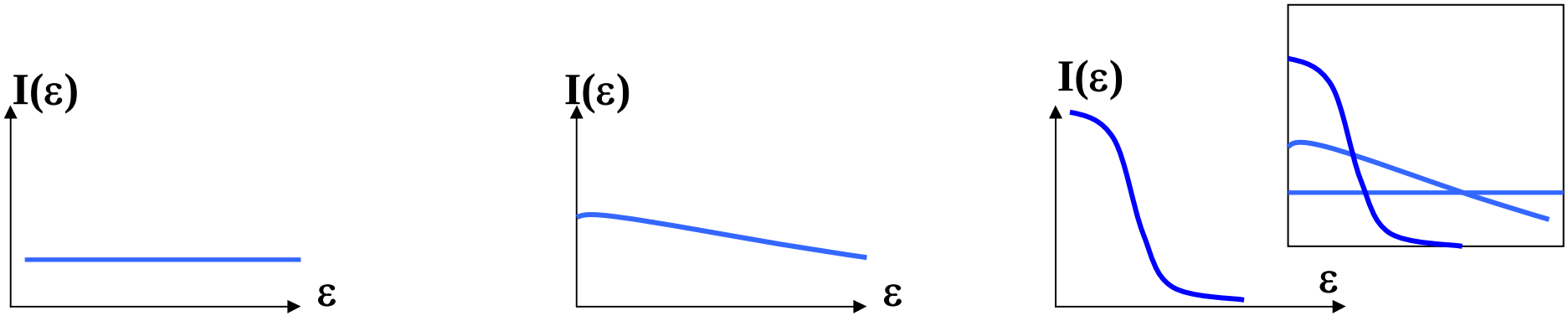

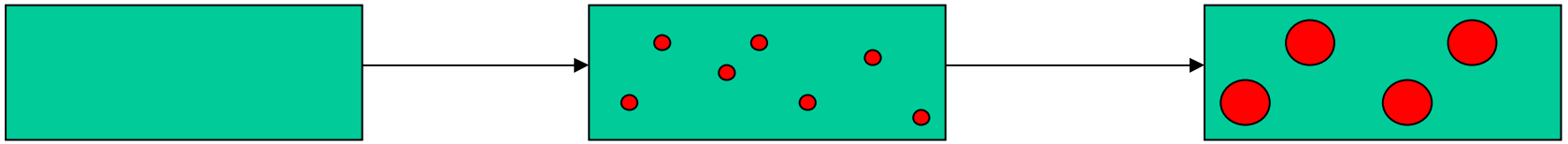

Isothermal transformation: Nanoclusters growth

LNLS SAXS beamline

G. Kellermann, F. Vicentin, E. Tamura, M. Rocha, H. Tolentino, A. Barbosa, A. F. Craievich e I. L. C. Torriani,
J. Appl. Cryst. (1997). 30, 880-883

Principais parâmetros da linha de SAXS do LNLS

- Fluxo: ~10^{10} fotons s^{-1} para 100 mA
- Comprimento de onda (λ): 1.38 – 1.8 Å.
- Vetor de espalhamento (for λ=1.61 Å):
  - 0.01 – 1 $Å^{-1}$ (distância amostra-detetor: 30 cm) ,
  - 0.005 – 0.2 $Å^{-1}$ (distância amostra-detetor: 160 cm).
- Resolução em energia ($\Delta E/E$): $5x10^{-3}$ @ 7.7 KeV.

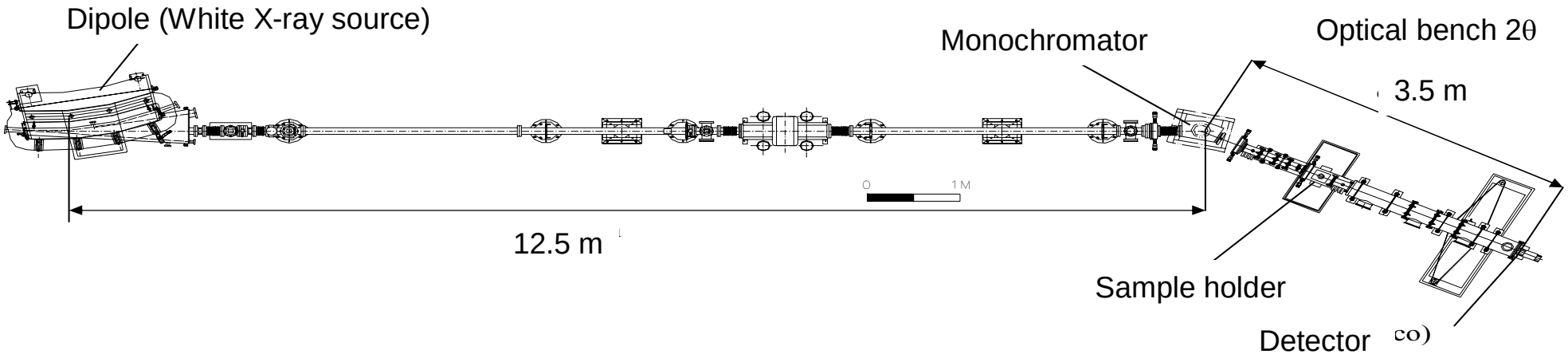

Bismuth droplets embedded in a soda-borate glass

Sample annealed 2 hours at 843 K

TEM study

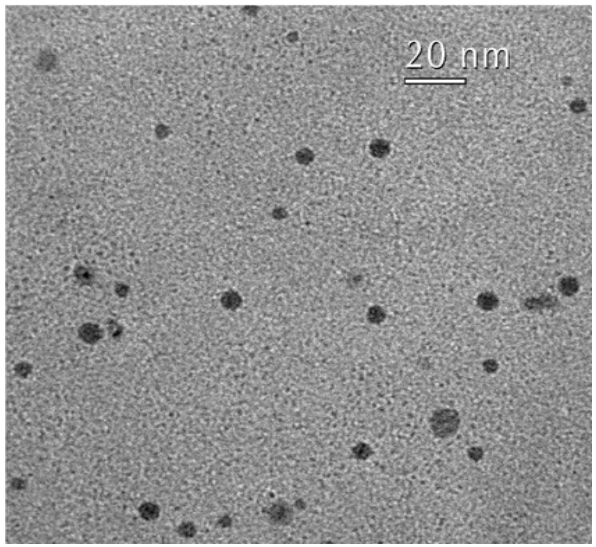

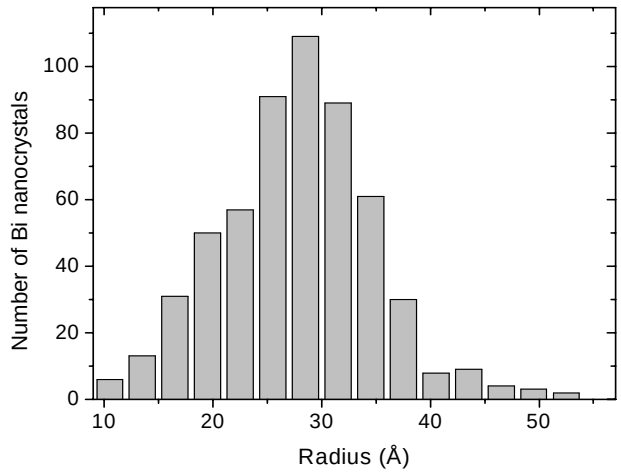

Spherical nano-objects embedded in a homogeneous matrix

$$I(q) = \int N(R).I_1(q,R)dR$$

$$I_1(q) = I_e(\rho_1 - \rho_2)^2 V_1 \int_0^R \left[1 - \frac{3r}{R} + \frac{1}{16}\left(\frac{r}{R}\right)^3\right] 4\pi.r^2 \frac{\sin qr}{qr} dr$$

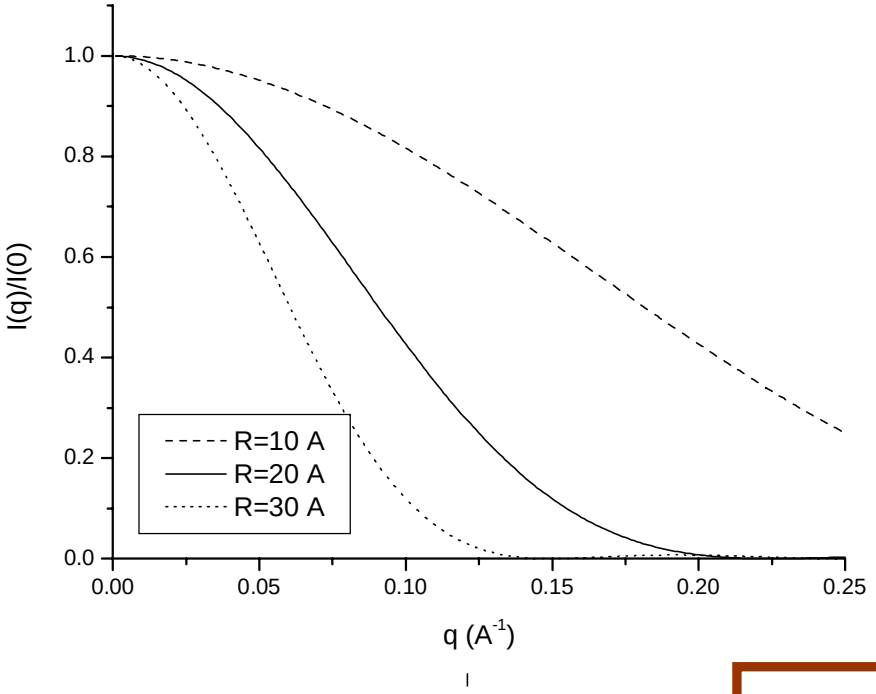

Monodisperse set of spheres

$$I_1(q) = I_e(\rho_1 - \rho_2)^2 . \left(\frac{4\pi R^3}{3}\right)^2 [\Phi(q)]^2$$

$$\Phi(q) = 3\frac{\sin qR - qR\cos qR}{(qR)^3}$$

GNOM package yields:

$$D(R) = \frac{4\pi}{3} R^3 .N(R)$$

Polydisperse set of spheres

$$I(q) = I_e(\rho_1 - \rho_2)^2 \left(\frac{4\pi}{3}\right)^2 \int N(R).R^6 \left[3\frac{\sin qR - qR\cos qR}{(qR)^3}\right]^2 dR$$

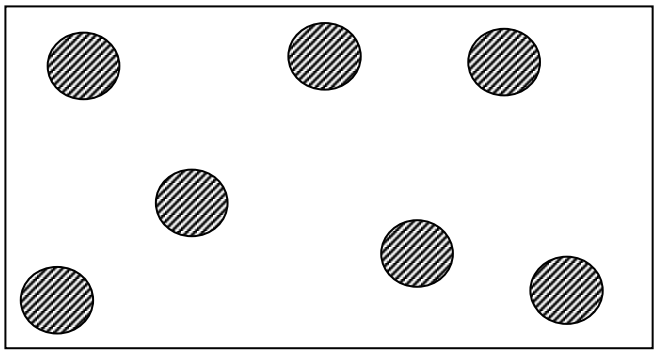

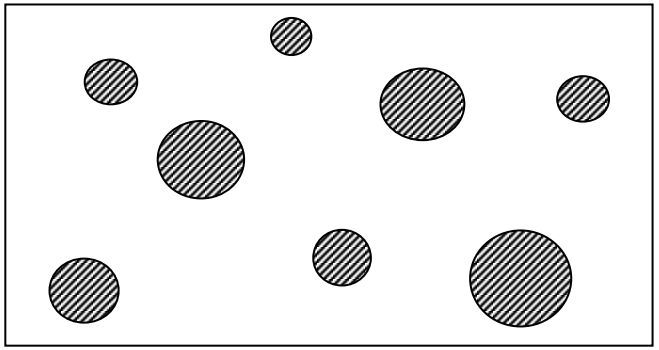

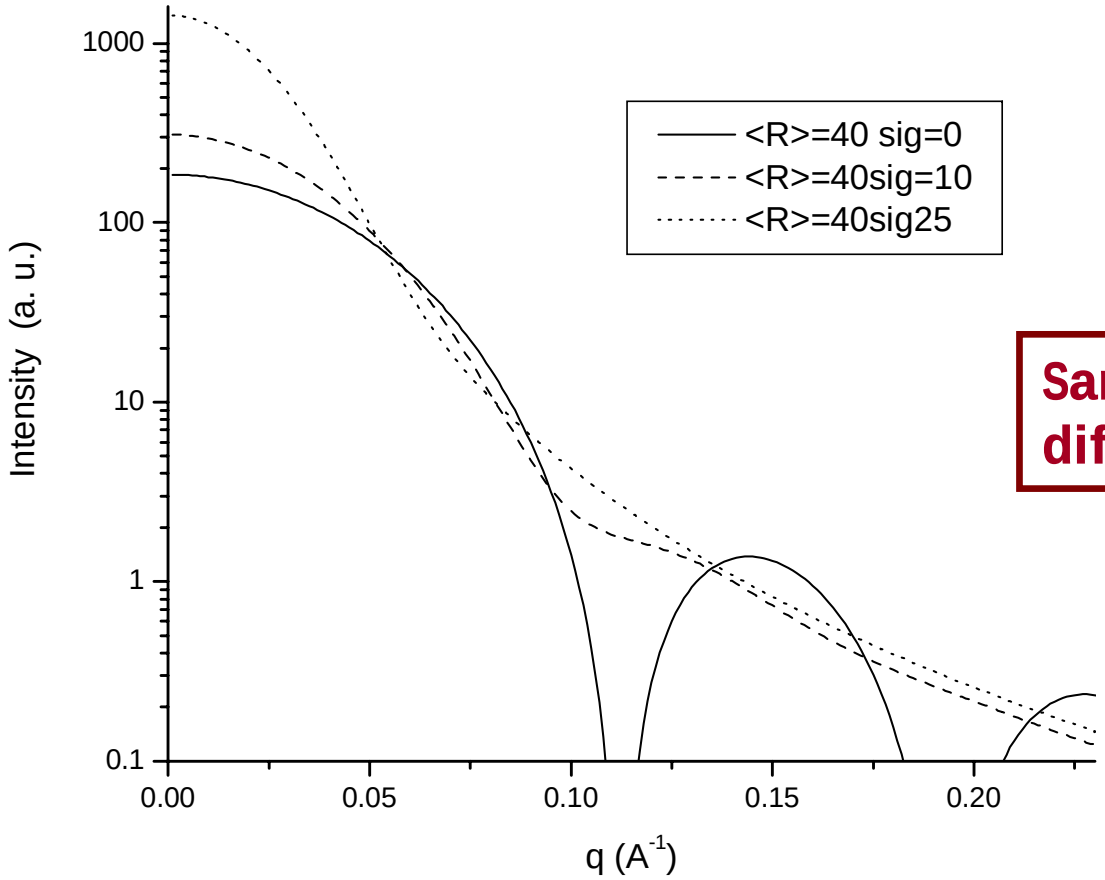

Same <R> and different dispersions

Dilute and isotropic system of polydisperse nano-objects

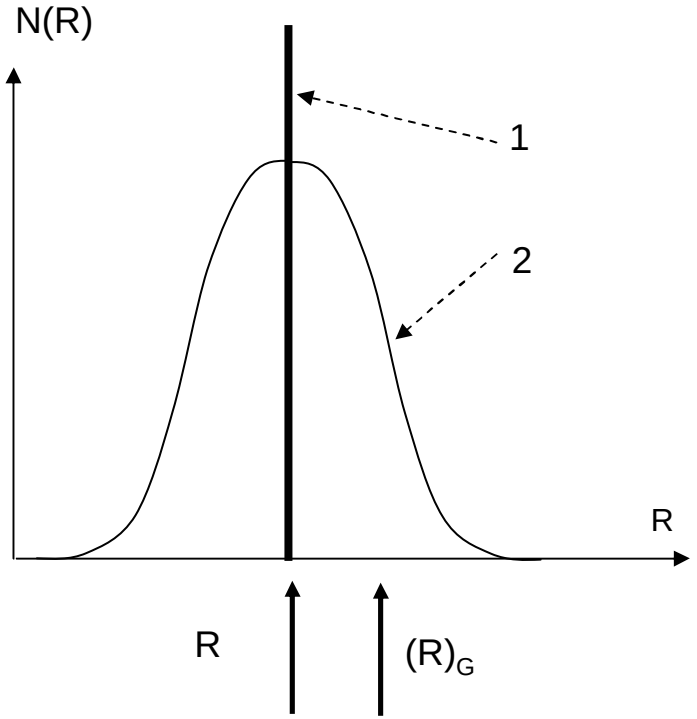

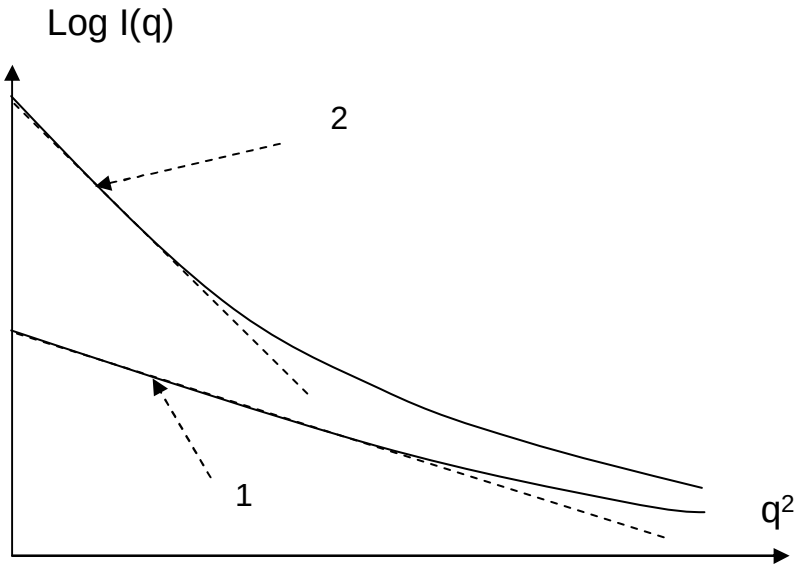

$$I(\vec{q}) = I_e(\rho_1 - \rho_2)^2 \int N(R_g)..V_1^2(R_g).e^{-\frac{R_g^2 q^2}{3}} dR_g$$

$$I(q) = NI_e(\rho_1 - \rho_2)^2 .\{V_1^2\} e^{-\frac{\{R\}_G^2 q^2}{3}}$$

$$I(q) = NI_e(\rho_1 - \rho_2)^2 \left[\frac{1}{N} \int N(R_g)..V_1^2(R_g).dR_g - \frac{q^2}{6N} \int N(R_g)..V_1^2(R_g).R_g^2 dR_g \right]$$

$$\{V_1^2\} = \frac{1}{N} \int N(R_g).V_1^2(R_g) dR_g$$

$$\{R\}_G = \left[\frac{1}{N} \int N(R_g).V_1^2 R_g^2 dR_g \right]^{1/2}$$

3. CLASSICAL THEORY OF DROPLET COARSENING

The formation of a new phase consisting of nanoclusters embedded in an initially homogeneous supersaturated matrix starts from a nucleation stage and is followed by a further growth promoted by the diffusion of doping atoms. This mechanism is named "nucleation and growth".

- According to the model proposed by Lifshitz-Slyosov (1961) [6] and Wagner (1961) [7] (LSW), when the supersaturation of the doping element in the matrix become small, *spherical clusters* with a radius R smaller than a critical radius R_c start to dissolve while those with radii larger that R_c still grow.

$$N(R,t) = f(t)\frac{4(R/R_c)^2}{9}\left(\frac{3}{3+R/R_c}\right)^{7/3} \times \left(\frac{3/2}{3/2-R/R_c}\right)^{11/3} e^{\left(\frac{R/R_c}{-3/2+R/R_c}\right)}$$

where $f(t)$ is a function of the annealing time. During the coarsening stage R_c coincides with $\langle R \rangle$. The concentration of solute atoms in the matrix c(t) and number density of clusters n(t) are time dependent functions.

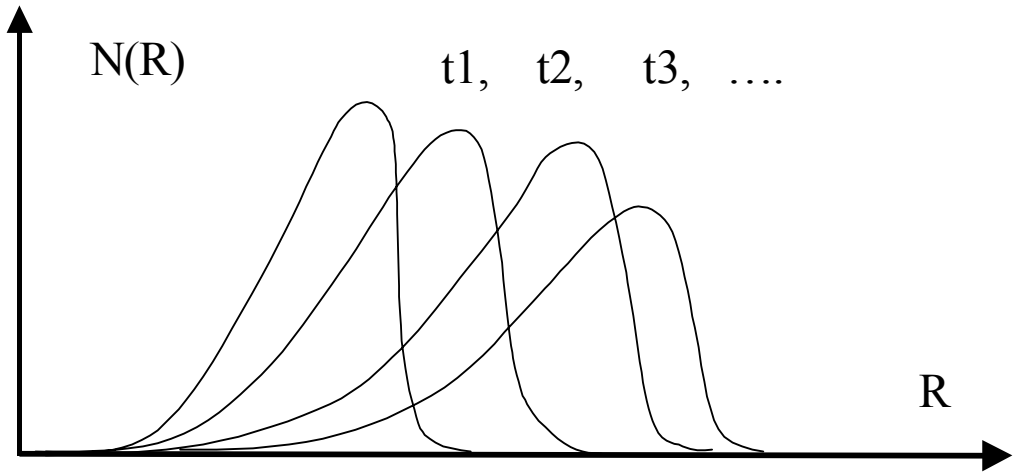

Rate equations

During the coarsening stage, the average radius <*R*> increases for increasing times while *n* progressively decreases. Quantitatively, according to the SLW model, the time dependence of the average droplet radius [<*R*>(t)], the number density *n(t)* and the solute concentration in the matrix c(t) satisfy the following equations [5-7]:

$$[< R >^3 (t)] =< R_0 >^3 + \kappa(t - t_0)$$; <R>: droplet average radius

$$n^{-1}(t) = n_0^{-1} + \beta(t - t_0)$$; n: droplet number density

$$c(t) = c^e + [\chi(t - t_0)]^{-1/3}$$; c(t): solute concentration in the matrix

$$\varphi(t) = \varphi_e - [\chi'(t - t_0)]^{-1/3}$$; φ(t): total droplet volume fraction

Determination of the atomic diffusion coefficient from SAXS results

The four rate parameters κ, β, χ and χ' are related to the atomic diffusion coefficient D of the solute:

$$\kappa = \frac{8\sigma v^2 c^e D}{9kT} \qquad \beta = \frac{4\sigma c^e v D}{(c_0 - c^e)kT}$$

$$\chi = \frac{D(kT)^2}{9\sigma^2 c_e^2 v} \qquad \chi' = \left(\frac{1/v - c_e}{1-\varphi_e}\right)^3 \chi$$

σ: free energy per unit of area of the interface between clusters and matrix,

υ: the volume of the solute; c^e: equilibrium solute concentration.

Since the parameters σ and c_e are in many cases not known,

these equations cannot directly be used to determine the diffusion coefficient D.

Assuming that $[(1/v) - c_e] \approx (1/v)$, we have

$$D = \frac{9}{4}(\kappa^2 \chi')^{1/3}$$

$$[< R >^3 (t)] =< R_0 >^3 + \kappa(t - t_0) \qquad \varphi(t) = \varphi_e - [\chi'(t - t_0)]^{-1/3}$$

Average radius (t) Total droplet volume fraction

$$\frac{d\Sigma}{d\Omega}(q) = r_0^{\,2} \cdot \left(\rho_p - \langle\rho\rangle\right)^2 \cdot \left(\frac{4\pi}{3}\right)^2 \int_0^\infty N(R) \cdot \left|P(q,R)\right|^2 \cdot R^6 \cdot dR$$

where $N(R)dR$ is the number of particles per unit volume with radius between R and $R+dR$. r_0 = 0.28179x10^{-14} m is the classical electron radius and $P(q,R)$ is the normalized form factor for a sphere defined by [9]:

$$P(q,R) = 3\frac{sen(qR) - qR\cos(qR)}{(qR)^3}$$

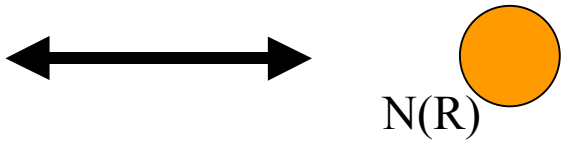

$$N(R) = \frac{n}{\sqrt{2\pi \exp(w^2)} \cdot wr} e^{-(\ln(R/r)/w)^2/2}$$

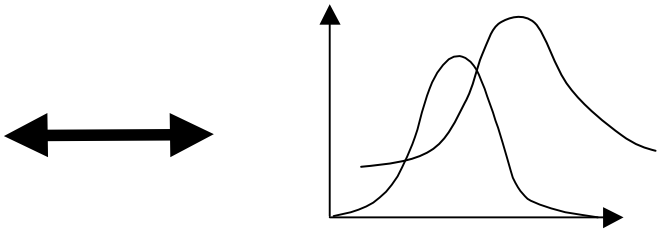

First, by a non-linear fitting procedure, we obtain the parameters r and w of the lognormal function

<R>(t) is then calculated

n(t) is obtained from:

$$n(t) = \int N(R,t)dR$$

Experimental determination of the diffusion coefficient of Bi and energy of activation from SAXS results

The volume fraction of the solute phase φ can be determined from the integrated scattering power Q in reciprocal space.

$$Q = 4\pi \int_{q=0}^{\infty} \frac{d\Sigma}{d\Omega}(q) \cdot q^2 dq .$$

This integral is related to the volume fraction φ by

$$Q = 8\pi^3 r_0^2 \Delta\rho^2 \varphi(1-\varphi)$$

Since in our case the Bi concentration is low (1-5%), we can safely assume that Δρ is a constant during the whole coarsening process. So,

$$\varphi(t) = \frac{1}{2} - \left(\frac{1}{4} - \frac{Q(t)}{4\pi^3 r_0^2 \Delta\rho^2} \right)^{1/2}$$

In situ SAXS at 833K

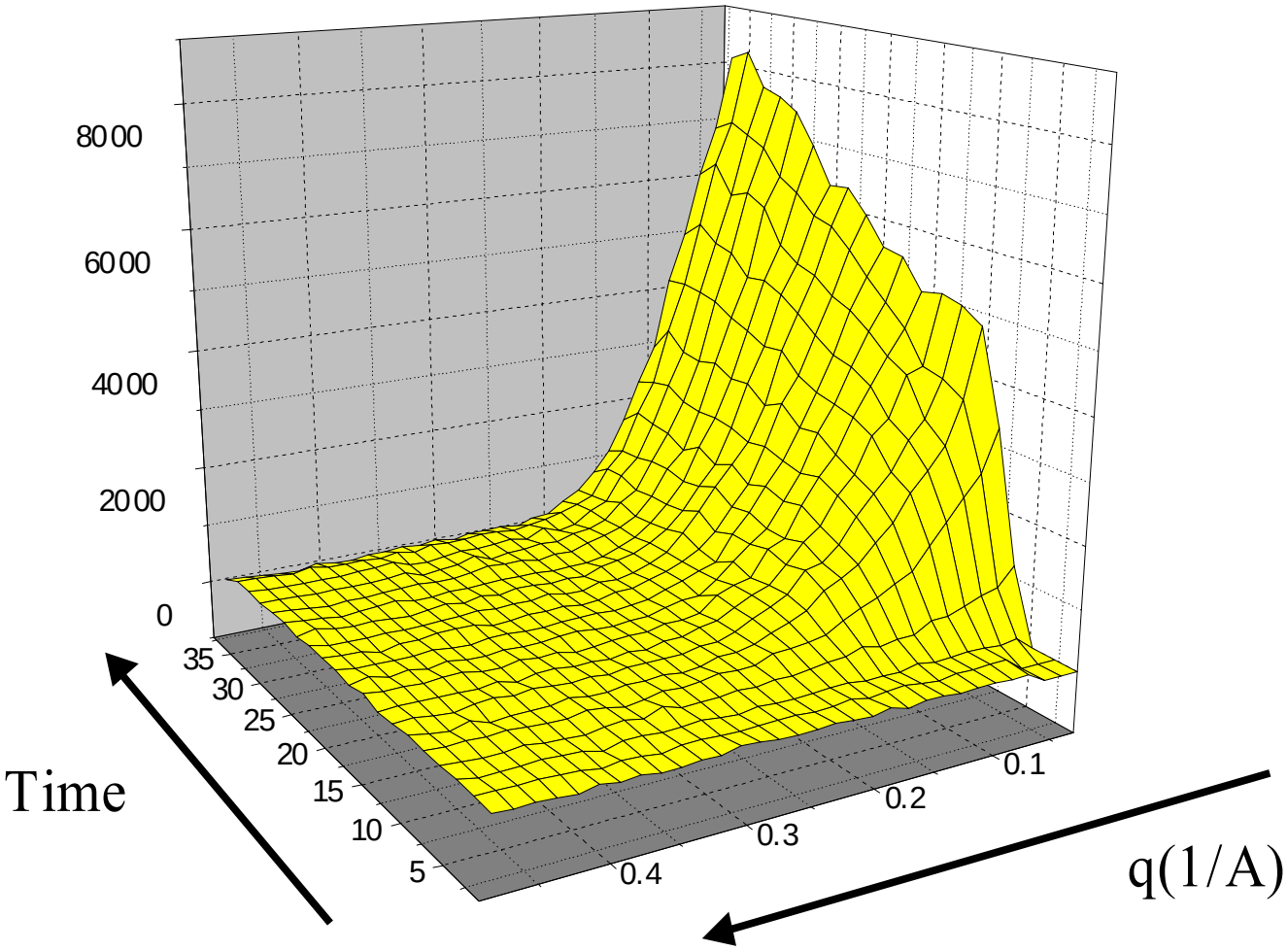

$$\frac{d\Sigma}{d\Omega}(q) = r_0^{\,2} \cdot \left(\rho_p - \langle\rho\rangle\right)^2 \cdot \left(\frac{4\pi}{3}\right)^2 \int_0^\infty N(R) \cdot \left|P(q,R)\right|^2 \cdot R^6 \cdot dR$$

Best fit of

$$\frac{d\Sigma}{d\Omega}(q)$$

to SAXS experimental results using LSW and lognormal N(t) functions

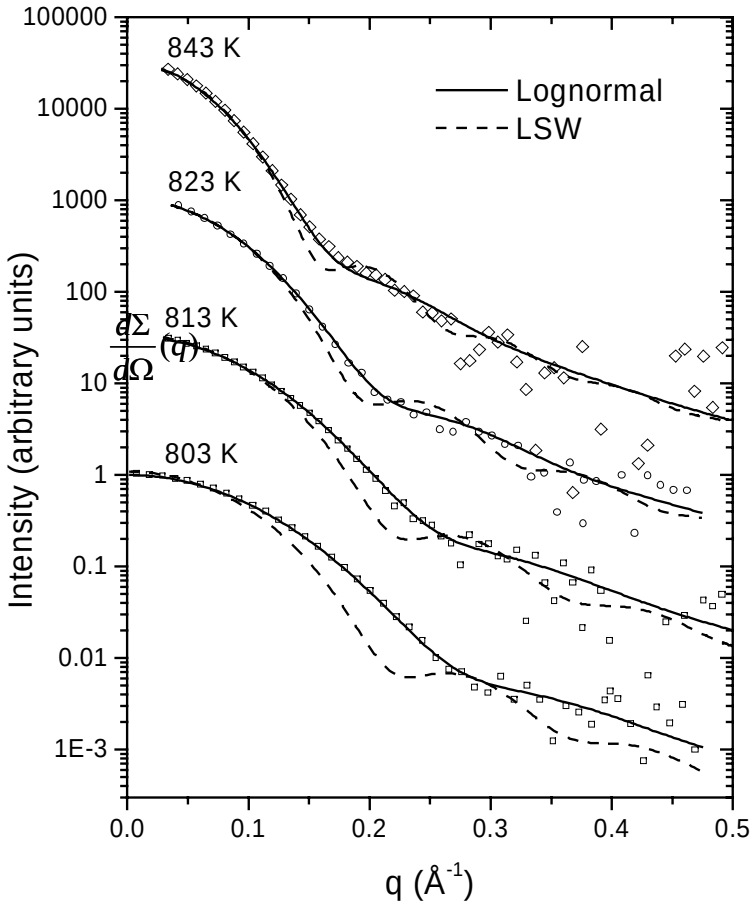

Experimenat SAXS results and calculated curves assuming a lognormal radius distribution

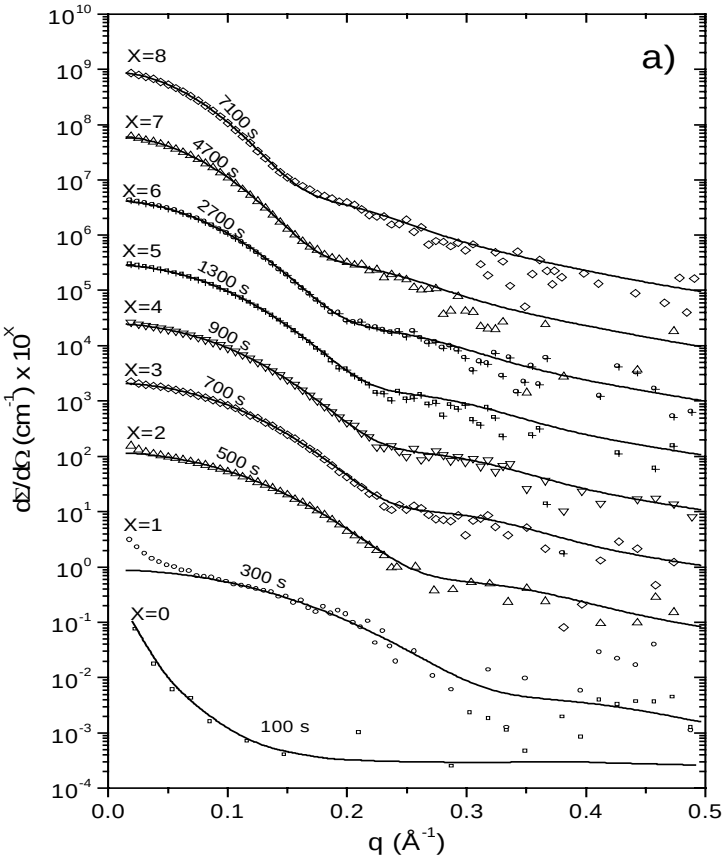

N(R,t) assuming a lognormal radius distribution

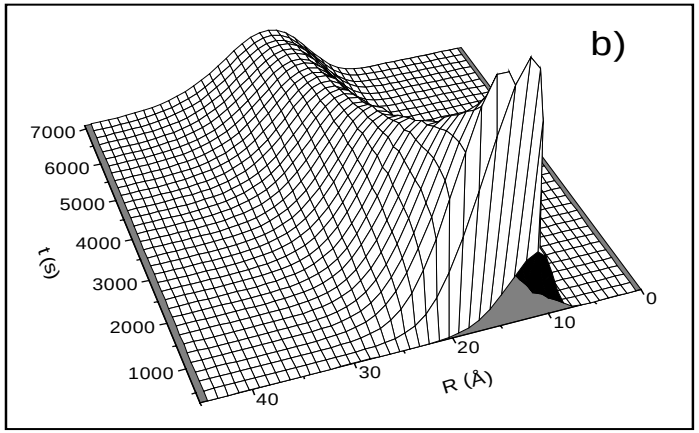

-Droplet radius

-Number density

-Relative radius dispersion

-Total droplet volume fraction

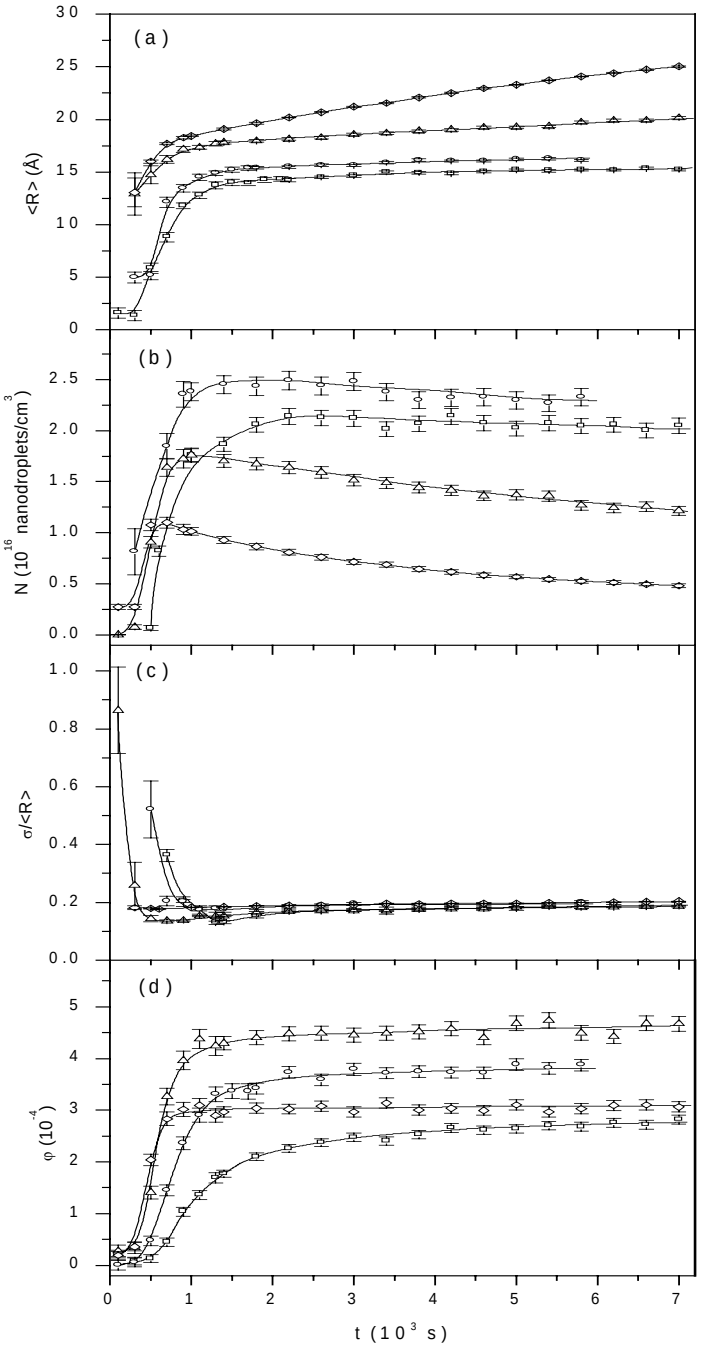

$$\langle R\rangle^3 = [\langle R\rangle^3] + \kappa\,(t-t_0)$$

$$n^{-1} = n^{-1}(t_0) + \beta\,(t-t_0)$$

$$\varphi = \varphi(0) + (\chi')^{-1/3}\,(t-t_0)^{-1/3}$$

$$D = (9/4)\,(\kappa^2\,\chi')^{1/3}$$

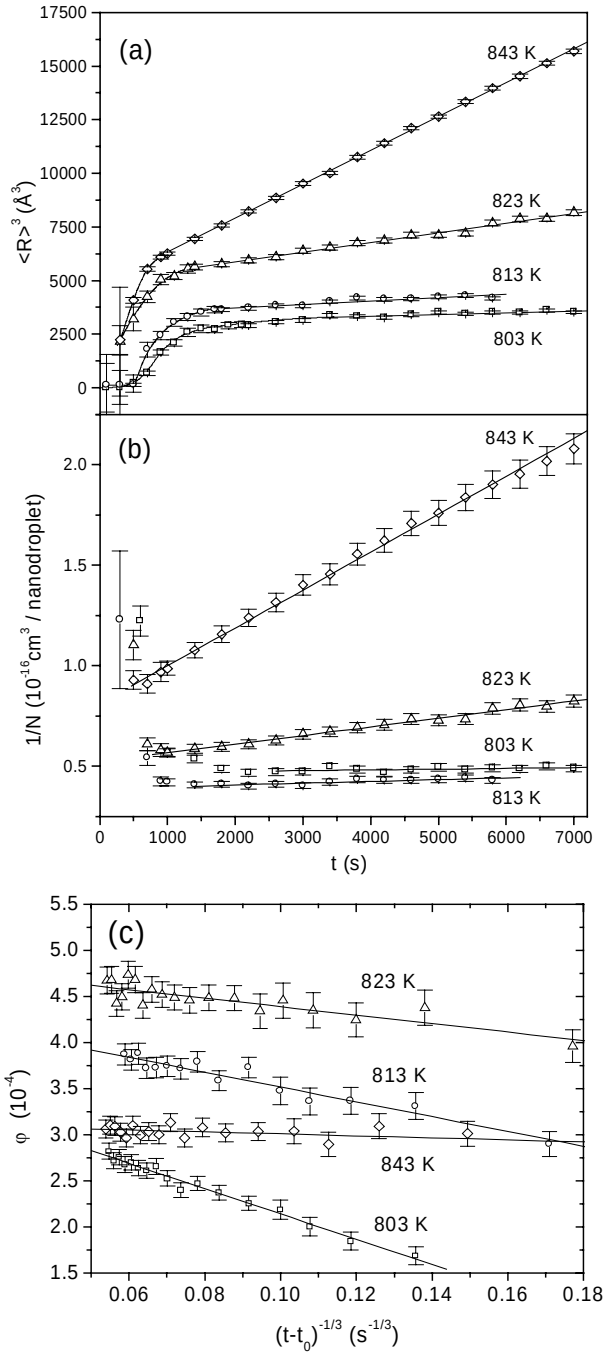

The activation energy for the diffusion of Bi atom was calculated from the slope in an Arrenhius plot [log D versus (1/T)]:

$$D=D_0\, e^{-E/RT}$$

$E=(64^{+}\text{-}3)$Kcal/mol

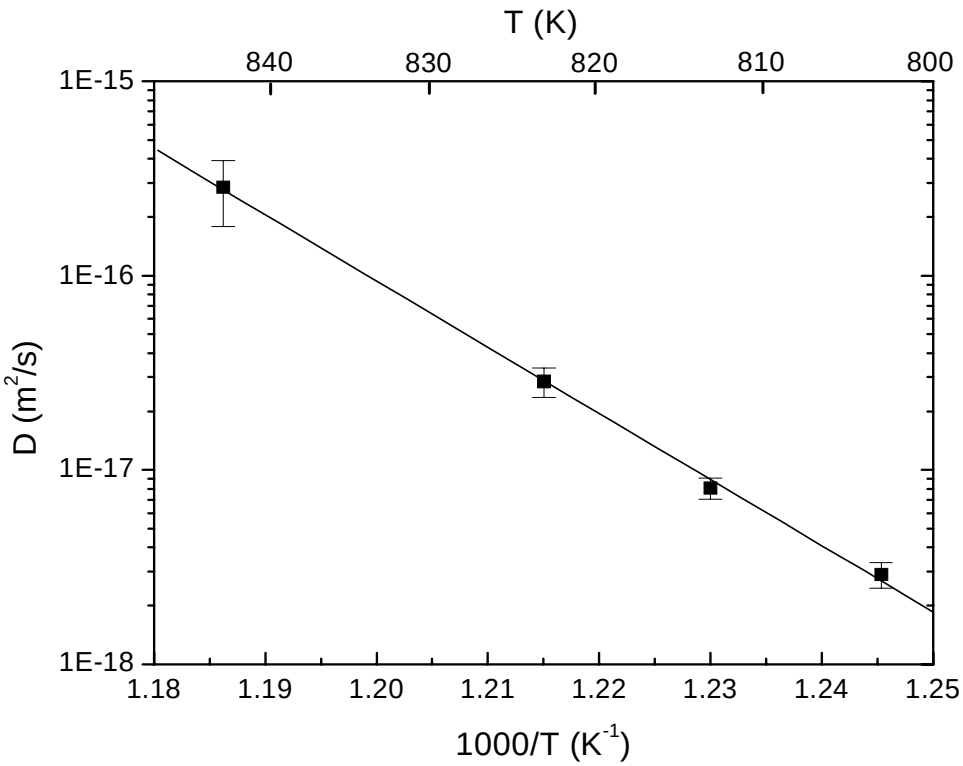

CONCLUSION

- Three stages were detected during the formation of Bi droplets embedded in a soda-borate glass:

i)an initial short incubation stage,

ii)a second fast growth stage during which the size of Bi clusters increases by atomic diffusion and aggregation of isolated Bi atoms,

iii)a final rather slow stage during which most of the isolated Bi atoms are already aggregated but the nanodroplets still grows by coarsening.

Stage (iii)

- The average radius and inverse density number of the Bi nanodroplets and the volume fraction of the new phase are well described by the equation predicted by the LSW model for coarsening.

- The ratio between the nanodroplets radius dispersion and their average value is a nearly time constant during coarsening as predicted by LWS theory, so indicating a dynamical scaling property or dynamical self-similarity of the structure.

- It was demonstrated that the radius distribution is better described by a lognormal function than by the function predicted by LSW model.

- The diffusion coefficients of Bi atoms through the studied soda-borate glass during coarsening was quantitatively calculated from a set of experimental curves of X-ray scattering power. This evaluation was performed for different annealing temperatures so as, from an Arrenhius plot, the activation energy $E=(64 \pm 3) \times 10^4$ J mol^{-1} was obtained.

Are

glass-metal nanocrystals nanocomposites

new materials?

Licurgus calice
(Lycurgus, King of Sparte)

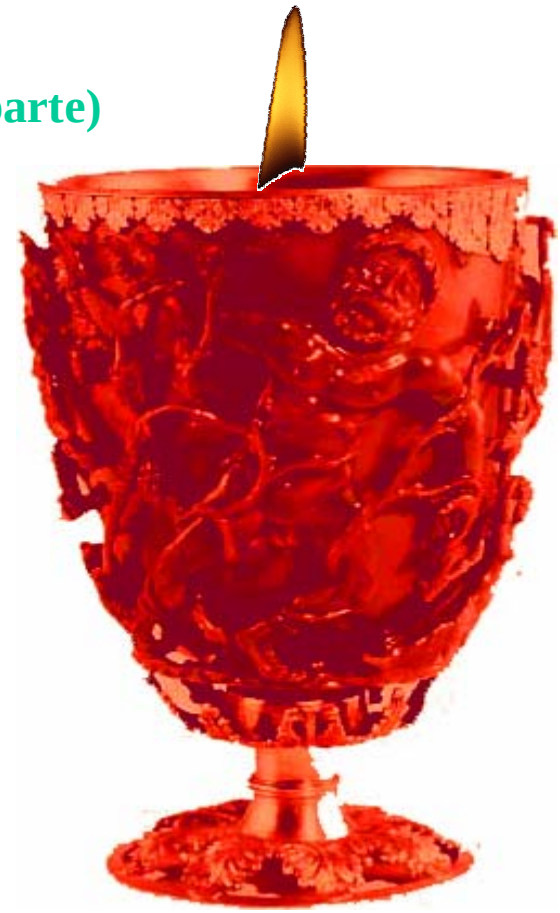

Roman object
(~2000 years old)

Soda-lime glass with
3.10^{-4} Ag e 4.10^{-5} Au

Structure and melting of Bi nanocrystals embedded in a B_2O_3-Na_2O glass

G. Kellermann and A. F. Craievich
Phys. Rev. B 65, 134204 (2002)

Differences between the structures of nanocrystals and bulk crystals

- Possible existence of non-crystallographic structures
- Lattice contraction or expansion
- Melting temperature (significant) variation (M. Takagi, 1954)

Theoretical dependence $T_m(R)$ for nanometric crystals

Couchman - Jesser (1977) e Allen *et al*., (1980)

$$T_m - T_b \propto 1/R$$

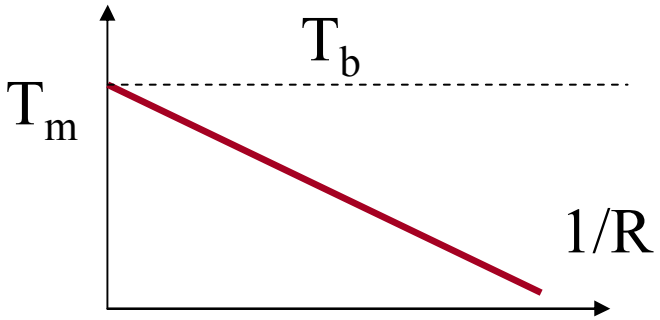

Glass containing spherical nanocrystals with a variety of sizes

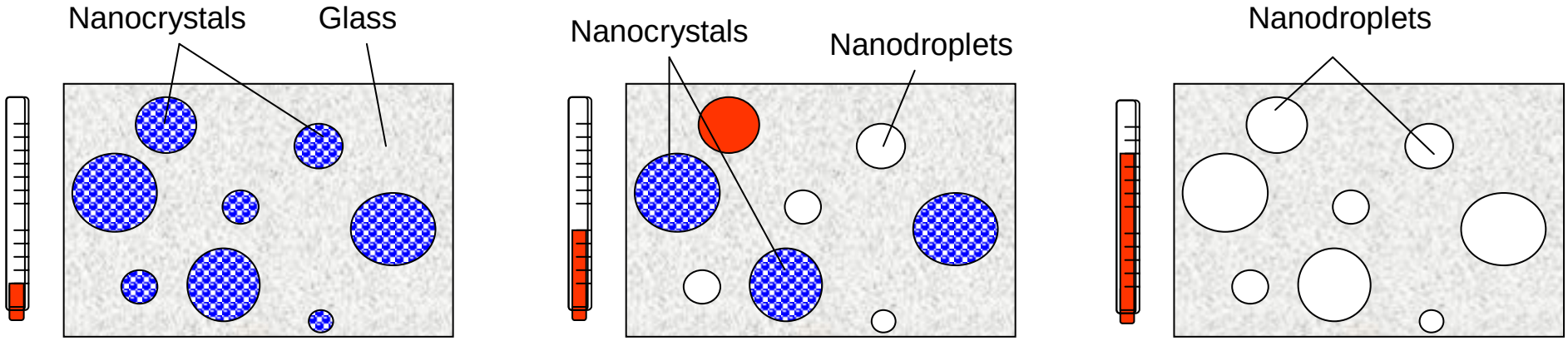

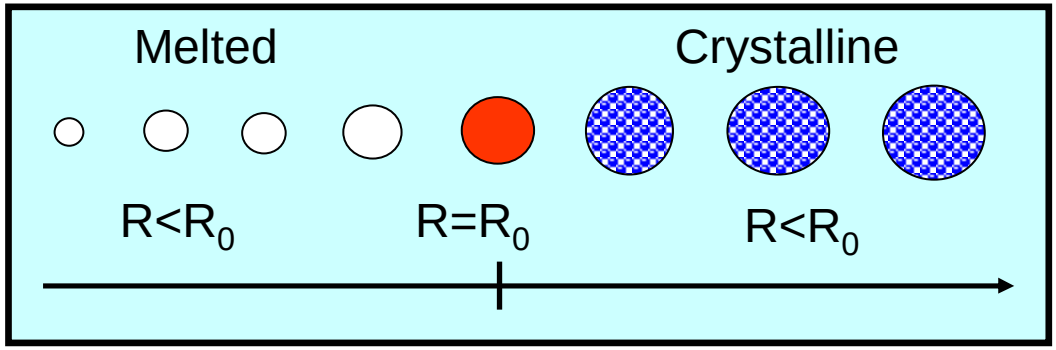

Current methods for the determination of T_m (R)

(Melting temperature versus nanocrystal radius)

- Transmission electron microscopy
- Optical techniques
- Calorimetry
- X-ray diffraction

These techniques probe a very large number of nanoclusters

Procedure

Combined SAXS and WAXS techniques

Experimental setup

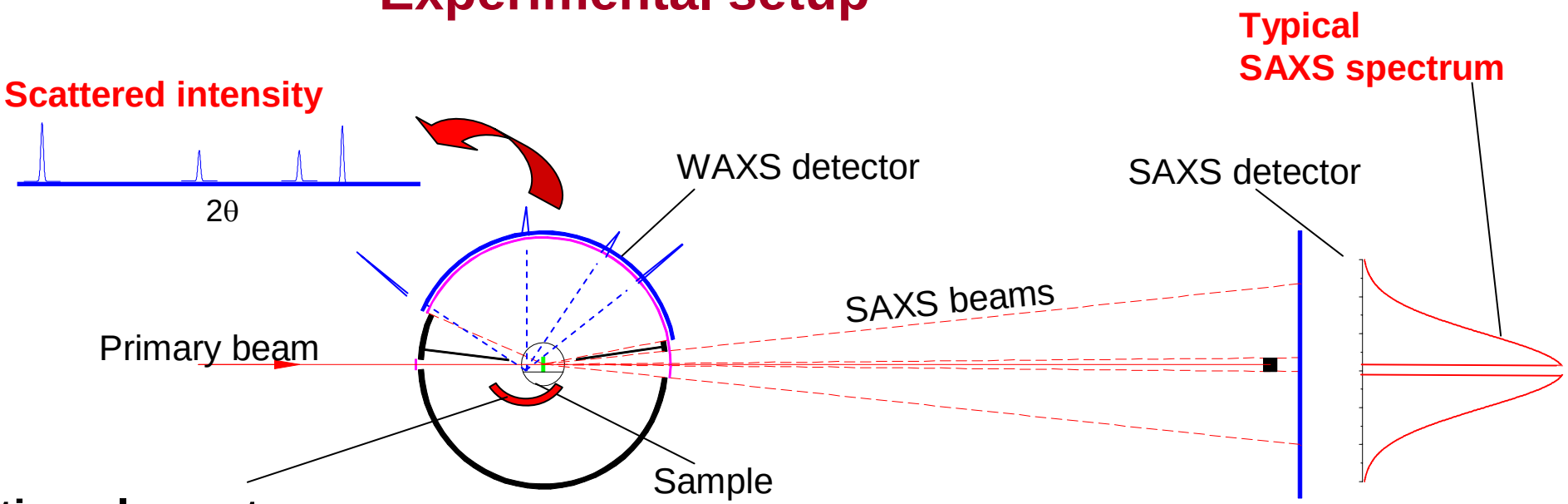

Structure as a function of temperature

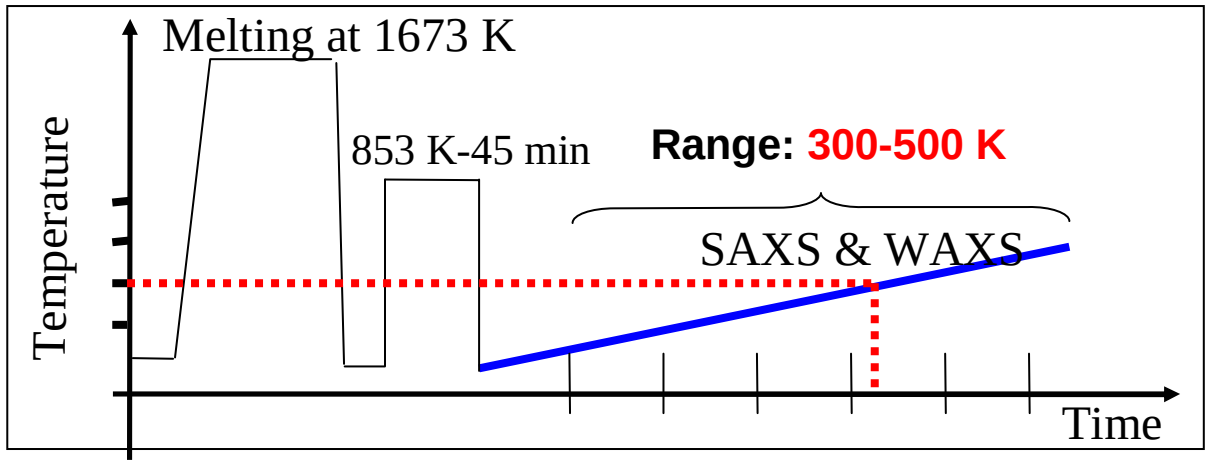

SAXS results

SAXS intensity

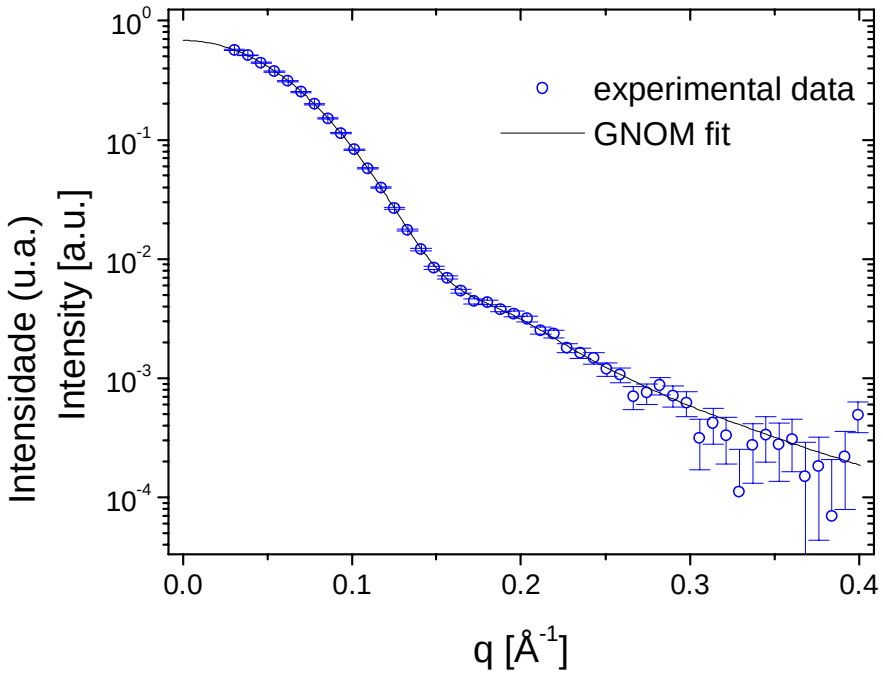

Volume distribution function

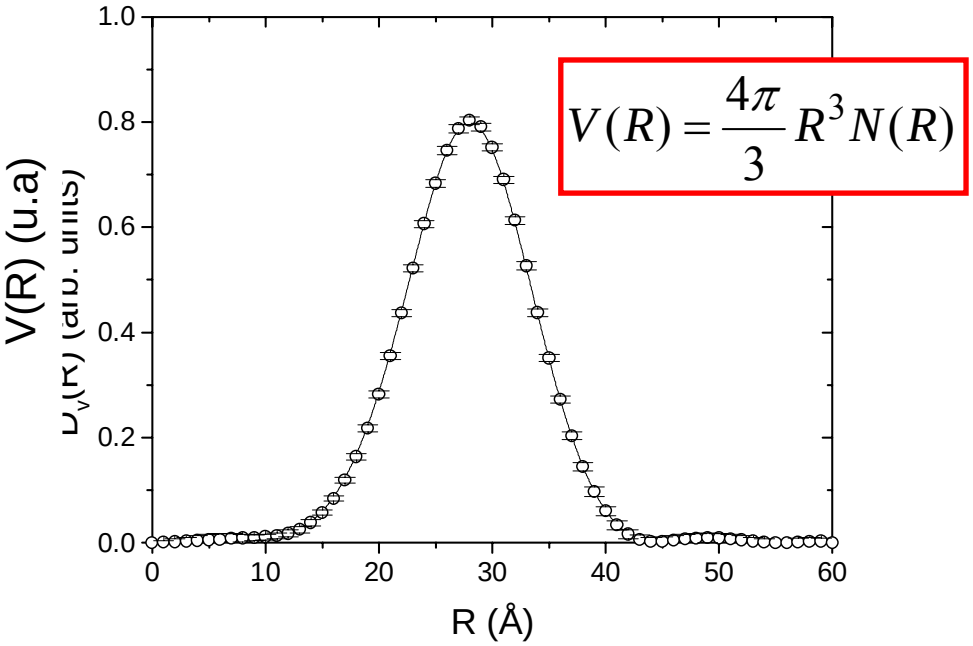

$$V(R) = \frac{4\pi}{3} R^3 N(R)$$

WAXS results

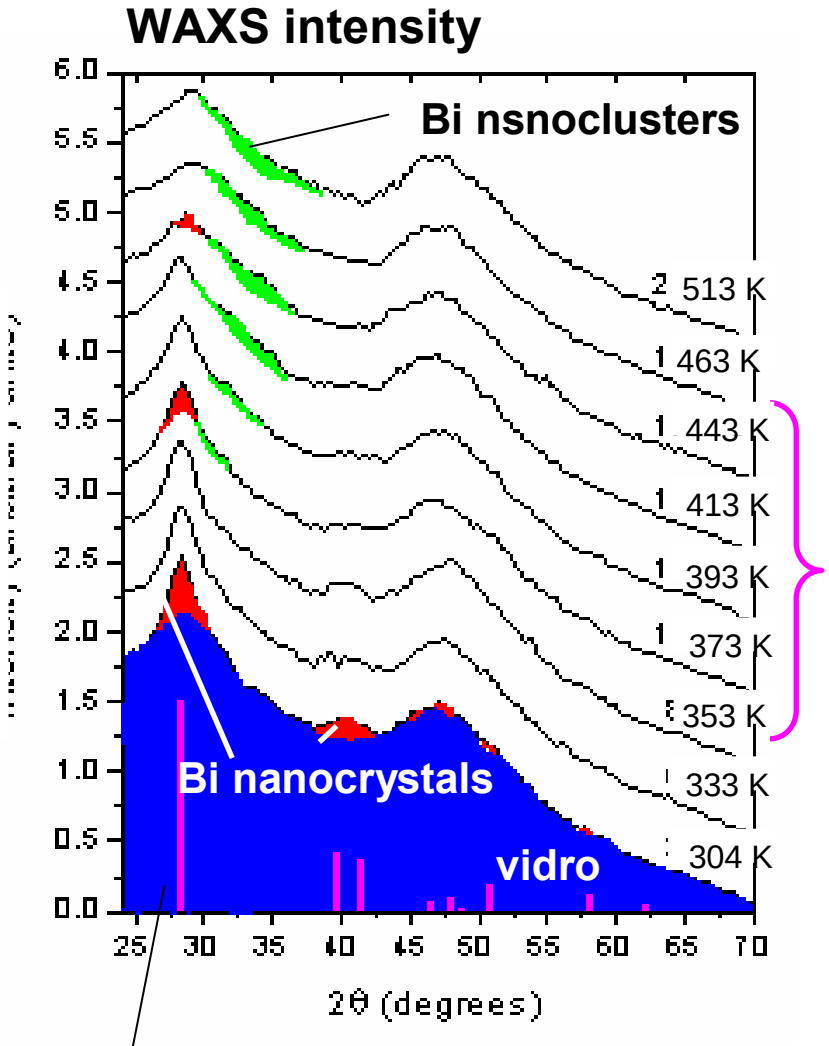

glass+nanodroplets

glass+nanocrystals+nanodroplets

glass+nanocrystals

WAXS results

Intensity scattered by Bi nanocrystals

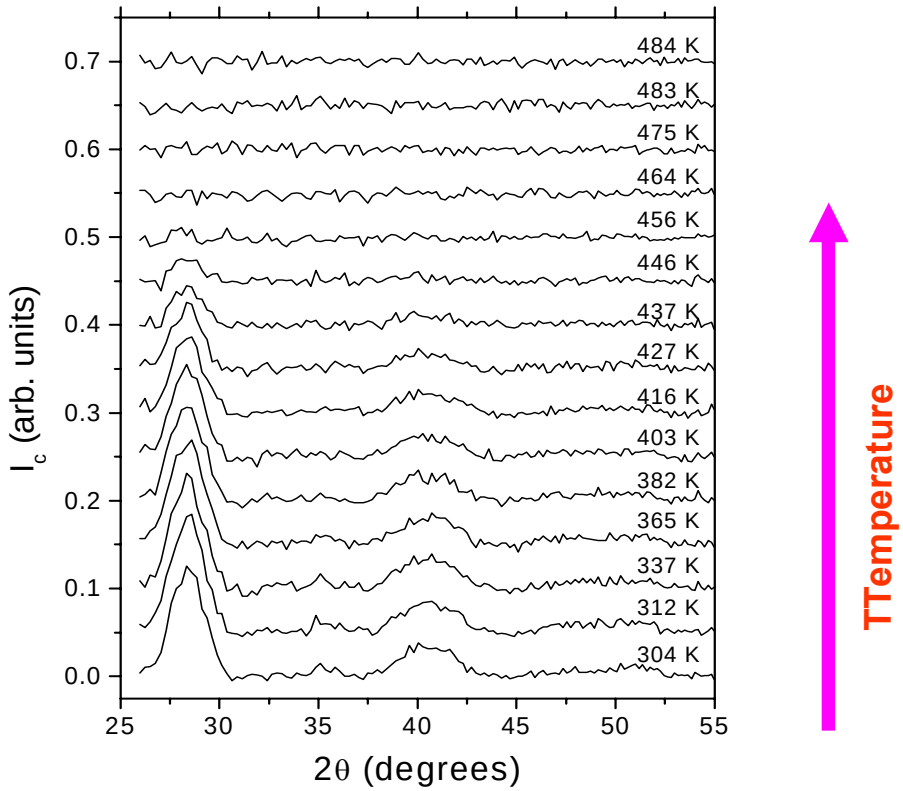

The area of Bragg peaks decreases continuously from 365 to 464 K (Δ T~100K). Above 464 K, all Bragg peaks desappear so indicating that all nanocrystals have melted.

How one can determine the connection between

melting temperature and nanocrystal radius

from WAXS and SAXS data ?

From SAXS results:

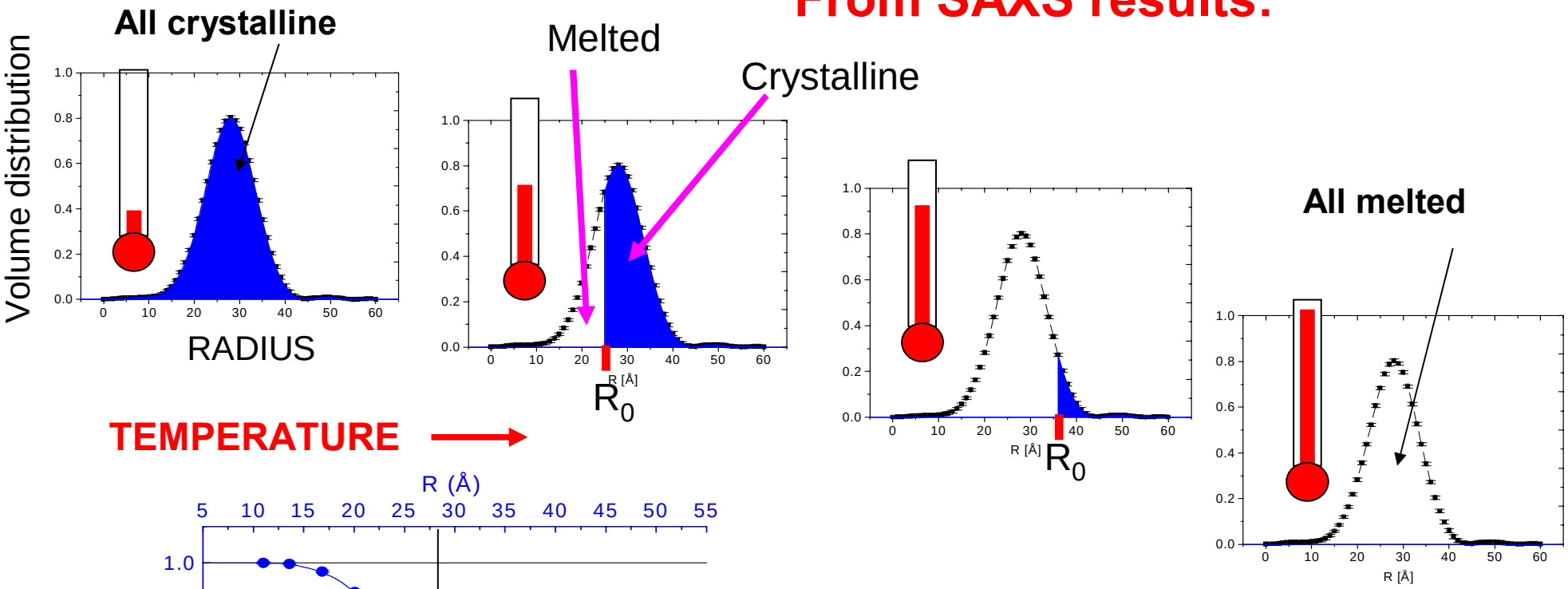

TEMPERATURE →

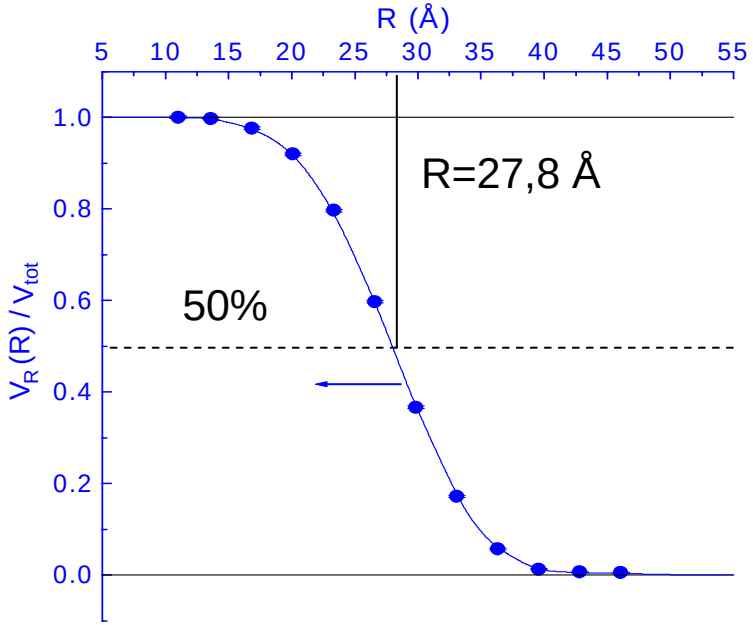

Volume fraction of the crystals with a radius > R

$$\frac{V_R(R_0)}{V_{tot}} = \frac{\int_{R_0}^{\infty} D_v(R') \cdot dR'}{\int_{0}^{\infty} D_v(R') \cdot dR'}$$

From WAXS results: Scattering intensity X Temperature

Scattering intensity produced by Bi nanocrystals

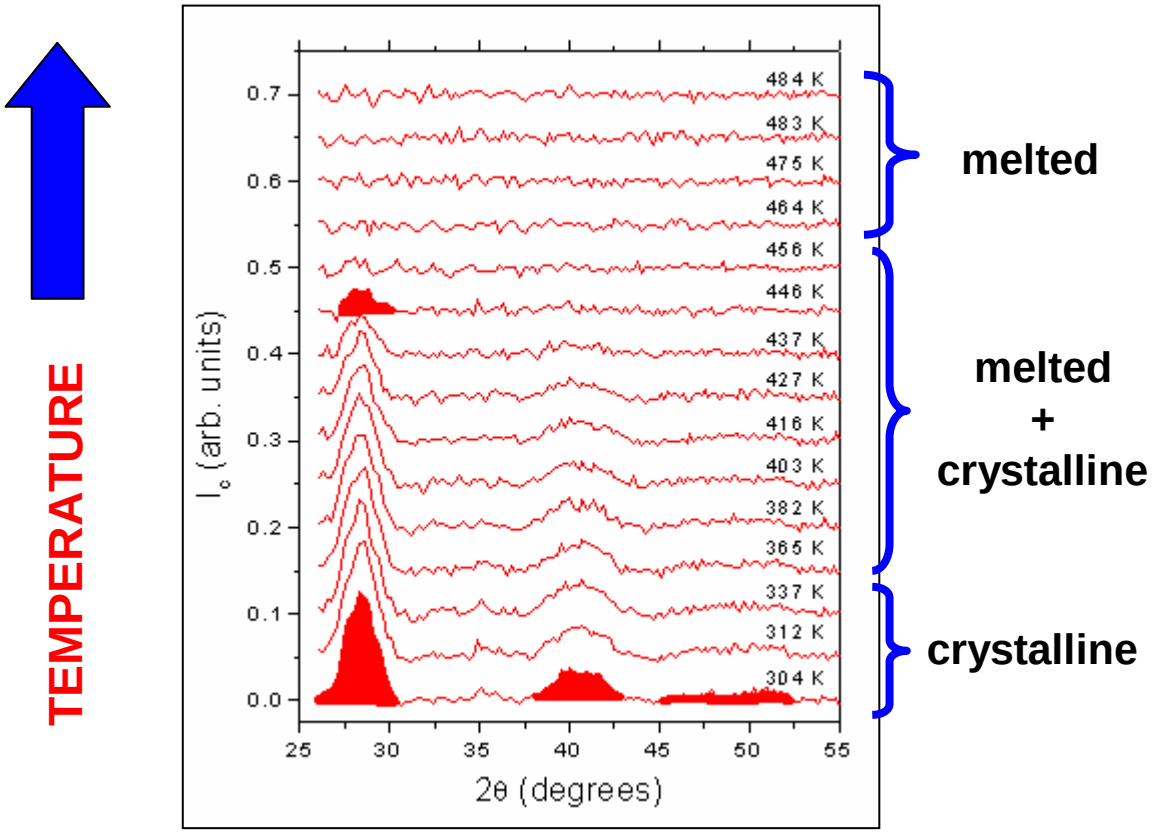

Fraction of Bi crystals

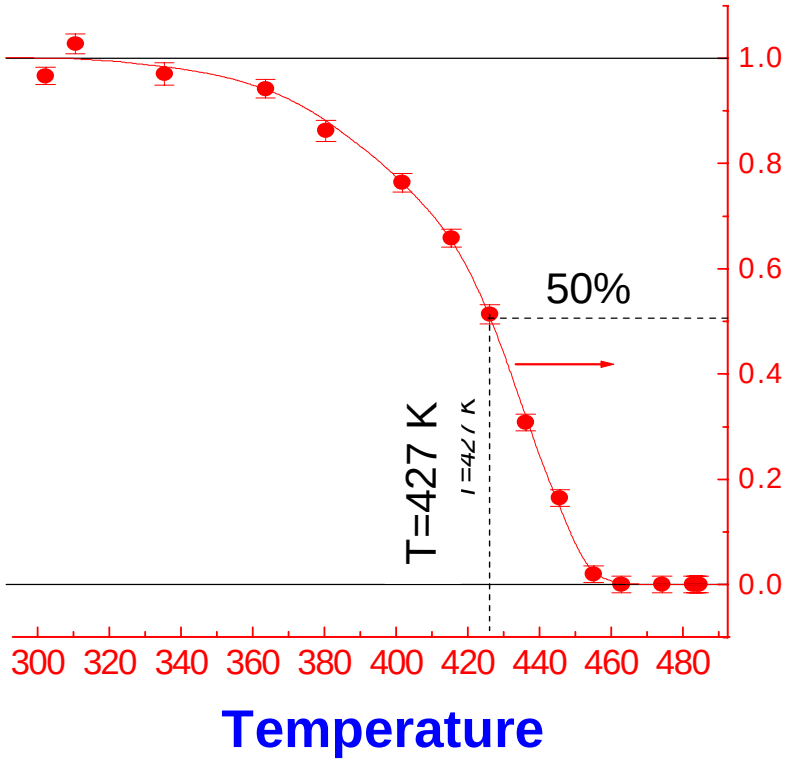

SAXS: Volume fraction with radius > R

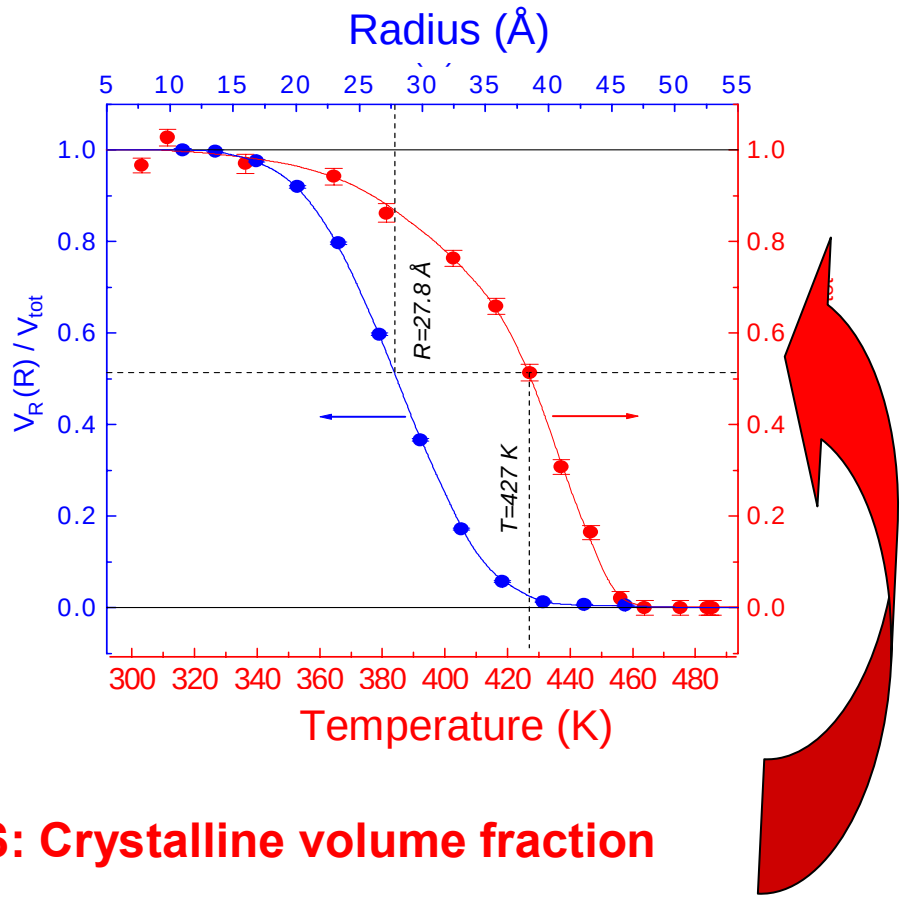

WAXS: Crystalline volume fraction

Melting temperature x Radius

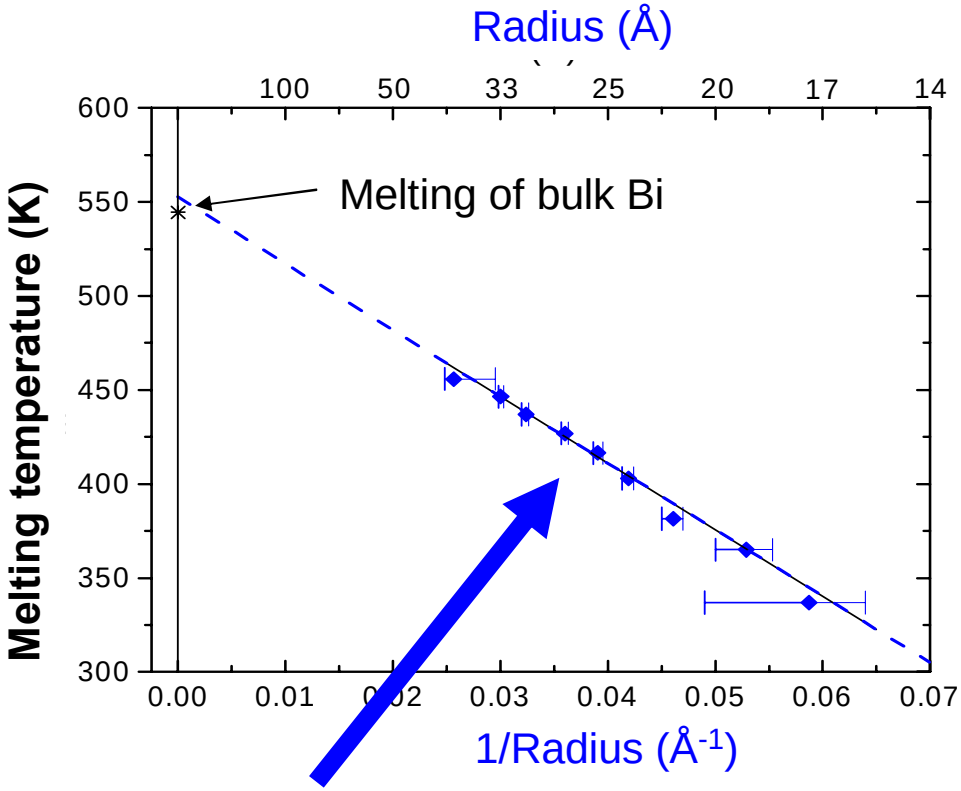

Linear dependence:

$$T_m - T_b \propto 1/R$$

Couchman - Jesser (1977) e Allen *et al.*, (1980)

Present and previous results

On substrate

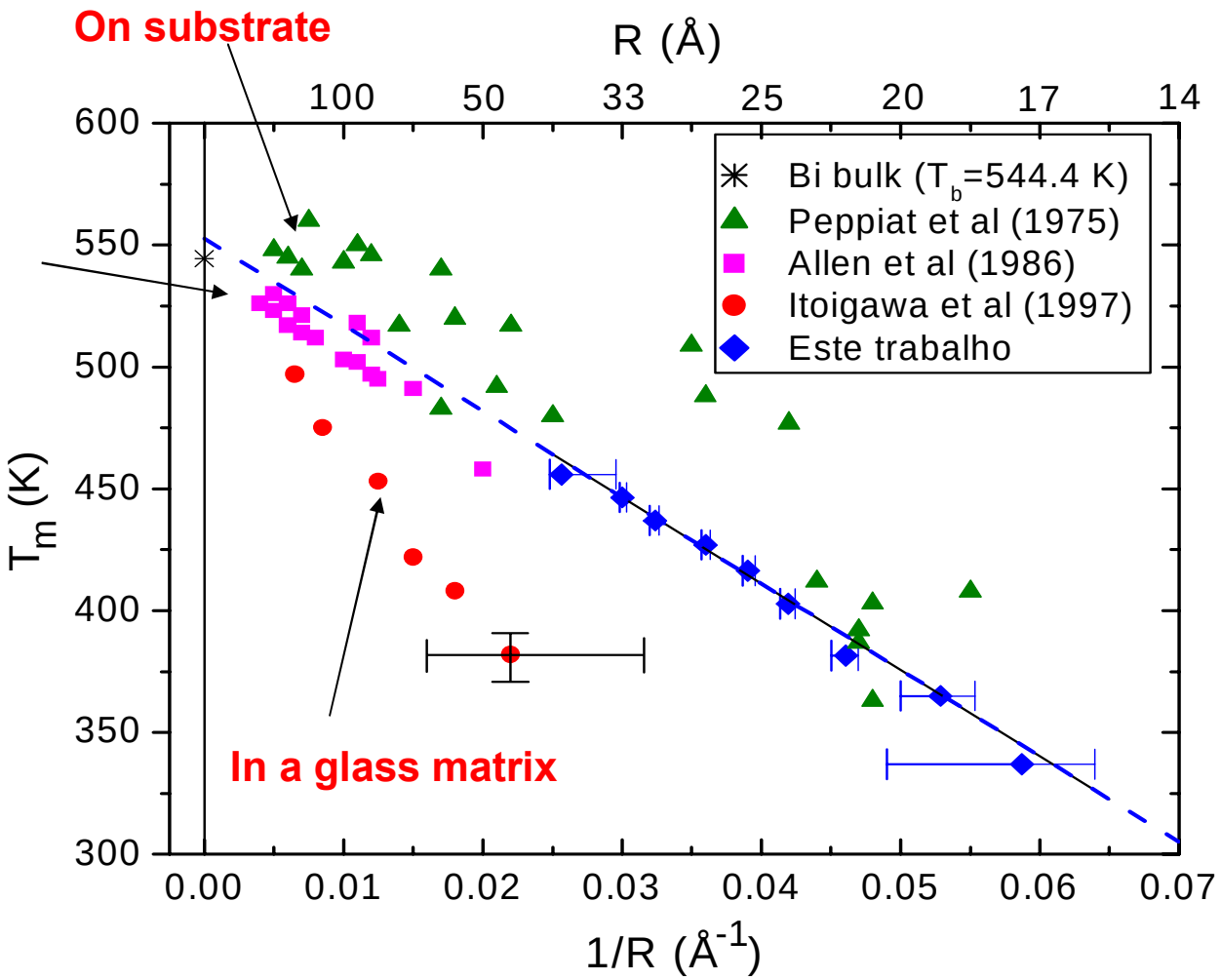

$\sigma_{gl} - \sigma_{gc} = 115 \times 10^{-3}$ J m^{-2}

Conclusion

- The combined use of WAXS and SAXS is useful in order to characterize the structure and determine the melting temperature of nanocrystals as a function of their radius. This procedure was demonstrated to be efficient even if the nanocrystals of different radii are all in the same sample.

- The melting temperature of spherical Bi nanocrystals embedded in a borate glass matrix is a linear function of 1/R
(in the range 17A<R<40A) in agreement with the prediction of Couchman and Jesser theory.

Isothermal aggregation of Ag atoms in sodium-borate glass

G. Kellermann and A. Craievich. Submitted, Physical Review B (2004)

Isothermal aggregation of Ag atoms in sodium-borate glass

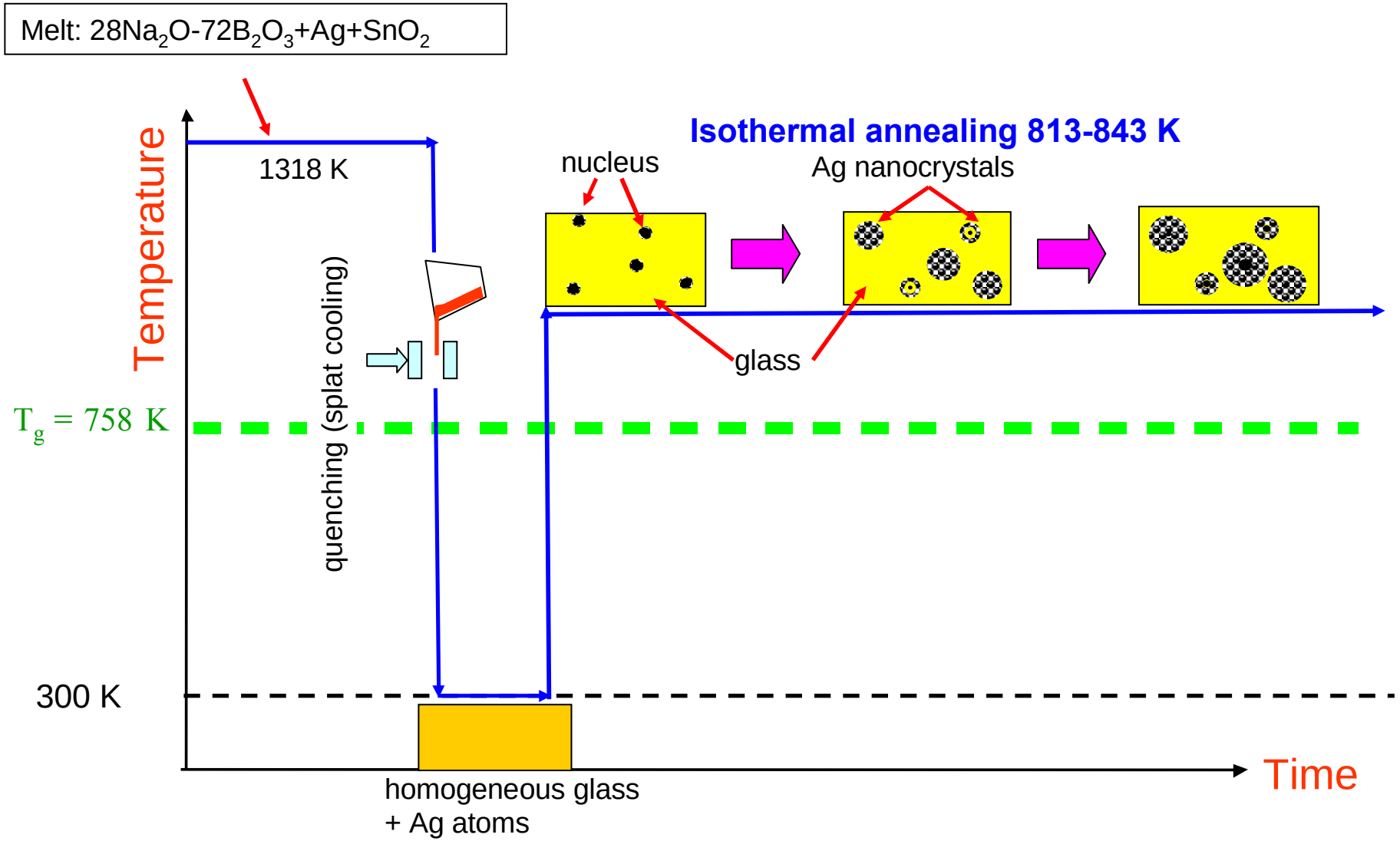

- **What are the mechanisms involved in the nanocrystals growth?**
- **How can them be determined?**

Small-angle x-ray scattering - SAXS

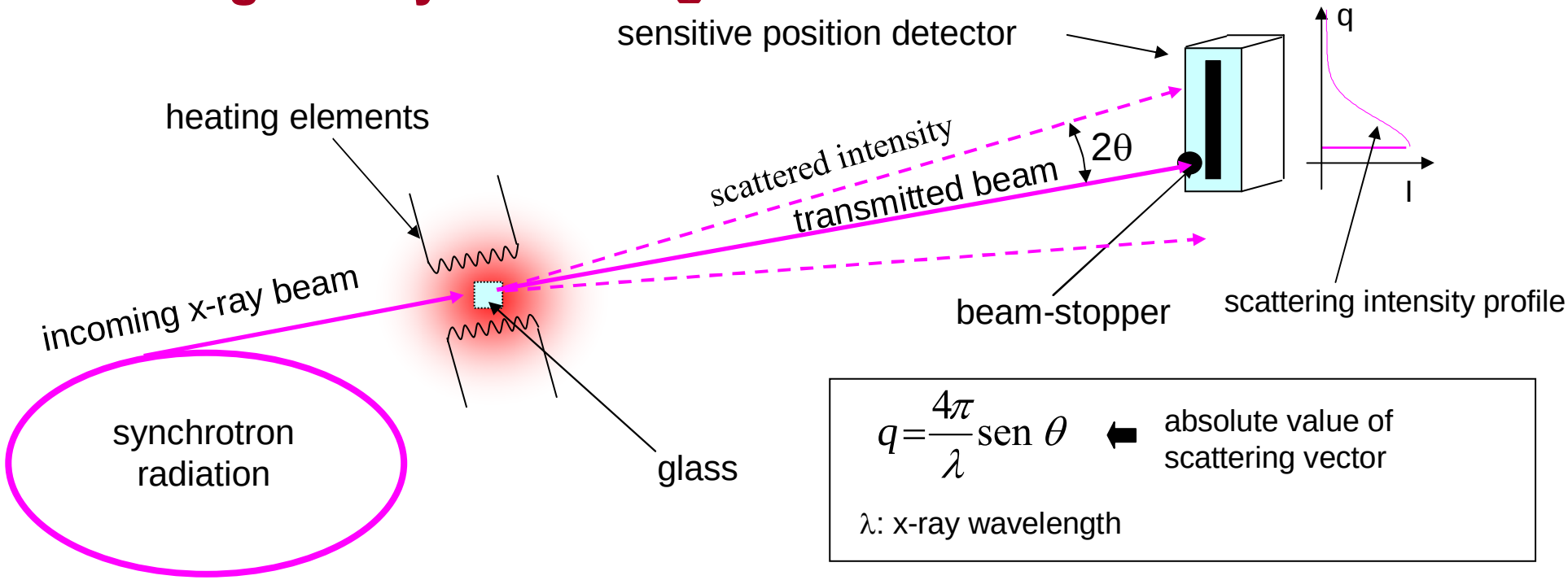

$$q = \frac{4\pi}{\lambda} \operatorname{sen} \theta$$ ⬅ absolute value of scattering vector

λ: x-ray wavelength

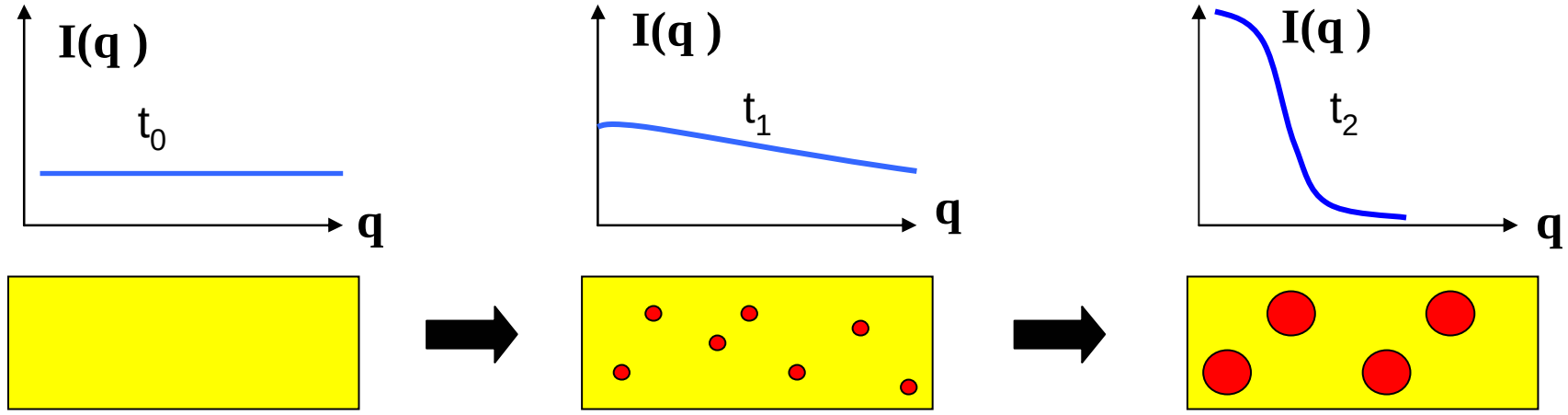

Isothermal transformation →

Isothermal annealing at 738 K (T_g = 758 K)

(Itoigawa et al., 1997)

Transmission electron Microscopy

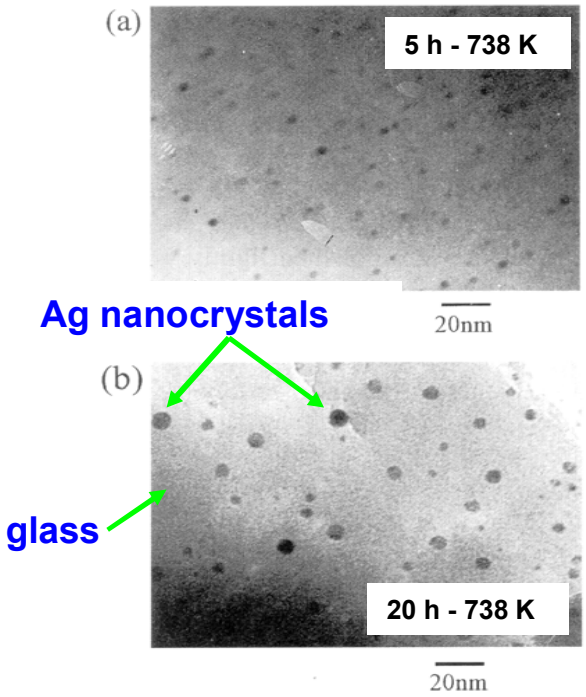

spherical shape

X-ray diffraction

glass + nanocrystals

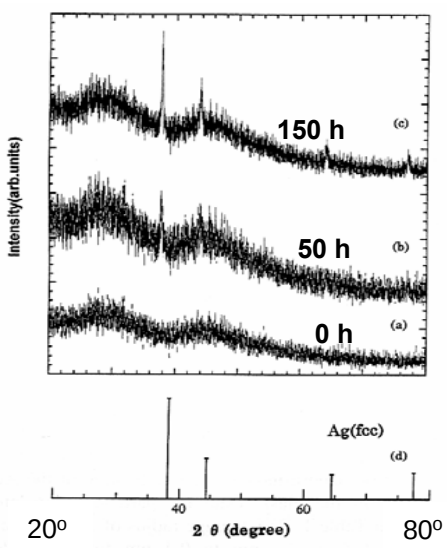

Selected area electron diffraction

single nanocrystal (R= 44 Å)

- **Structure: fcc, cubic closed-packed**

- shape
- electron density of nanocrystals

SAXS intensity

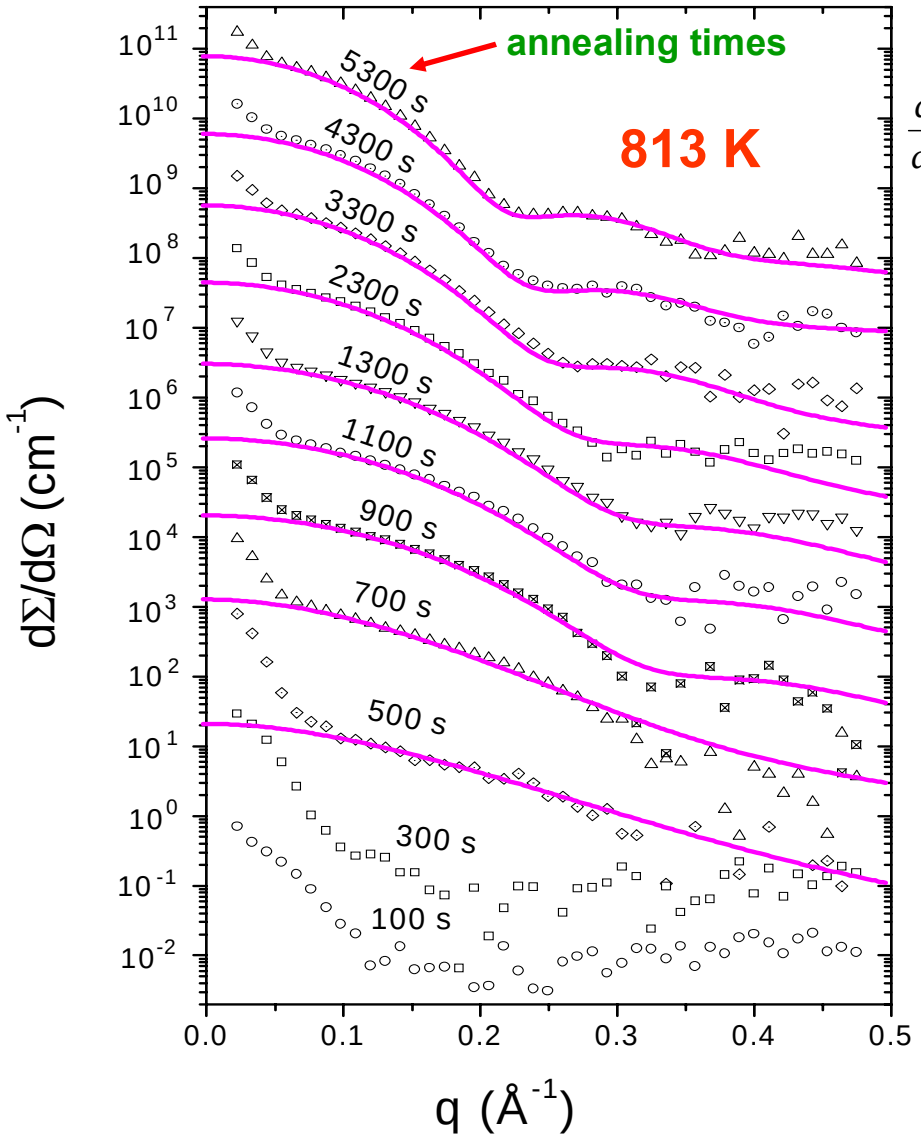

SAXS intensity for a diluted set of spherical particles is given by:

$$\frac{d\Sigma}{d\Omega}(q) = r_0^{\,2} \cdot \left(\rho_p - \langle\rho\rangle\right)^2 \left(\frac{4\pi}{3}\right)^2 \cdot \int_0^{\infty} N(R) \cdot \left[3\,\frac{\mathrm{sen}(qR) - qR\cdot\cos(qR)}{(qR)^3}\right]^2 \cdot R^6 \cdot dR$$

Log-normal function

$$N(R) = \frac{n}{\sqrt{2\pi\exp(w^2)}\cdot wr}\, e^{-(\ln(R/r)/w)^2/2}$$

Nanocrystals size distribution at different annealing times: N(R,t)

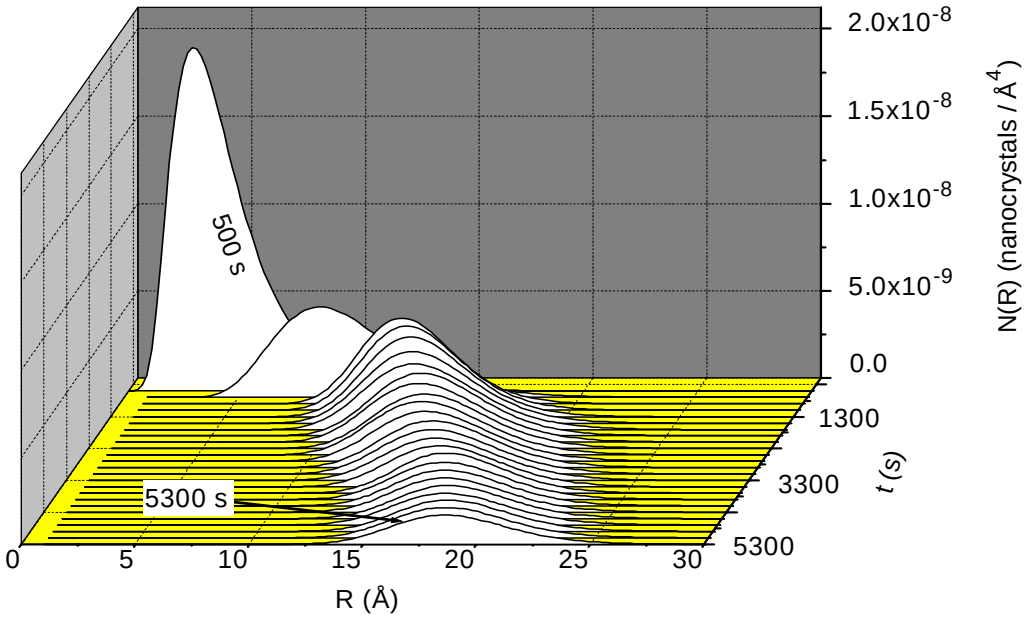

Isothermal aggregation of Ag atoms in sodium-borate glass

N(R,t)

Average radius

$$< R >= \frac{\int_{R_{min}}^{R_{max}} R \cdot N(R) \cdot dR}{n_{Total}}$$

Number density

$$n_{total} = \int_{R_{min}}^{R_{max}} N(R) dR$$

Volume fraction

$$\varphi(t) = \frac{4\pi}{3} \int_{R_{min}}^{R_{max}} N(R) \cdot R^3 dR$$

Relative size dispersion

$$\sigma / < R >= \frac{\sqrt{\int_{R_{min}}^{R_{max}} (R - < R >)^2 \cdot N(R) \cdot dR}}{< R >}$$

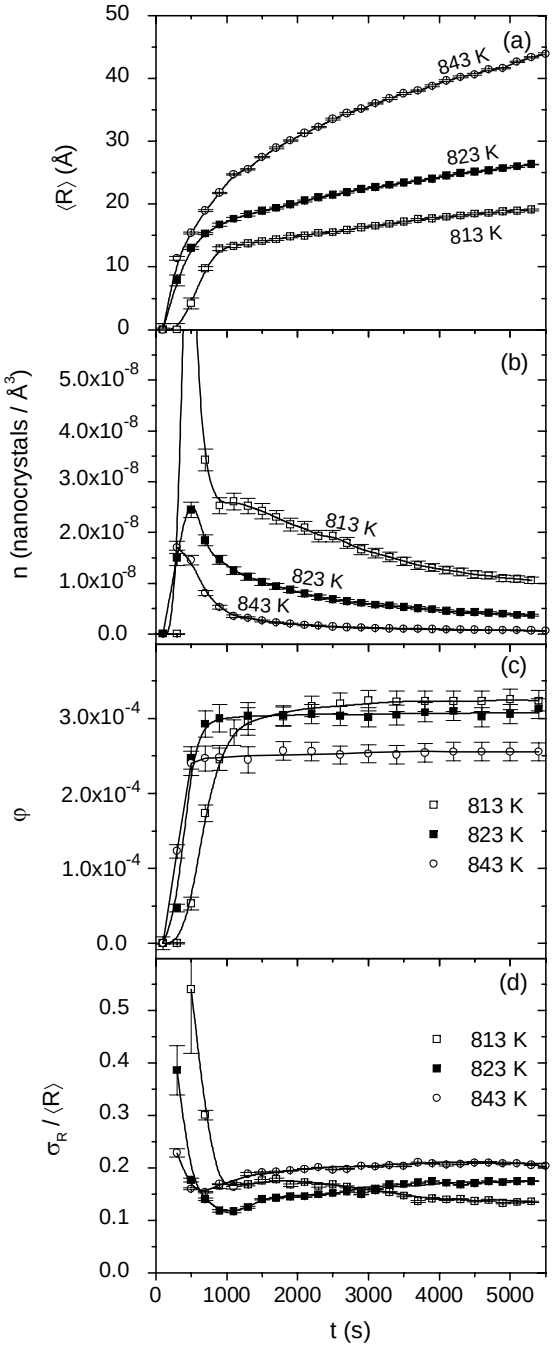

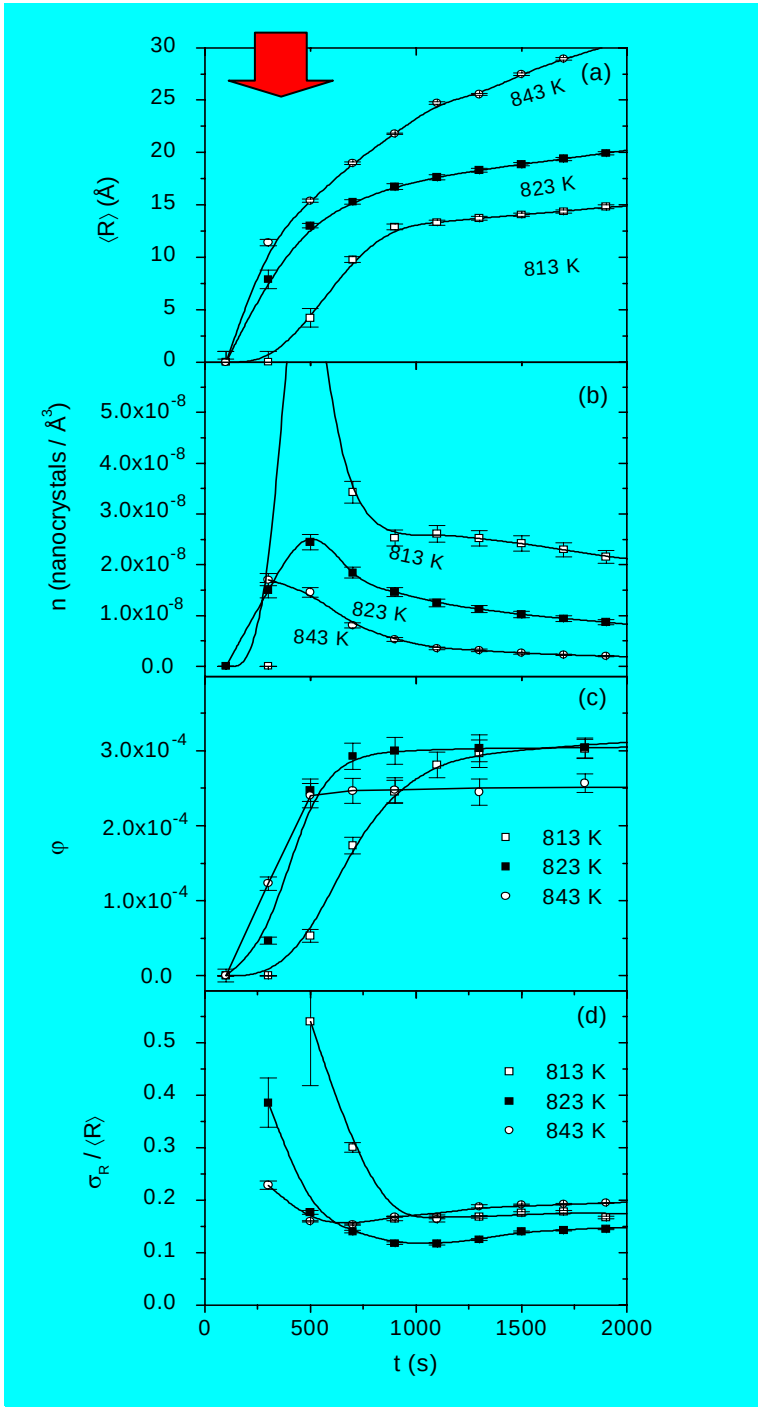

Nucleation and growth

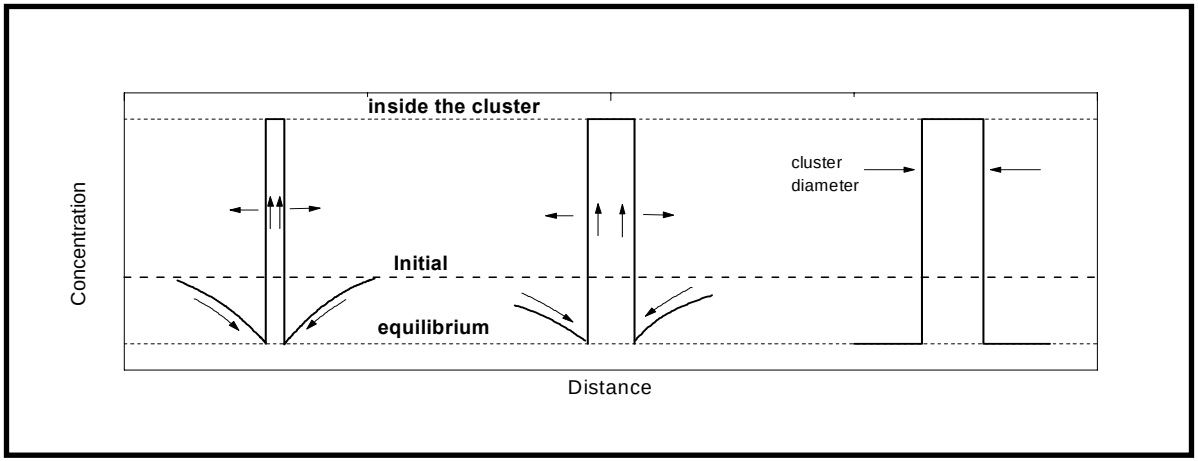

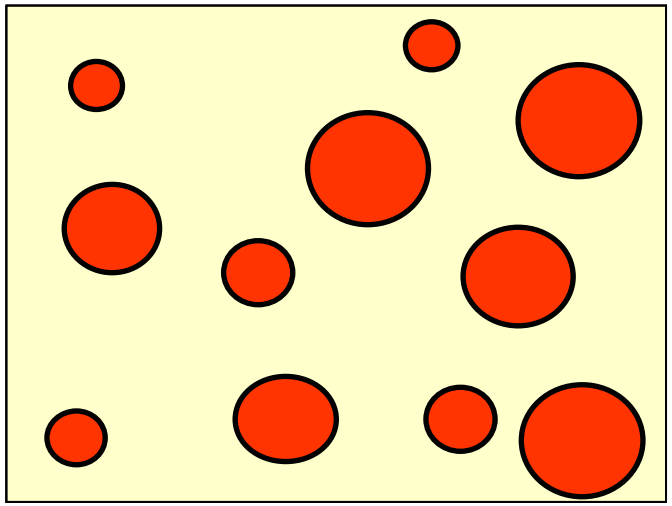

Coarsening

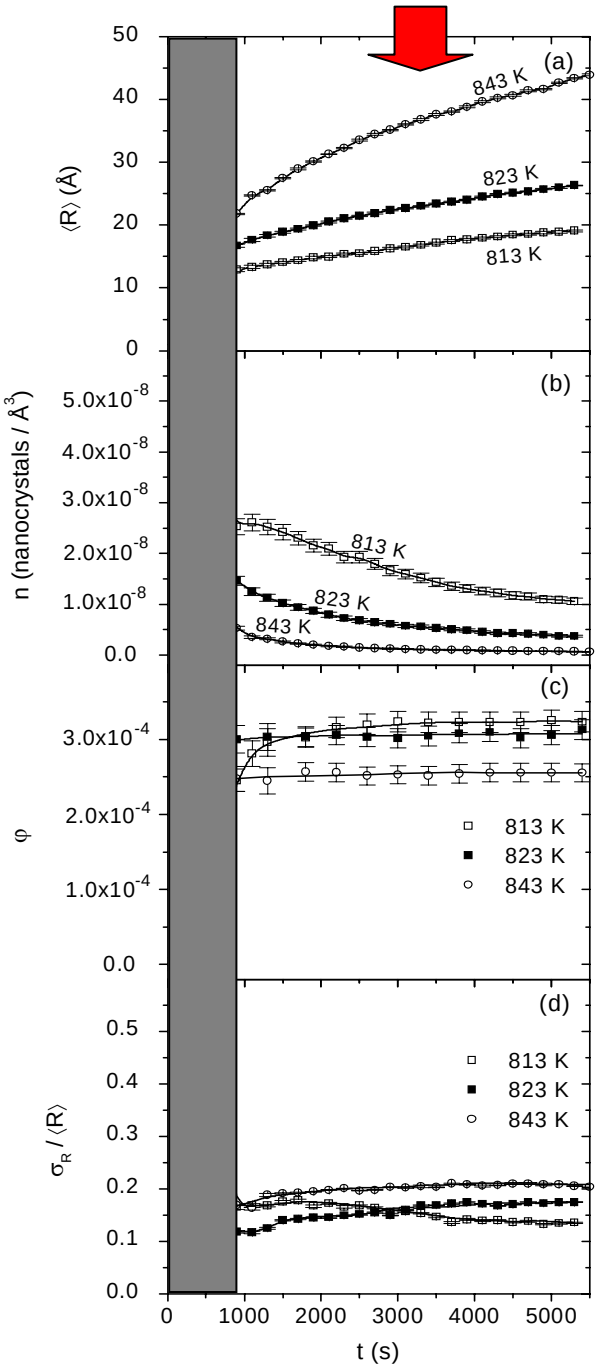
(a)
843 K
823 K
813 K
⟨R⟩ (Å)
(b)
813 K
823 K
843 K
n (nanocrystals / Å^3)
(c)
813 K
823 K
843 K
φ
(d)
813 K
823 K
843 K
σ_R / ⟨R⟩
t (s)

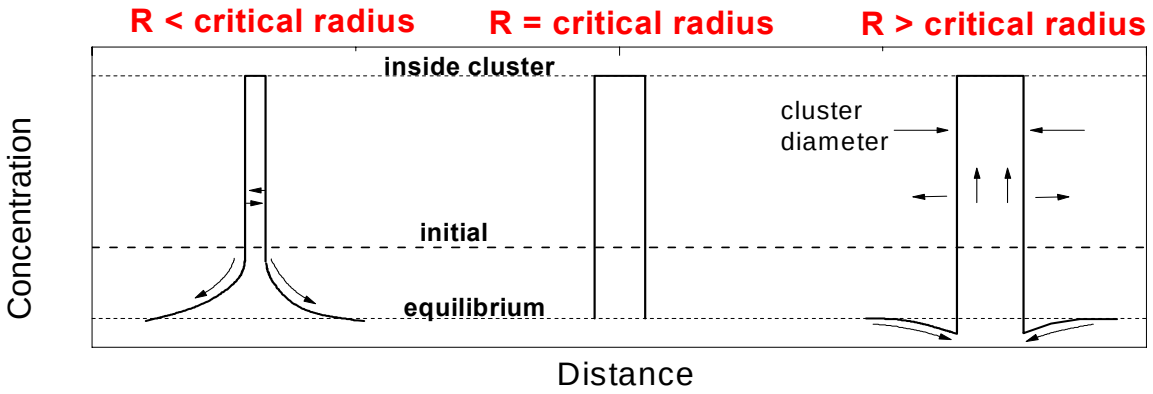
R < critical radius
R = critical radius
R > critical radius
inside cluster
cluster
diameter
initial
equilibrium
Concentration
Distance

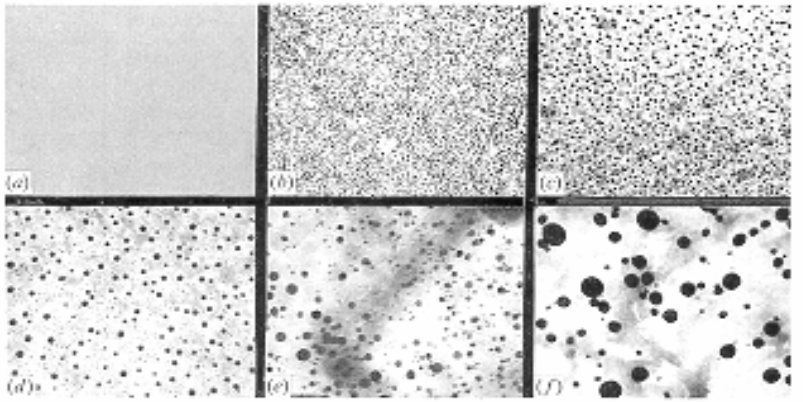

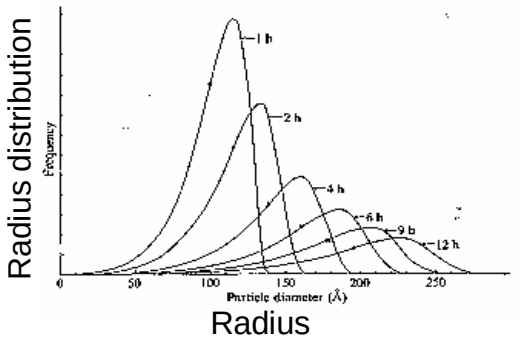
Radius distribution
Frequency
1 h
2 h
4 h
6 h
9 h
12 h
Particle diameter (Å)
Radius

Lifshitz-Slyosov (1961) and Wagner (1961) model for coarsening (LSW)

<R>: average radius

$$\left[\langle R\rangle(t)\right]^3 = \left[\langle R\rangle_0\right]^3 + \alpha(t - t_0),$$

$$\alpha = \frac{8\gamma v^2 c_e D}{9kT}$$

n: number density

$$\frac{1}{n(t)} = \frac{1}{n_0} + \beta(t - t_0)$$

$$\beta = \frac{4\gamma c_e v D}{(c_i - c_e)kT}$$

t_0: starting time for coarsening
$\langle R_0\rangle$: average radius at $t = t_0$
n_0: cluster number density at $t = t_0$
γ: free energy per unity area of the interface between clusters and matrix
ν: atomic volume of solute
c_e: concentration of solute in the matrix at equilibrium
c_e: initial concentration of solute
D: diffusion coefficient of solute
k: Boltzmann constant
T: absolute temperature (Kelvin)

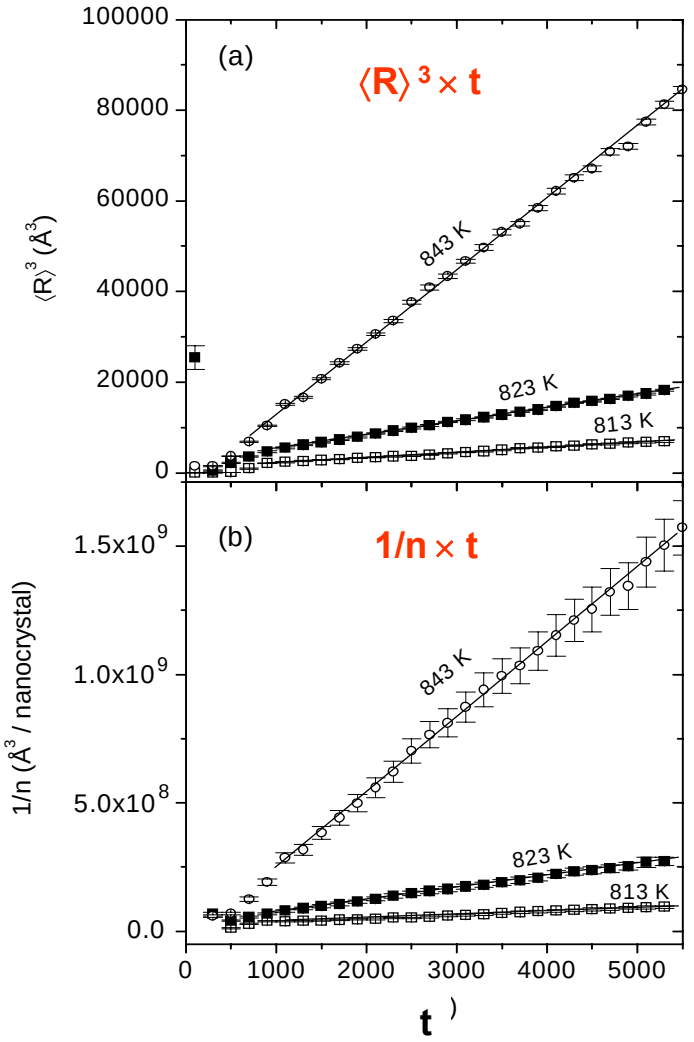

Relative size dispersion

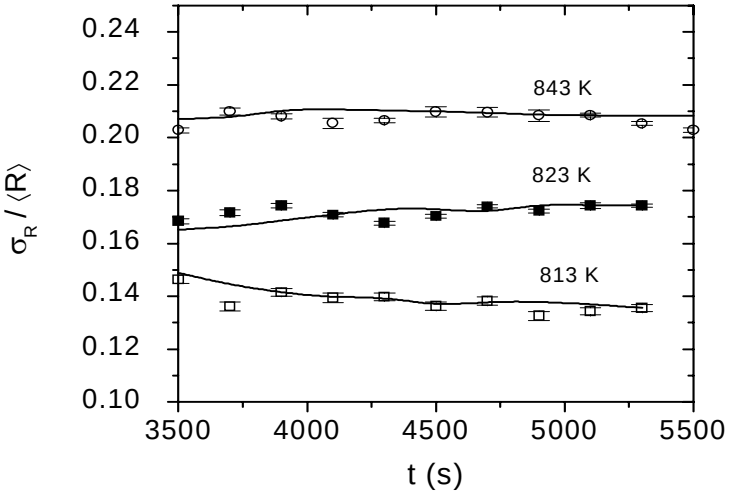

Bi

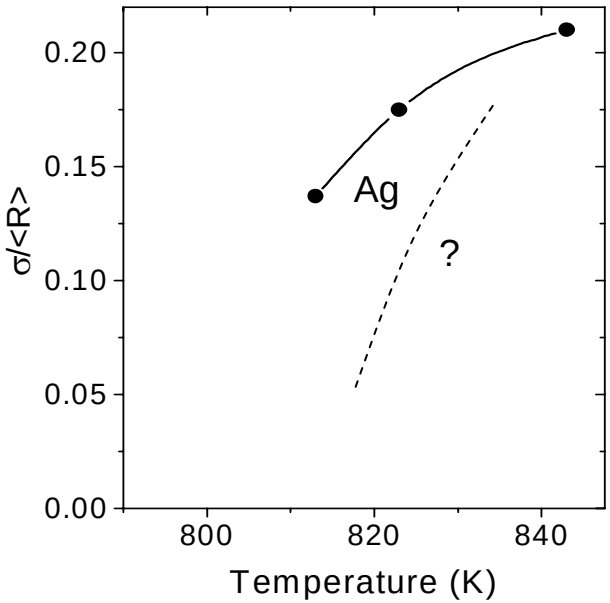

Absence of elastic strain
(T>> T_g temperature)

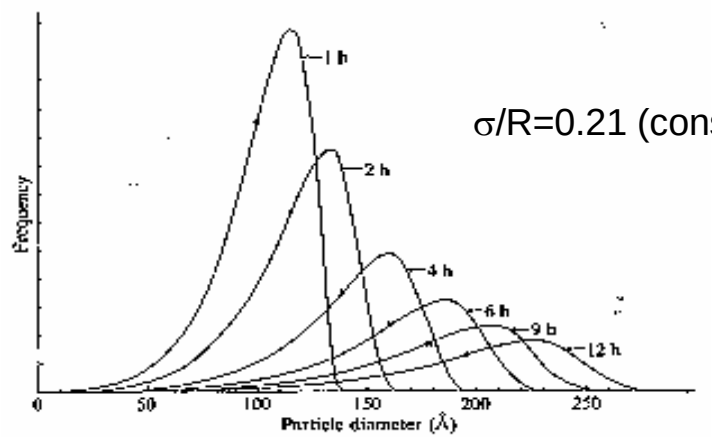

σ/R=0.21 (constant)

Lifshitz-Slyosov (1961) and Wagner (1961)

Presence of elastic strain
(close to T_g temperature)

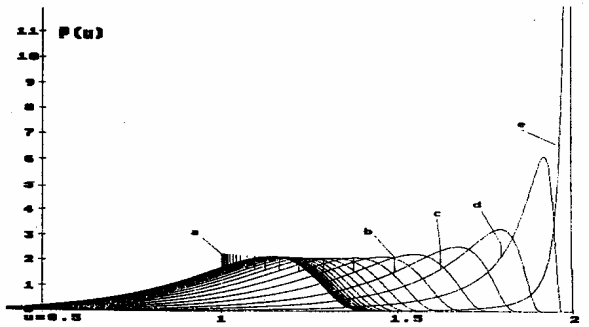

J. Schmelzer and J. Moller, (1992)

CONCLUSIONS

•The formation and growth of Ag nanocrystals occurs from the very beginning of the thermal annealing.

•An initial incubation stage is followed by (i) a stage during which nanocrystals grows by atomic diffusion and aggregation of individual Ag atoms, and (ii) a final stage during which nanocrystals grows by coarsening.

Coarsening process:

• The time dependences of the average radius, inverse of number density and the fraction of total volume occupied by Ag nanocrystals are well described by the equations predicted by the LSW model for coarsening.

•The radius distribution of nanocrystals is better described by a log-normal function than by the function predicted by LSW model.

•The ratio between the nanodroplets radius dispersion and their radius is nearly time constant during the whole coarsening process as predicted by the LWS theory, $(\sigma/\langle R\rangle \neq f(t)=0.21)$, so indicating a dynamical scaling property or dynamical self-similarity of the structure.

•The ratio between size dispersion and the average radius decrease for decreasing annealing temperatures, from $(\sigma/\langle R\rangle) = 0.21$ down to $(\sigma/\langle R\rangle) = 0.14)$. This effect was attributed to strains induced by differences between the diffusion coefficient of Ag atoms and those of the components elements of the glass matrix. This effect of strains is actually expected to be progressively more important for decreasing annealing temperatures.

Structure and melting of Bi nanocrystals embedded in a B_2O_3-Na_2O glass

G. Kellermann
Laboratório Nacional de Luz Síncrotron and Instituto de Física Gleb Wataghin, Universidade Estadual de Campinas, Campinas SP, Brazil

A. F. Craievich
Instituto de Física, Universidade de São Paulo, São Paulo SP, Brazil

(Received 6 August 2001; revised manuscript received 20 November 2001; published 19 March 2002)

A composite material consisting of spherical Bi nanoclusters (nanocrystals and/or liquid nanodroplets) embedded in a $28Na_2O$-$72B_2O_3$ glass was studied by the wide-angle x-ray scattering (WAXS) and small-angle x-ray scattering (SAXS) techniques over the temperature range in which the Bi crystal-liquid transition occurs. Because of the wide radius distribution of Bi clusters and due to the dependence of the melting temperature on crystal radius, the overall transition occurs over a wide range, from 365 up to 464 K. In this transition range, large Bi nanocrystals coexist with small liquid droplets. A weak contraction in **a** and **c** lattice parameters of rhombohedral Bi nanocrystals with respect to the bulk crystal was detected. As expected, the average radius of crystalline Bi clusters, deduced from WAXS data, increases for increasing temperatures over the whole solid-to-liquid transition range. The SAXS spectrum recorded at different temperatures within the transition range is essentially invariant, indicating that the radius distribution of Bi nanoclusters (nanocrystals and nanodroplets) is temperature independent. The volume distribution of Bi nanoclusters is a single-mode function with the radius ranging from about 15 up to 41 Å with a maximum at 28 Å. The integral of Bragg peaks of Bi nanocrystals decreases for increasing temperatures as a consequence of the progressive melting of nanocrystals of increasing size. By combining the results of WAXS and SAXS experiments, we determined the melting temperature of the nanocrystals as a function their radius suppressing unwanted size dispersion effects. Our results clearly indicate a linear dependence of the melting temperature on nanocrystal reciprocal radius, thus confirming previous theoretical predictions.

DOI: 10.1103/PhysRevB.65.134204 PACS number(s): 65.80.+n, 61.46.+w, 61.10.−i

I. INTRODUCTION

The structure and properties of nanostructured materials may strongly differ from those of common, coarse-grained, solids. The existence of noncrystallographic structures and lattice contraction effects was already reported for a number of nanocrystals.[1–4] Another well-known effect is the strong decrease in the melting temperature for decreasing nanocrystal size. This effect was first reported by Takagi.[5]

A number of experimental techniques have been used up to now to study the size dependence of the melting temperature of nanocrystals. In most of the published articles, results obtained by transmission electron microscopy (TEM) were reported. In TEM experiments changes in nanocrystal shape, from polyhedral to spheroidal, were observed. On the other hand, differences in the structure of nanocrystals of varying size were detected by electron diffraction and dark-field electron microscopy. Optical techniques, differential scanning calorimetry and x-ray diffraction were also used to investigate these materials. A detailed description of the solid-liquid phase transition in nanostructured materials was reported by Kofman *et al.*[6]

We here present an experimental study of the structure and melting behavior of Bi nanocrystals embedded in a $28Na_2O$-$72B_2O_3$-glass matrix. The glass-Bi nanocrystal composite was studied by simultaneous small-angle x-ray scattering (SAXS) and wide-angle x-ray scattering (WAXS) at varying temperatures. Combined use of SAXS and WAXS techniques allowed us to determine the melting temperature of Bi nanocrystals as a function of their radius using a single sample.

The dependence of the melting temperature on the radius of Bi nanocrystals determined in the present work was compared to those obtained by previous authors[7–9] and with the prediction of a simple theoretical model.[10]

II. NANOCRYSTAL-TO-LIQUID TRANSITION

A theoretical thermodynamic approach developed by Couchman and Jesser[10] connects the melting temperature T_m of free small spherical crystals with their radius R. The $T_m(R)$ function is given by[10]

$$T_m = T_b\left[1 - \frac{3(\sigma_c/\rho_c - \sigma_l/\rho_l)}{RL_m}\right], \tag{1}$$

where T_b is the melting temperature corresponding to macroscopic crystals, L_m is the latent heath of fusion per unit mass, σ_c and σ_l are the surface energies of crystalline and liquid clusters, respectively, and ρ_c and ρ_l are the densities of the crystalline and liquid phases, respectively.

Equation (1) implies that T_m is a linear and decreasing function of $1/R$. The limit value of T_m for $(1/R)$ approaching zero is equal to T_b. For very large values of $1/R$, with R approaching atomic dimensions, the crystalline and liquid phases are not well defined and so Eq. (1) no longer applies.

For particles embedded in a glass matrix Eq. (1) still holds if σ_c and σ_l are substituted by the interfacial energy between the glass and crystals, σ_{gc}, and between the glass and liquid droplets, σ_{gl}, respectively. An additional term K_E

takes into account the difference in density of the strain energy due to volume changes during the melting.[11] Consequently, for nanocrystals embedded in a homogenous glass matrix, Eq. (1) becomes

$$T_m = T_b\left[1 - \frac{3(\sigma_{gc}/\rho_c - \sigma_{gl}/\rho_l)}{RL_m} - K_E\right]. \quad (2)$$

III. EXPERIMENT

The starting raw materials were Na_2CO_3, B_2O_3, Bi_2O_3, and SnO. SnO was added as a reducing agent for Bi_2O_3. This mixture was melted in an electrical furnace under vacuum (10^{-1} mbar) at 1313 K. A $28Na_2O$-$72B_2O_3$ glass containing dispersed Bi nanocrystals was obtained by an initial quenching using the splat-cooling technique, an isothermal annealing of 45 min at 853 K, and a slow final cooling down to room temperature.[9] The isothermal annealing at 853 K promotes the nucleation and growth of *liquid* Bi droplets. (The melting temperature of bulk Bi is 544.4 K.) After annealing, the glass sample was cooled down to room temperature at which all liquid droplets have crystallized. The resulting glass-nanocrystal composite was then studied at different temperatures, from 304 to 503 K, using combined WAXS and SAXS techniques.

The SAXS and WAXS experiments were performed at the SAS beamline of the National Synchrotron Light Laboratory (LNLS), Campinas, Brazil.[12] The two types of spectrum were recorded using one-dimension gas x-ray position-sensitive detectors. X-ray monitors placed before and after the sample measured the intensity of the incoming and transmitted x-ray beam intensity in order to determine the sample attenuation. SAXS spectra were normalized to equivalent intensity of the direct beam in order to compensate for the continuous decrease in the emission of the synchrotron source. The SAXS intensity was determined as a function of the modulus of the scattering vector $q = 4\pi \sin\theta/\lambda$, λ being the wavelength of the x-ray beam ($\lambda = 1.61$ Å) and θ half the scattering angle. An alumina standard sample was used for the precise measurement of the scattering angle and for the determination of the instrumental effects on the broadening of WAXS peaks. WAXS and SAXS experiments were simultaneously performed so that both techniques probed the same sample volume.

IV. RESULTS AND DISCUSSION

A. Small-angle x-ray scattering measurements

The overall, low-resolution, structure of the studied glass-metallic Bi nanocomposite was characterized by SAXS. Previous observations by TEM (Ref. 9) indicated that the studied material is composed of a homogeneous glass matrix in which spherical or nearly spherical Bi clusters of different sizes are embedded. The SAXS technique was employed in order to determine the volume distribution of Bi clusters as a function of their radius, the average radius and the total volume occupied by them.

WAXS results indicated that spherical Bi nanocrystals and Bi liquid droplets coexist within a wide temperature range. The SAXS technique probes all Bi nanoclusters regardless of the (crystalline or liquid) physical state.

The SAXS intensity produced by a two-electron density system composed of a dilute set of spherical and homogeneous nanoclusters embedded in an also homogeneous matrix is given by[13]

$$I_{\mathrm{SAXS}}(q) = (\rho_p - \rho_m)^2\left(\frac{4\pi}{3}\right)^2 \int_0^\infty D_n(R)R^6[F(qR)]^2 dR, \quad (3)$$

where $D_n(R)$ is the cluster number distribution function, ρ_p and ρ_m are the electron densities of the particles (nanoclusters) and matrix, respectively, and $F(qR)$ is defined by[13]

$$F(qR) = 3\,\frac{\sin(qR) - qR\cos(qR)}{(qR)^3}. \quad (4)$$

The cluster volume distribution function $D_v(R) = 4\pi R^3 D_n(R)/3$ was determined from the SAXS intensity profiles plotted in Fig. 1(a) using the GNOM package.[14] The best fit to experimental SAXS data is also shown in Fig. 1(a), and the corresponding $D_v(R)$ function is plotted in Fig. 1(b). The good agreement between the experimental and calculated spectra confirms the validity of the proposed model for the studied material.

The experimental results demonstrated that, under the above-mentioned annealing condition, $D_v(R)$ is a single-mode function of nanocrystal radius. The nanocluster radii range from about 15 up to 40 Å and the maximum of $D_v(R)$ is at $R = 28$ Å. The average radius $\langle R\rangle$ and the relative radius dispersion σ_R are $\langle R\rangle = 24.1 \pm 0.2$ Å and $\sigma_R = 0.236 \pm 0.004$, respectively.

As we will see in the next section, WAXS results demonstrated that below 365 K all Bi clusters are crystalline, above 464 K all are in liquid state, and within the 365–464 K range nanocrystals and liquid droplets coexist. Since all SAXS intensity spectra recorded at different temperatures, from 304 up to 503 K, are essentially equivalent, we concluded that the radius distribution of the clusters (crystals and liquid droplets) is essentially independent of the temperature and physical state.

B. Wide-angle x-ray scattering measurements

In order to study the structure of Bi nanoclusters at different temperatures, WAXS measurements were performed during the heating of the glass-metallic Bi composite from room temperature up to 503 K. Figure 2(a) shows the WAXS spectra, corresponding to the sample held at 304 and 503 K. The spectra corresponding to temperatures above 304 K exhibit weak and wide Bragg peaks corresponding to Bi nanocrystals superposed onto the scattering halo produced by the glass matrix.

The analysis of the diffraction patterns indicates that Bi nanocrystals are rhombohedral as in bulk state. These peaks continuously decrease in intensity for increasing temperatures.

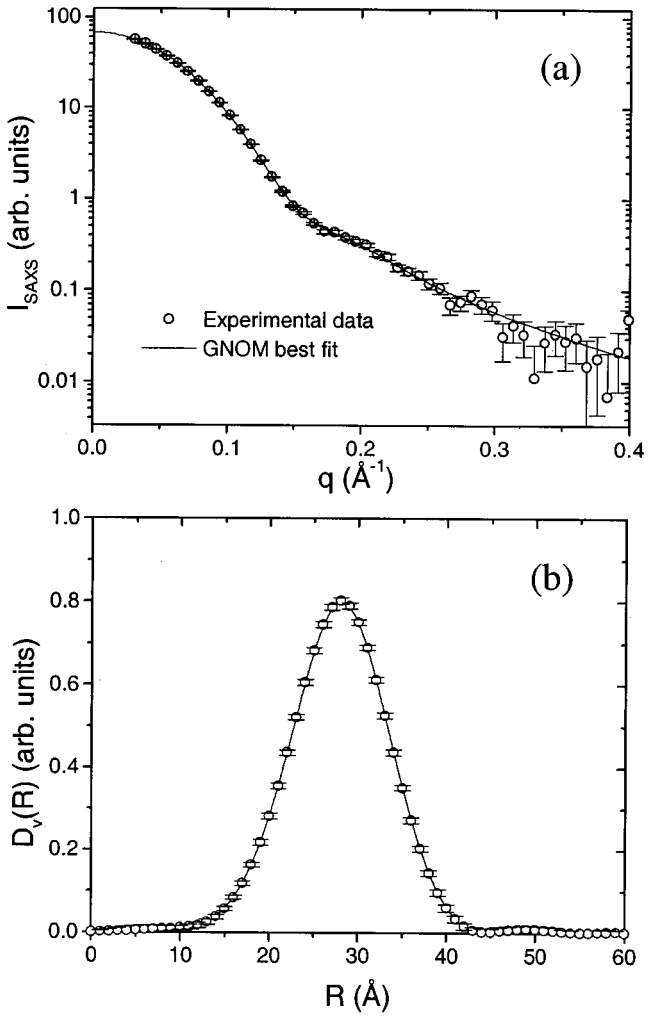

FIG. 1. (a) SAXS intensity produced by Bi nanocrystals embedded in a borate glass at room temperature. The open circles are the experimental data and the solid line is the best fit using GNOM program. (b) Nanocrystal volume distribution function. SAXS intensity spectra determined at different temperatures from 304 up to 503 K are essentially equivalent.

The progressive melting of Bi nanocrystals for increasing temperatures provides an additional contribution to the wide halo associated with the noncrystalline part of the material (liquid Bi and sodium-borate glass). So the total WAXS intensity can be written as

$$I_{\mathrm{WAXS}}(T,\theta)=I_c(T,\theta)+I_g(\theta)+I_l(T,\theta), \tag{5}$$

where $I_c(\theta,T)$ is the WAXS intensity produced by Bi nanocrystals, $I_g(\theta)$ the intensity coming from the glass matrix, and $I_l(\theta,T)$ the intensity contribution from the melted Bi droplets. The intensity $I_g(\theta)$ is assumed to be independent of the temperature T over the range $304\ \mathrm{K}<T<503\ \mathrm{K}$.

The contribution from the glass matrix was removed by subtracting the WAXS intensity $[I_g(\theta)+I_l(T_F,\theta)]$ measured at high temperature ($T_F=503$ K), at which all Bi nanoclusters are melted and so no Bragg peaks from the crystalline structure are present. The resulting intensity $J(T,\theta)$ is given by

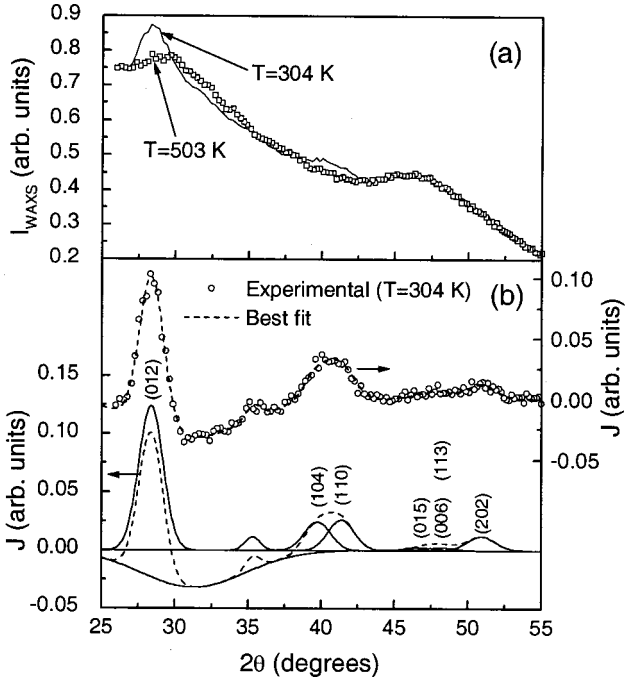

FIG. 2. (a) WAXS spectra at 304 and 503 K corresponding to Bi crystalline nanoclusters and liquid nanoclusters, respectively. In the spectrum corresponding to $T=503$ K, the additional contribution from melted Bi clusters is clearly apparent. (b) Difference between the WAXS intensities measured at 304 and 503 K: $[I_{\mathrm{WAXS}}(T=304\ \mathrm{K},\theta)-I_{\mathrm{WAXS}}(T=503\ \mathrm{K},\theta)]$. The solid lines correspond to the Gaussian functions determined from the best fit. Only one weak peak at $2\theta\approx35°$ was not identified.

$$J(T,\theta)=I_c(T,\theta)+I_l(T,\theta)-I_l(T_F,\theta). \tag{6}$$

In order to determine the average radius and lattice parameters of Bi nanocrystals, the diffraction peaks of the $J(T,\theta)$ functions were fitted by Gaussian functions. The fitting parameters of the modeled Gaussian functions were the **a** and **c** lattice parameters of the hexagonal unit cell, the integrated area of the diffraction peaks, and integral width of the (012) Bragg profile. The integral width $\Delta(2\theta)_{012}$ could be precisely determined because the (012) peak is relatively strong and does not overlap with other peaks (Fig. 2). For the fittings of the theoretical profile to the (104), (110), and (202) experimental peaks, it was assumed that all nanocrystals are spherical. Under this assumption, the integral widths $\Delta(2\theta)$ of these weak peaks are not independent parameters and are related to $\Delta(2\theta)_{012}$, as will be described later, by the Scherrer equation. The acceptable quality of the fitting of the theoretical curves to the experimental ones (Fig. 2) *a posteriori* justifies the mentioned assumption.

Since for $T<T_F$ we have $I_l(T,\theta)<I_l(T_F,\theta)$, a negative contribution due to the increase in scattering intensity introduced by the melted Bi particles is expected. A Gaussian function for this difference was also assumed in the fitting procedure.

Taking into account the small volume fraction occupied by the nanocrystals and the consequent weak Bragg peaks and high relative statistical errors in the scattering intensity,

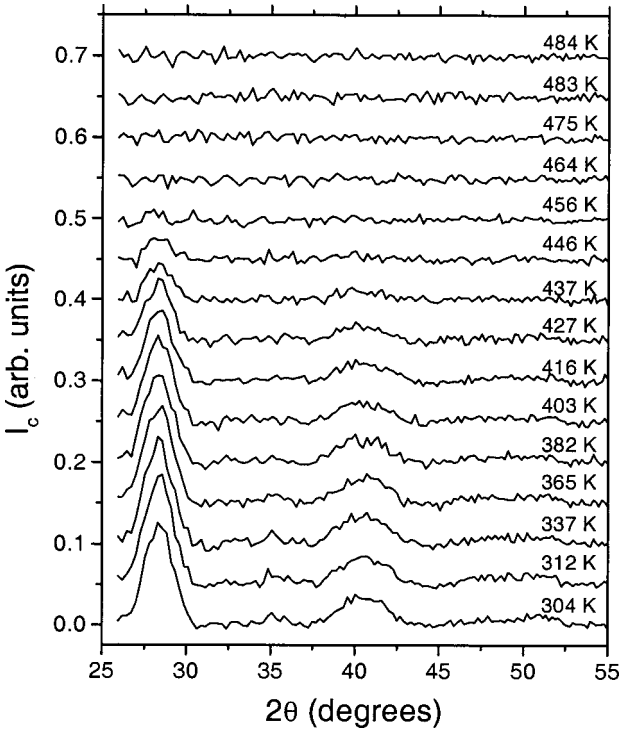

FIG. 3. WAXS pattern corresponding to the Bi nanocrystals after subtraction of the contributions of the glass matrix and of the melted Bi clusters. The curves are vertically displaced for clarity.

the Gaussian function was demonstrated to be an acceptable approximation for the peak profile in the fitting procedure.

The $J(T,\theta)$ function at $T=304$ K and the modeled function that best fit to it are shown in Fig. 2(b). Both curves are in good agreement. The same procedure was applied to all WAXS spectra. From the values of the adjusted coefficients of the modeled curves, the temperature dependence of the volume fraction of crystalline phase and the average radius and lattice parameters of Bi nanocrystals were determined.

By subtracting the contribution from the glass matrix and from melted Bi particles, the WAXS peak profiles of Bi nanocrystals $I_c(T,\theta)$ were obtained. The results are plotted in Fig. 3. The area of the Bragg peaks exhibits a monotonous and continuous decrease between 365 and 464 K. Above 464 K the Bi Bragg peaks vanish, indicating that all nanocrystals have melted.

The values of the lattice parameters experimentally determined are noticeably smaller than those of bulk Bi (**a** $=4.5470$ Å, **c** $=11.8616$ Å—JCPDS PDF card 44-1246). The observed lattice contraction is a consequence of the expected surface tension effect that becomes relevant for very small crystals. The contraction of the **c** parameter, 0.8%, is higher than that of **a**, 0.4%. This anisotropy was also reported by Yu *et al.*[15] for Bi nanocrystals produced by an electrohydrodynamic technique.

The average chord length in the direction perpendicular to the reflecting planes $\langle M\rangle$ was determined from the integral width of the Bragg reflection $\Delta(2\theta)$ using the Scherrer equation[16]

$$\langle M\rangle_{hkl}=\frac{\lambda}{\Delta(2\theta)_{hkl}\cos\theta_{hkl}}, \tag{7}$$

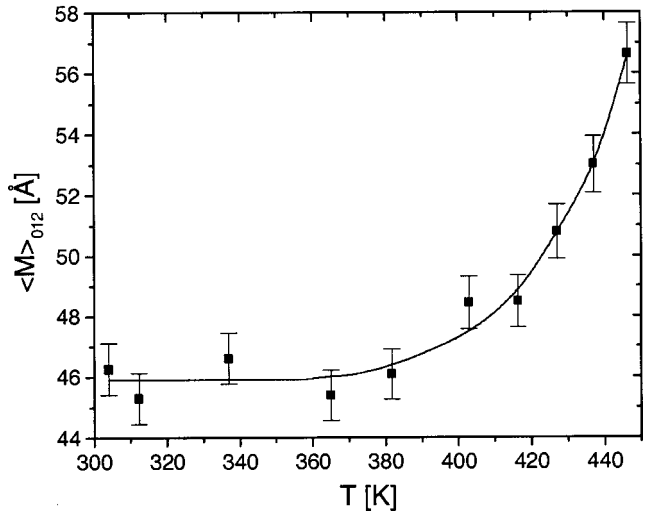

FIG. 4. Average chord length of Bi nanocrystals at different temperatures. Above 370 K, a progressive increase in $\langle M\rangle_{012}$ for increasing T is observed.

where *hkl* are the Miller indexes of the reflecting planes and θ_{hkl} are the Bragg angles. Assuming a Gaussian profile, we have $\Delta(2\theta)=\sqrt{2\pi}\sigma$, where σ is the standard deviation.

The average size parameters $\langle M\rangle_{012}$ obtained by the fitting procedure described before are shown in Fig. 4. A progressive increase in $\langle M\rangle_{012}$ is observed for increasing temperatures. This trend is expected because small Bi nanocrystals melt at lower temperatures than large ones,[7–9] thus shifting the average size of crystalline clusters toward higher values. At lower temperatures (<365 K) no variation in the average cluster size is observed and $\langle M\rangle_{012}$ is equal to 45.9 ± 0.8 Å.

In the case of a system composed of a high number of randomly oriented nanocrystals with a known shape and size distribution, $\langle M\rangle$ can be calculated directly using its geometrical definition:[16]

$$\langle M\rangle=\frac{\int M\,d\nu_M}{V}, \tag{8}$$

where $d\nu_M/V$ is the volume fraction of the crystalline phase for which the chord lengths in the direction normal to the reflecting plane lies between M and $M+dM$. For spherical nanocrystals with a volume distribution function given by $D_\nu(R)$, we have

$$\langle M\rangle_{\rm sph}=\frac{3}{2}\frac{\int_0^\infty D_\nu(R)R\,dR}{\int_0^\infty D_\nu(R)dR}. \tag{9}$$

Using the $D_\nu(R)$ function calculated from the SAXS profile corresponding to Bi nanocrystals at 304 K (Sec. IV A), Eq. (9) yields $\langle M\rangle=41.9\pm0.4$ Å. This value is slightly smaller than that obtained from the width of WAXS Bragg peaks ($\langle M\rangle=45.9\pm0.8$ Å). This difference was attributed to probable minor deviations of nanocrystals from spherical

shape. As a matter of fact, the existence of some faceted nanocrystals coexisting with spherical ones was previously observed by TEM.[9]

The integral of Bragg peaks is proportional to the volume of the crystalline phase[17] and so proportional to the quotient $V_c(T)/V_{\rm tot}$, $V_c(T)$ being the volume occupied by the nanocrystals and $V_{\rm tot}$ the total volume of the nanoclusters (nanocrystals+liquid nanodroplets). Assuming that at 304 K all Bi clusters are in crystalline state, the crystalline volume fraction $V_c(T)/V_{\rm tot}$ can easily be determined from the values of the integral of the strongest Bragg peak, I_{012}, after correction for the effect produced by the temperature dependence of the Debye-Waller factor. So the crystalline volume fraction is given by[16]

$$\frac{V_c(T)}{V_{\rm tot}} = \frac{I_{012}(T)/e^{-2W(T)}}{I_{012}(304\ {\rm K})/e^{-2W(304\ {\rm K})}}, \tag{10}$$

where

$$W = \frac{1.14\times 10^4}{M_a\Theta}\frac{\sin^2\theta_{012}}{\lambda^2}\frac{T}{\Theta}\left[\frac{1}{4}\frac{\Theta}{T}+\varphi\left(\frac{\Theta}{T}\right)\right],$$

M_a and Θ being the Bi atomic mass and the Debye temperature of Bi crystals, respectively, φ is a tabulated function,[16] and λ is expressed in angstroms. The fraction $V_c(T)/V_{\rm tot}$ starts to slowly decrease at 365 K and vanishes at about 464 K, thus indicating that at this temperature all crystals have melted. The wide temperature range of the crystal to liquid transition ($\sim$100 K) is the expected consequence of a strong dependence of the melting temperature on nanocrystal radius.

C. Dependence of the melting temperature on nanocrystal radius

The knowledge of (i) the cluster (nanocrystals +nanodroplets) volume distribution $D_\nu(R)$, determined by SAXS, and (ii) the temperature dependence of the fraction of clusters in crystalline state, $V_c(T)/V_{\rm tot}$, calculated from WAXS results, made possible the evaluation of the melting temperature of Bi crystals as a function of their reciprocal radius, $T_m(1/R)$.

Previous observations have shown that the melting of nanocrystals starts in a region close to the surface and then propagates toward the bulk.[18–21] We have implicitly assumed that the times involved in this process are much shorter than those of our measurements.

The fraction of spherical clusters (nanocrystals +liquid droplets) with a radius $R'>R$, $V_R(R)/V_{\rm tot}$, can be determined from the volume distribution function determined by SAXS (Sec. IV A) as follows:

$$\frac{V_R(R)}{V_{\rm tot}} = \frac{\int_R^\infty D_\nu(R')dR'}{\int_0^\infty D_\nu(R')dR'}. \tag{11}$$

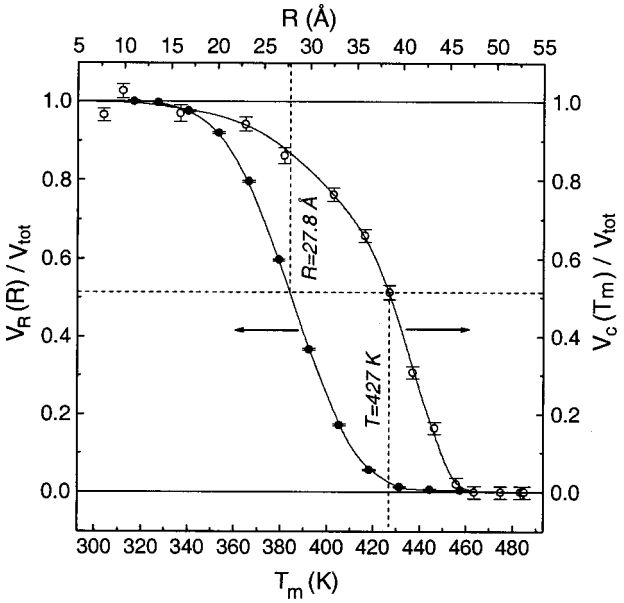

FIG. 5. Volume fraction of the Bi clusters in crystalline state determined by SAXS $[V_R(R)/V_{\rm tot}]$ and by WAXS $[V_c(T)/V_{\rm tot}]$. From these two curves the function $T_m(R)$ was determined. The procedure for the determination of Bi nanocrystals melting temperature corresponding to $R=27.8$ Å is indicated.

Assuming that Bi nanoclusters with $R'>R$ are crystalline and those with $R'<R$ are in liquid state, the clusters with $R'=R$ melt at $T=T_m$ and so

$$\frac{V_c(T_m)}{V_{\rm tot}} = \frac{V_R(R)}{V_{\rm tot}}.$$

Thus from Eqs. (10) and (11) we have

$$\frac{I_{012}(T)/e^{-2W(T)}}{I_{012}(304\ {\rm K})/e^{-2W(304\ {\rm K})}} = \frac{\int_R^\infty D_\nu(R')dR'}{\int_0^\infty D_\nu(R')dR'}. \tag{12}$$

The experimental functions corresponding to both sides of Eq. (12) are plotted in Fig. 5. The numerical solution of Eq. (12) yields the $T_m(R)$ function relating the melting temperature T_m and the nanocrystal radius R.

The results of the calculations of T_m are plotted in Fig. 6 as a function of the reciprocal radius for a direct verification of the theoretical linear dependence predicted by Eq. (2). Previous determinations of the melting temperature of Bi nanocrystals on a solid substrate[7,8] and embedded in the same glass matrix as in this work[9] are also plotted in Fig. 6. These studies were performed using transmission electron microscopy and thermal analysis. In all previous reported measurements the melting temperature corresponds to a set of nanocrystals with a more or less wide radius distribution.

The melting temperature for $(1/R)$ extrapolated to zero coincides with T_b within the experimental error, so that the strain energy parameter K_E is negligible for the studied system. The difference in crystal-glass and liquid-glass interfacial energies, determined from the slope of the straight line

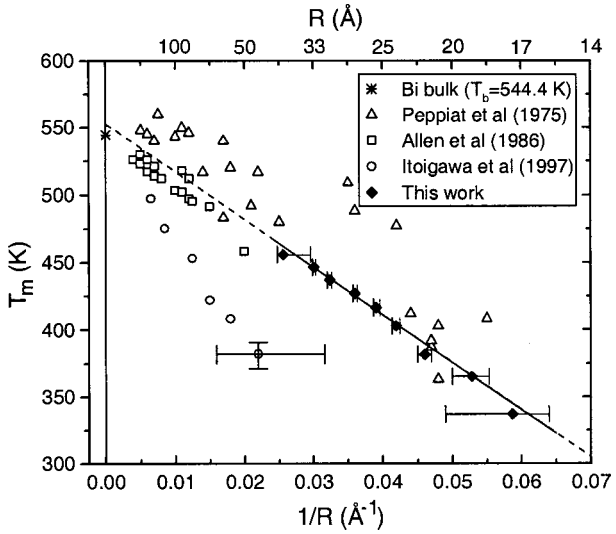

FIG. 6. Melting temperature T_m as a function of the nanocrystal reciprocal radius $1/R$. The straight line was determined by weighted linear regression. The results are in good agreement with the linear dependence predicted by Couchman-Jesser (Ref. 10) theory.

obtained by least-squares fitting of our experimental results, is $(\sigma_{gc}-\sigma_{gl})=115\times10^{-3}\ \mathrm{J\,m^{-2}}$. This value is much smaller than that reported in a previous investigation of the same system $(255\times10^{-3}\ \mathrm{J\,m^{-2}})$.[9]

The T_m versus $1/R$ plot of our experimental results (Fig. 6) clearly follows the linear behavior predicted by Eq. (2). The dispersion of the experimental T_m values from the linear behavior predicted by the theory is much smaller than those observed in previous investigations using other techniques.

V. CONCLUSION

The presented results demonstrate that the simultaneous use of WAXS and SAXS techniques, together with a synchrotron x-ray source and position-sensitive x-ray detection, yield useful and precise information on the structure and on the crystal-liquid transition of nanocrystals embedded in a glass matrix. This procedure makes possible the determination of the melting temperature as a function of nanocrystal radius suppressing unwanted effects of size dispersion.

The crystallographic lattice of Bi nanocrystals embedded in a sodium-borate glass matrix is rhombohedral like in the bulk state. The lattice parameters (**a** and **c**, hexagonal unit cell) exhibit a weak and increasing contraction for decreasing nanocrystal sizes.

The melting temperature of Bi nanocrystals embedded in a sodium-borate glass is a linear and decreasing function of the reciprocal radius as predicted by simple thermodynamical arguments. The difference between the crystal-glass and liquid-glass interface energies was found to be equal to $115\times10^{-3}\ \mathrm{J\,m^{-2}}$, this value being lower than that previously reported in the literature for the same system.[9] We have assigned this discrepancy to probable systematic errors in previous determinations of $T_m(R)$ produced by the wide nanocrystal size dispersion in the analyzed samples. This systematic error is absent in the present work.

ACKNOWLEDGMENT

The financial support provided by FAPESP and PRONEX/CNPq is acknowledged.

[1] C. Solliard, Surf. Sci. **106**, 58 (1981).
[2] J. Woltersdorf, A. S. Nepijko, and E. Pippel, Surf. Sci. **106**, 64 (1981).
[3] G. Apai, J. F. Hamilton, J. Stohr, and A. Thompson, Phys. Rev. Lett. **43**, 165 (1979).
[4] Z. M. Stadnik, P. Griesbach, G. Dehe, P. Gütlich, T. Kohara, and G. Stroink, Phys. Rev. B **35**, 6588 (1987).
[5] M. Takagi, J. Phys. Soc. Jpn. **9**, 359 (1954).
[6] R. Kofman, P. Cheyssac, and R. Garrigos, *Phase Transitions* (Gordon and Breach, London, 1990).
[7] S. J. Peppiatt, Proc. R. Soc. London, Ser. A **345**, 401 (1975).
[8] G. L. Allen, R. A. Bayles, W. W. Gile, and W. A. Jesser, Thin Solid Films **144**, 297 (1986).
[9] H. Itoigawa, T. Kamiyama, and Y. Nakamura, J. Non-Cryst. Solids **210**, 95 (1997).
[10] P. R. Couchman and W. A. Jesser, Nature (London) **269**, 481 (1977).
[11] G. L. Allen, W. W. Gile, and W. A. Jesser, Acta Metall. **28**, 1695 (1980).
[12] G. Kellermann, F. Vicentin, E. Tamura, M. Rocha, H. Tolentino, A. Barbosa, A. Craievich, and I. Torriani, J. Appl. Crystallogr. **30**, 880 (1997).
[13] O. Glatter and O. Kratky, *Small Angle X-ray Scattering* (Academic, London, 1982).
[14] A. V. Semenyuk and D. I. Svergun, J. Appl. Crystallogr. **24**, 537 (1991).
[15] X. F. Yu, X. Liu, K. Zhang, and Z. Q. Hu, J. Phys.: Condens. Matter **11**, 937 (1999).
[16] A. Guinier, *X-ray Diffraction in Crystals, Imperfect Crystals and Amorphous Bodies* (Freeman, San Francisco, 1963).
[17] R. Jenkins and R. L. Snyder, *Introduction to X-ray Powder Diffractometry* (Wiley, New York, 1996).
[18] J. T. McKinney, E. R. Jones, and M. B. Webb, Phys. Rev. **160**, 523 (1967).
[19] J. J. Lander, *Progress in Solid State Chemistry* (Pergamon, New York, 1965).
[20] R. M. Goodman and G. A. Somorjai, J. Chem. Phys. **52**, 6325 (1970).
[21] J. Klaestrup-Kristensen and R. M. J. Cotterill, *Physics of Non-Equilibrium Systems: Fluctuations, Instabilities and Phase Transitions* (Leinden, Nordhoff, 1975).

Isothermal aggregation of Bi atoms embedded in a soda borate glass: Coarsening of liquid nanodroplets and atomic diffusion

G. Kellermann[1,2,*] and A. F. Craievich[3]
[1]*Laboratório Nacional de Luz Síncrotron, C.P. 6192, 13084-971 Campinas SP, Brazil*
[2]*Instituto de Física "Gleb Wataghin," UNICAMP, C.P. 6165, 13083-970 Campinas SP, Brazil*
[3]*Instituto de Física, USP, C.P. 66318, CEP 05315-970, São Paulo SP, Brazil*
(Received 8 August 2002; revised 26 November 2002; published 7 February 2003)

The process of nucleation and growth of liquid Bi nanodroplets embedded in a soda borate glass submitted to isothermal annealing at different temperatures was studied by small-angle x-ray scattering (SAXS) and transmission-electron microscopy. The experimental results indicate that the formation and growth of Bi droplets occur in two successive stages after a short incubation period. The first is characterized by the nucleation and growth of spherical droplets promoted by atomic diffusion and aggregation of isolated Bi atoms and the second one by a subsequent droplet coarsening. The experimental functions describing the time variation of the droplet average radius and density number at advanced stages of the growth process agree with the classical Lifshitz-Slyozov-Wagner (LSW) theory. However, the radius distribution was demonstrated to be well described by a log-normal function thus differing from the prediction of the LSW model. The atomic diffusion coefficient of Bi was determined from SAXS results for several annealing temperatures and, from it, the activation energy for the diffusion process was inferred.

DOI: 10.1103/PhysRevB.67.085405 PACS number(s): 61.10.Eq, 66.10.Cb, 81.10.Jt

I. INTRODUCTION

Nanometer-sized metallic particles have attracted the interest of many scientists due to their potential uses as catalysts and heat-exchange materials. Due to their singular optical properties, particular interest was addressed to composite materials consisting of metallic clusters embedded in glass matrices. A detailed review of the properties and characterization techniques of metal nanoclusters was reported by Gonella and Mazzoldi.[1]

This is a study of the kinetics of formation and growth of liquid Bi clusters embedded in a soda borate glass. Initially homogeneous and Bi-doped glass samples are studied by *in situ* small-angle x-ray scattering (SAXS) during isothermal annealing at temperatures close to the soda borate glass transition ($\sim$800–850 K). The annealing temperatures being well above the melting temperature of bulk Bi crystals ($T_m = 544.4$ K), the spherical clusters are in the liquid state from the first stages until the end of their growth. From the results of SAXS experiments, the radius distribution function, the time dependence of the average radius, the radius dispersion, and the number density of the liquid nanodroplets are determined. These experimental results are compared to those predicted by the classical theories of growth of spherical droplets embedded in a supersaturated matrix.

In addition, the coefficients of diffusion of Bi atoms through the glass matrix are determined from SAXS results at several temperatures and, from this, the energy of activation for the diffusion process is evaluated. Complementary measurements of transmission-electronic microscopy (TEM) and x-ray-absorption near-edge structure (XANES) are performed in order to verify the shape of the Bi nanoclusters and estimate the total concentration of Bi in the glass, respectively.

This study is a detailed *in situ* characterization, at high temperature, of the formation of a Bi liquid droplet-soda borate glass nanocomposite. After cooling down to room temperature, this system transforms into a Bi nanocrystal-glass nanocomposite. The structure and melting behavior of these Bi nanocrystals embedded in a glass matrix have recently been investigated and published elsewhere.[2]

II. EXPERIMENT

The starting raw materials were Na_2CO_3, B_2O_3, Bi_2O_3, and SnO. SnO was added as a reducing agent for Bi_2O_3. This mixture was melted in an electrical furnace under vacuum (10^{-1} mbar) at 1313 K. A $28Na_2O$-$72B_2O_3$ glass containing dispersed Bi atoms was obtained by fast quenching of the melted glass down to room temperature using the splat-cooling technique. The obtained 100-μm-thick glass plates were homogeneous and transparent to visible light. The quenching procedure prevents glass crystallization and suppresses, or strongly reduces, the formation of Bi clusters during cooling. The SAXS intensity produced by the glass samples was measured *in situ*, during isothermal annealing at temperatures ranging from 803 up to 843 K in a specially designed high-temperature cell.[3] After isothermal annealing, the sample was cooled down to room temperature and studied by TEM.

The SAXS experiments were performed at the SAS beamline of the National Synchrotron Light Laboratory (LNLS), Campinas, Brazil.[4] The SAXS intensity was recorded using a one-dimension gas x-ray position-sensitive detector. X-ray monitors placed before and after the sample measured the intensity of the incoming and transmitted x-ray beam intensity in order to determine the sample attenuation. SAXS spectra were normalized to equivalent intensities of the direct beam to compensate for the continuous decrease in the emission of the synchrotron source. The SAXS intensity was determined as a function of the modulus of the scattering

vector $q=(4\pi \sin\theta)/\lambda$, λ being the wavelength of the x-ray beam ($\lambda=1.61$ Å) and θ half of the scattering angle. The parasitic scattering was subtracted from the total SAXS intensity. Because of the small area of the cross section of the transmitted x-ray beam at the detection plane and the narrow resolution slit used for the detector, the SAXS curves were essentially free from smearing effects. The SAXS intensity was determined in absolute units by using water as a standard.[5]

The TEM study was performed at LME/LNLS, Campinas, Brazil, using a JEM-3010 UHR microscope operating at 300 kV at room temperature. The glass containing the Bi nanocrystals (solidified Bi droplets) was very finely grinded and mixed with isopropanol (100 mg of glass per ml of alcohol). The mixture was maintained in an ultrasonic bath during 10 min and then dropped on a 30-Å carbon film deposited on a cupped grid. After drying, the very thin glass grains, well adhered to the grid, were observed in the microscope.

III. CLASSICAL THEORY OF DROPLET COARSENING

A. Basic aspects

The formation of a second phase consisting of nanoclusters embedded in an supersaturated homogeneous matrix containing doping atoms starts by a nucleation stage and is followed by a further cluster growth promoted by the diffusion and aggregation of initially isolated doping atoms. This mechanism is named ''nucleation and growth.'' According to the model proposed by Lifshitz-Slyosov[6] and Wagner[7] (LSW), when the supersaturation of the doping element in the matrix becomes small, *spherical clusters* with a radius R smaller than a critical radius R_c start to dissolve while those with radii larger than R_c still grow. This is consequence of the driving force for coarsening that promotes the decrease of the area of the interface between the clusters and the matrix phase thus reducing the total interface energy. The cluster radius distribution $N(R,t)$ for different times t of isothermal annealing during the coarsening regime predicted by the LSW model is independent of the initial size distribution $N(R,0)$ and is given by[6]

$$N(R,t)=f(t)\frac{4(R/R_c)^2}{9}\left(\frac{3}{3+R/R_c}\right)^{7/3}\left(\frac{3/2}{3/2-R/R_c}\right)^{11/3}\times\exp\left(\frac{-R/R_c}{3/2-R/R_c}\right), \quad (1)$$

where $f(t)$ is a function of the annealing time only. During the coarsening stage R_c coincides with the cluster average radius $\langle R\rangle$. The cluster average radius $\langle R\rangle(t)$, the concentration of solute atoms in the matrix $c(t)$, and the number density of clusters $n(t)$ are time-dependent functions. The density number can be determined as $n(t)=\int N(R,t)dR$.

During the coarsening stage, $\langle R\rangle(t)$ increases for increasing times while $n(t)$ progressively decreases. Quantitatively, according to the LSW model, the time dependence of $\langle R\rangle\times(t)$, $n(t)$, and $c(t)$ satisfy the following equations:[6–8]

$$\langle R\rangle^3(t)=\langle R_0\rangle^3+\kappa(t-t_0) \quad (t\geqslant t_0), \quad (2)$$

$$n^{-1}(t)=n_0^{-1}+\beta(t-t_0) \quad (t\geqslant t_0), \quad (3)$$

$$c(t)=c_e+\chi^{-1/3}(t-t_0)^{-1/3} \quad (t\geqslant t_0), \quad (4)$$

where $\langle R_0\rangle$ and n_0 are the average radius and number density of the clusters, respectively, at the starting time for coarsening $t=t_0$ and c_e is the concentration of solute atoms (number per unit volume) in the matrix at equilibrium. An equation equivalent to Eq. (4) can be written in terms of the volume fraction of the new phase,[9]

$$\varphi(t)=\varphi_e-\chi'^{-1/3}(t-t_0)^{-1/3} \quad (t\geqslant t_0), \quad (5)$$

where φ_e is the volume fraction of the new phase at equilibrium. Equations (2)–(5) hold for annealing times $t\geqslant t_0$. The equations derived from the LSW model apply to *dilute* two-phase systems composed of spherical clusters occupying a low fraction of the total volume.

B. Determination of the atomic diffusion coefficient from SAXS results

The four rate parameters κ, β, χ, and χ' in Eqs. (2)–(5), respectively, are related to the atomic diffusion coefficient D of the solute as follows:[6–9]

$$\kappa=\frac{8\sigma\nu^2c_eD}{9kT}, \quad (6)$$

$$\beta=\frac{4\sigma c_e\nu D}{(c_i-c_e)kT}, \quad (7)$$

$$\chi=\frac{D(kT)^2}{9\sigma^2c_e^2\nu}, \quad (8)$$

$$\chi'=\left(\frac{1/\nu-c_e}{1-\varphi_e}\right)^3\chi, \quad (9)$$

where σ is the free energy per unit of area of the interface between clusters and the matrix, ν the atomic volume of the solute, c_i the initial concentration of solute in the matrix, k the Boltzmann constant, and T the absolute temperature. Since the parameters σ and c_e are in many cases not known, Eqs. (6)–(9) cannot generally be used to determine the diffusion coefficient D.

By combining Eqs. (6) and (8) we have

$$\kappa^2\chi=\left(\frac{4}{9}\nu D\right)^3$$

and thus

$$D=\frac{9}{4\nu}(\kappa^2\chi)^{1/3}.$$

Finally, using Eq. (9) and assuming that $[(1/\nu)-c_e]\approx 1/\nu$, we have

$$D=\frac{9(1-\varphi_e)}{4}(\kappa^2\chi')^{1/3}. \quad (10)$$

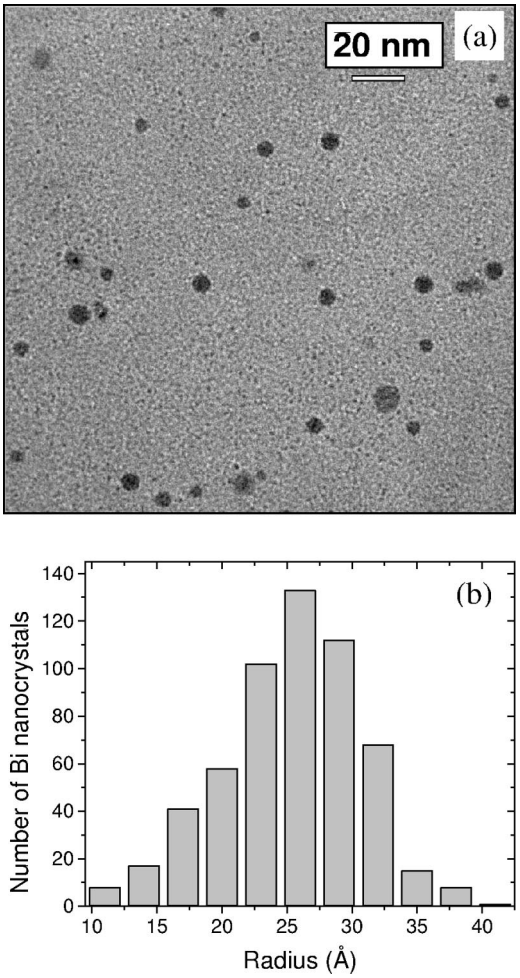

FIG. 1. (a) Transmission-electron microscopy bright field image corresponding to a thin sample annealed 2 h at 843 K. (b) Histogram of droplet radii.

If, beside c_i, c_e, φ_e, and T, also D, σ, and ν are approximately constant during the whole coarsening process, the rate parameters κ, β, χ, and χ' [Eqs. (2)–(5) respectively] are expected to have *constant values along the whole coarsening process*, i.e., under the mentioned conditions, the LSW theory predicts that during the cluster coarsening process $\langle R\rangle^3(t)$ and $n^{-1}(t)$ are linear functions of the annealing time and $c(t)$ and $\varphi(t)$ are linear functions of $(t-t_0)^{-1/3}$. Since the relevant parameters φ_e, κ, and χ' are easily determined from SAXS results in an absolute scale, Eq. (10) can be applied to the determination of D without the explicit knowledge of σ and c_e.

IV. RESULTS AND DISCUSSION

A. Transmission-electron microscopy

The TEM image given in Fig. 1(a) shows Bi nanocrystals embedded in the soda borate glass matrix corresponding to a sample held during 2 h at 843 K and cooled down to room temperature. The image demonstrates that Bi nanocrystals have a nearly spherical shape. Figure 1(b) shows the histogram of the number of Bi nanocrystals as a function of their radii. The analysis of the TEM image indicates a single-mode radius distribution function [Fig. 1(b)].

The average nanocrystal radius $\langle R\rangle$ and the relative radius dispersion $\sigma_R/\langle R\rangle$ are (25 ± 2) Å and (0.21 ± 0.01), respectively. The histogram was obtained from the measured diameters of 560 nanocrystals corresponding to different grains of the glass-Bi nanocrystals composite. The estimated resolution limit for size determination was 18 Å (minimum measurable radius: 9 Å). The diameter of each nanocrystal was determined from the diameter of a circle that best fit the perimeter of their projected images.

In order to compare the radius distribution function derived from the TEM image with those from SAXS experiments, we have considered that the radius distribution of Bi nanocrystals obtained by TEM at room temperature is essentially the same as the radius distribution of liquid Bi nanodroplets in the precursor sample just before cooling. This is a reasonable assumption because the temperature range of the liquid-to-crystal transition is well below the softening temperature of the glass matrix.[2]

B. Small-angle x-ray scattering

1. Formation and growth of the new phase

We wish to characterize the mechanisms of formation and growth, during isothermal annealing, of a dilute and isotropic set of spherical Bi droplets embedded in an initially homogeneous Bi supersaturated glass. We remind the reader that the Bi clusters are in a liquid state because the annealing temperatures ($\approx$800–850 K) are well above the melting temperature of Bi nanocrystals.[2] The shape of the liquid droplets is expected to be spherical as a consequence of the dominant effect of surface tension. As will be described below, under these conditions the SAXS intensity is a particularly simple function of the modulus of the scattering vector.

In general, the scattering intensity in absolute units, or scattering power, is given by the differential scattering cross section $d\Sigma/d\Omega$. For a dilute set of spherical droplets with constant electron density ρ_p embedded in a homogeneous matrix with a constant electron density $\langle\rho\rangle$, the scattering power is given by[10]

$$\frac{d\Sigma}{d\Omega}(q)=r_0^2(\Delta\rho)^2\left(\frac{4\pi}{3}\right)^2\int_0^\infty N(R)P(q,R)R^6dR, \quad (11)$$

where $\Delta\rho=\rho_p-\langle\rho\rangle$ and $N(R)dR$ is the number of droplets per unit volume with radii between R and $R+dR$. $r_0=0.28179\times10^{-14}$ m is the classical electron radius and $P(q,R)$ is the normalized form factor for a sphere defined by[10]

$$P(q,R)=\left[3\frac{\sin(qR)-qR\cos(qR)}{(qR)^3}\right]^2. \quad (12)$$

An additional and essentially q-independent contribution to the scattering intensity produced by electron-density fluctuations in the matrix is experimentally determined by using Porod plots[10] and subtracted from the total scattering intensity.

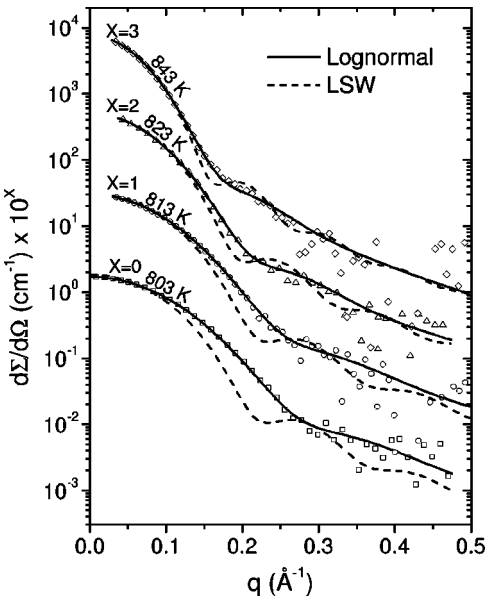

FIG. 2. Scattering power corresponding to samples annealed during 100 min at the indicated temperatures. Modeled curves using the functions defined by Eqs. (1) and (13) are also plotted. The curves from $x=1-3$ are multiplied by increasing powers of 10 for clarity.

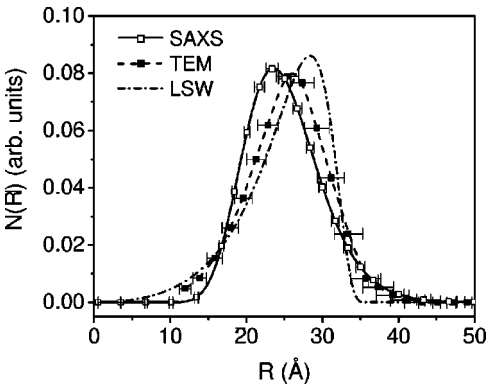

FIG. 3. Nanocrystal radius distributions $N(R)$ corresponding to a sample annealed at 843 K during 2 h. These functions were obtained from (i) an experimental SAXS curve assuming a log-normal radius distribution and (ii) the TEM histogram displayed in Fig. 1(b). Both radius distribution functions yield the same average radius ($\langle R\rangle=25$ Å). The third curve is the radius distribution function predicted by the LSW model [Eq. (1)] for same average radius. The areas under the curves are normalized to unity.

According to our already mentioned TEM results, the assumptions regarding the dilute nature of the solution and the spherical shape of the clusters apply to the system that we study here. The Bi concentration in the samples, determined from absorption x-ray spectroscopy (XANES) measurements, is of the order of 10^{-5} mol/cm^3. The electron densities of the initial glass matrix $\langle\rho\rangle$ and of Bi nanodroplets ρ_p were determined from the known nominal composition and mass density of the glass and from the mass density of bulk melted Bi, respectively. Due to the decreasing trend in the number of Bi atoms dissolved in the glass matrix, a variation in the difference between the electron density of Bi nanodroplets and the glass matrix ($\Delta\rho=\rho_p-\langle\rho\rangle$) is expected. Because of the small Bi concentration, this difference is only very slightly modified during the whole annealing process and so it was assumed to maintain a constant value.

The experimental SAXS intensity curves at advanced stages of thermal annealing were modeled assuming the radius distribution predicted by LSW theory, Eq. (1). As an alternative attempt, the scattering intensity curves were modeled assuming a log-normal radius distribution function defined by

$$N(R)=\frac{n}{\sqrt{2\pi e^{w^2}}wr}\exp\left\{-\frac{1}{2}\frac{[\ln(R/r)]^2}{w^2}\right\}, \qquad (13)$$

where r, w, and n are fitting parameters, n being the droplet number density.

The scattering power (SAXS intensity in absolute units) corresponding to 100 min of isothermal annealing and the best modeled curves for both size distribution functions [Eqs. (1) and (13)] are plotted in Fig. 2. The best fit using Eq. (1) leads to a function that exhibits significant deviations from the experimental results. On the other hand, the curves obtained by assuming a log-normal radius distribution function [Eq. (13)] fitted very well the experimental data except at the very beginning of the process.

In order to compare the radius distribution functions derived from SAXS and TEM results, we have focused on a particular sample annealed during 2 h at 843 K. In Fig. 3 the log-normal radius distribution function [Eq. (13)] determined from a SAXS experiment and that deduced from a TEM image [Fig. 1(b)] are plotted together with the distribution predicted by the LSW model [Eq. (1)] for $\langle R\rangle=25$ Å. The presented results indicate that even though the radius distribution determined from SAXS and TEM analyses are not identical, the average radius obtained using both methods is the same ($\langle R\rangle=25$ Å). The error bars are ±0.1 Å and ±2 Å for SAXS and TEM, respectively. The relative dispersions of the distribution function $N(R)$ determined from SAXS and TEM results are $\sigma_R/\langle R\rangle=0.190\pm0.005$ and $\sigma_R/\langle R\rangle=0.21\pm0.01$, respectively. This indicates that both techniques lead to average radius and radius dispersion in very good agreement. The differences in the distribution profile may be due to the rather low sampling in TEM analysis and/or to the inherent approximation associated to the use of a log-normal function for the analysis of SAXS results.

As it can be seen in Fig. 3, the shape of the radius distribution function $N(R)$ determined from SAXS results is not identical to that predicted by the LSW model. In fact, deviations of the experimental radius distribution from that predicted by the LSW theory [Eq. (1)] have already been reported in a number of previous investigations.[8,9] The reported deviations may be, at least partially, due to systematic errors associated to the procedure used for size determination. In the present work, the different shape may be also related to the more or less good approximation involved in the assumption of a log-normal function for the radius distribution. However, the structural parameters whose time de-

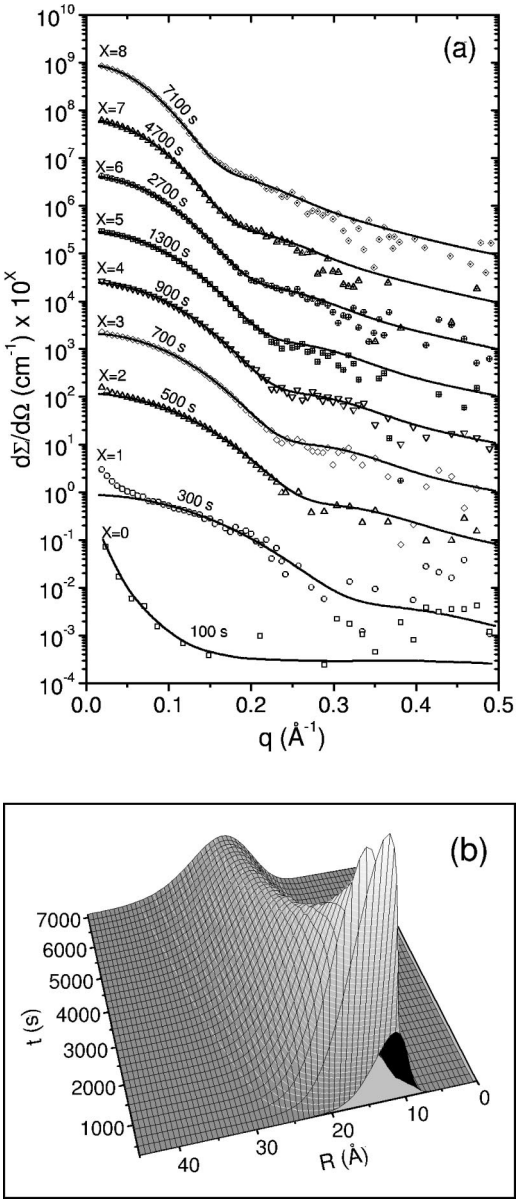

FIG. 4. (a) Scattering power corresponding to a sample annealed at 843 K during the indicated time periods. The continuous line is the modeled function assuming a log-normal radius distribution. The curves from $x=1-8$ are multiplied by increasing powers of 10 for clarity. (b) Radius distribution as a function of the annealing time determined from data plotted in (a).

pendence is used here in order to characterize the mechanism of Bi droplet growth (i.e., $\langle R\rangle$, n, and φ) depend on integrals involving the $N(R)$ function and not on its detailed shape. As we will see in the next section, in spite of the mentioned discrepancy in the profile of the $N(R)$ function, the experimentally observed time dependencies of $\langle R\rangle$, n, and φ agree very well with those predicted by the LSW model.

The scattering power corresponding to different periods of annealing at 843 K and the modeled curves according to Eqs. (11) and (13) are plotted in Fig. 4(a). At the beginning of thermal treatment, corresponding to the induction period, only a very weak and q-independent scattering, except at the very small angles, is observed. The scattering at very small angles is attributed to the existence of a few and rather large Bi clusters in the as-quenched glass. In the above fitting procedure, the data corresponding to very small angles were not considered.

The log-normal distributions $N(R,t)$ associated to the modeled scattering power curves for different annealing times are plotted in Fig. 4(b). The results evidence an initial stage with very fast nucleation and growth of the Bi nanodroplets, indicated by the increase of the area under $N(R,t)$ curves, and a shift of the maximum of the radius distribution toward higher R values. The nucleation and growth period is about 10 min at 843 K and longer at lower temperatures. After this transient period, a continuous reduction in the number of nanodroplets occurs. On the other hand, the maximum of the distribution continuously shifts toward higher R values thus indicating a continuous growth of nanodroplets from the beginning until the end of the coarsening process. The fitting procedure applied to the whole set of scattering curves yielded the time variations in average radius, number density, and relative radius dispersion of nanodroplets, $\langle R\rangle \times(t)$, $n(t)$, and $[\sigma_R/\langle R\rangle](t)$, respectively.

Figure 5(a) displays the dependence of $\langle R\rangle^3$ on the annealing time. After the induction period, a very fast growth of nanodroplets is observed. Later, it follows a stage in which nanodroplets grow at a lower rate until the end of the annealing process. The linear dependence of the experimental $\langle R\rangle^3(t)$ function agrees with the prediction of LSW coarsening theory [Eq. (2)]. As expected, the $\langle R\rangle^3(t)$ growth rate—slope κ—is an increasing function of the temperature.

The function $n^{-1}(t)$ is plotted in Fig. 5(b). The fast increase in the number density of nanodroplets at the beginning of the thermal treatment indicates an initial nucleation stage. Later, a continuous reduction of nanodroplet number density is observed. The linear dependence of $n^{-1}(t)$ on the annealing time also agrees with the prediction of LSW theory [Eq. (3)].

In Fig. 5(c), the ratios $\sigma_R/\langle R\rangle$ are displayed as functions of the annealing time for different annealing temperatures. High values of these ratios are observed at the beginning of the annealing. This is an expected consequence of the continuous nucleation of additional clusters in this stage. As a consequence of the decreasing Bi concentration in the glass matrix, the rate of nucleation decreases and $\sigma_R/\langle R\rangle$ falls to a minimum. After this period, when coarsening starts, $\sigma_R/\langle R\rangle$ increases very slightly and at advanced stages becomes nearly constant. The invariance of $\sigma_R/\langle R\rangle$ with respect to the annealing time in this stage indicates that the radius distribution becomes time independent under scaling of the average nanodroplet radius. During advanced stages of annealing $\sigma_R/\langle R\rangle$ is equal to 0.20, in agreement with the value of 0.21 determined from TEM images and $\sigma_R/\langle R\rangle=0.21$ predicted by LSW theory.

2. Experimental determination of the diffusion coefficient and the energy of activation for Bi diffusion from SAXS results

The volume fraction of the solute phase φ can be determined from the integrated scattering power in reciprocal

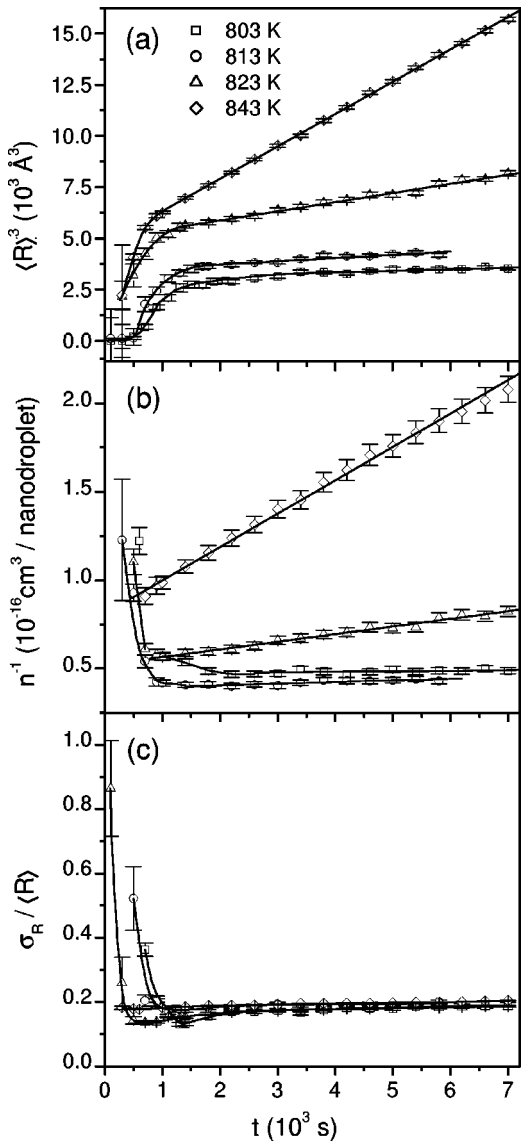

FIG. 5. (a) Cubic average radius $\langle R\rangle^3$, (b) reciprocal number density n^{-1}, and (c) relative radius dispersion $\sigma_R/\langle R\rangle$ as functions of the annealing time at the indicated annealing temperatures.

space Q. For systems in which the new phase is formed by randomly oriented precipitates of any shape, the scattering power is a function of the modulus of the scattering vector q and so the integral Q is given by[10]

$$Q=4\pi\int_{q=0}^{\infty}\frac{d\Sigma}{d\Omega}(q)q^2dq. \tag{14}$$

This integral is related to the volume fraction φ by[10]

$$Q=8\pi^3r_0^2\Delta\rho^2\varphi(1-\varphi). \tag{15}$$

Since in our case the initial Bi concentration in glass is very low (volume fraction $\sim 10^{-4}$), we can safely assume that $\Delta\rho$ is a constant during the whole coarsening process. So, for the new phase occupying the smaller volume fraction, we have

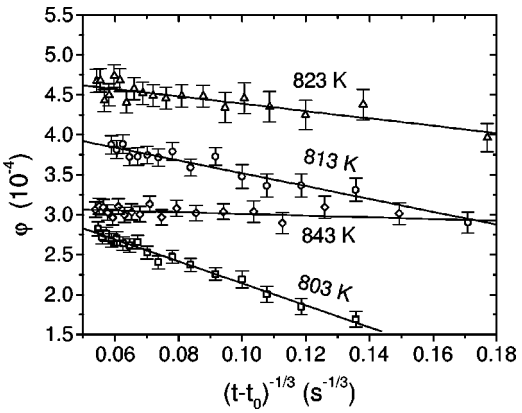

FIG. 6. Total volume fraction of Bi droplets, φ, as a function of $(t-t_0)^{-1/3}$ for the indicated annealing temperatures.

$$\varphi(t)=\frac{1}{2}-\left[\frac{1}{4}-\frac{Q(t)}{8\pi^3r_0^2\Delta\rho^2}\right]^{1/2}. \tag{16}$$

The volume fraction $\varphi(t)$ can also be calculated from the known $N(R,t)$ function

$$\varphi(t)=\frac{4\pi}{3}\int N(R,t)R^3dR. \tag{17}$$

The use of Eq. (16) is preferable because it is a direct calculation from the experimental SAXS curves that yields a more precise $\varphi(t)$ function than that obtained by applying Eq. (17).

Our experimental SAXS results were applied to the determination of the integral Q and, from Eq. (16), the time dependence of the fraction of the total volume occupied by the Bi droplets, $\varphi(t)$, was inferred. A fast increase of $\varphi(t)$ during the first period of annealing indicates that, during this stage, nanodroplets grow mainly by the incorporation of Bi atoms dissolved in the glass that diffuse toward them. After this period $\varphi(t)$ increases at a much smaller rate and is a linear function of $(t-t_0)^{-1/3}$. The $\varphi(t)$ functions versus $(t-t_0)^{-1/3}$ corresponding to the different annealing temperatures are plotted in Fig. 6.

We can see in Figs. 5(a), 5(b), and 6 that the experimental functions $\langle R\rangle^3(t)$ and $n(t)^{-1}$ exhibit a linear dependence on the annealing time and $\varphi(t)$ is a linear function of $(t-t_0)^{-1/3}$, in agreement with the predictions of LSW theory. We stress that this good agreement is actually expected for the studied system because it obeys the basic conditions of validity of the LSW model, i.e., a spherical shape and low total volume fraction of the droplets.

From the slopes of the linear parts of the curves plotted in Figs. 5(a) and 6, we have determined the rate parameters κ and χ', respectively, at different temperatures and, applying Eq. (10), the diffusion coefficients D of Bi through the soda-borate glass were inferred. Since the $\log D$ versus $(1/T)$ plot displayed in Fig. 7 indicates a linear dependence, the diffusion coefficient actually obeys the Arrhenius law:

$$D(T)\propto e^{-E/\mathcal{R}T}, \tag{18}$$

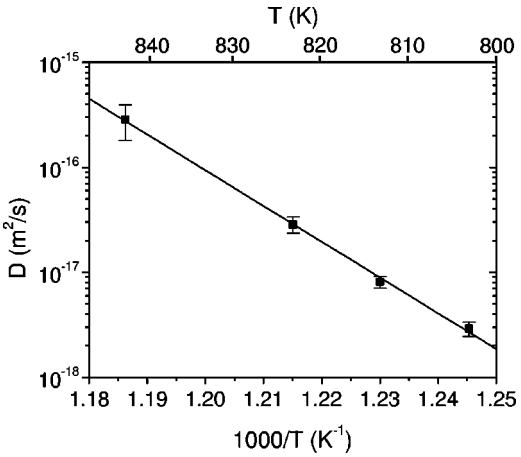

FIG. 7. Arrhenius plot for the diffusion coefficients of Bi atoms through a soda borate glass matrix at different annealing temperatures.

where E is the activation energy for the diffusion process and $\mathcal{R}$ is the gas constant. From the slope of the straight line in a $\log D$ versus $(1/T)$ plot (Fig. 7) the value of the activation energy for Bi diffusion through the soda borate glass $E = (64 \pm 3) \times 10^4$ J mol^{-1} was obtained.

V. CONCLUSION

Our experimental SAXS and TEM results regarding the formation and growth of Bi liquid droplets embedded in the studied Bi-doped soda borate glass evidence a clustering process involving three distinct stages: (i) an initial short incubation stage, (ii) a second fast growth stage during which the size of Bi clusters increases by atomic diffusion and aggregation of isolated Bi atoms, and (iii) a final rather slow stage during which most of the isolated Bi atoms are already aggregated but the nanodroplets still grow by coarsening. The stage of nucleation and growth is characterized by an induction period of the formation of precursor Bi nuclei and by their growth promoted by atomic diffusion of isolated Bi atoms through the glass matrix. This leads to a nanocomposite consisting of a depleted matrix in which spherical nanodroplets with a single-mode radius distribution are homogeneously dispersed.

At more advanced stages of annealing, the time variations of the average radius, the density number of the Bi nanodroplets, and the volume fraction of the new phase are well described by the equations predicted by the LSW model for coarsening. The ratio between the nanodroplets' radius dispersion and their average value is nearly time constant during coarsening as predicted by LSW theory, thus indicating a dynamical scaling property or dynamical self-similarity of the structure. On the other hand, it was demonstrated that the radius distribution is better described by a log-normal function than by the function predicted by the LSW model.

The diffusion coefficients of Bi atoms through the studied soda borate glass during coarsening were quantitatively determined from a set of experimental curves of x-ray scattering power. This evaluation was performed for different annealing temperatures, so from an Arrhenius plot, the activation energy of the diffusion process was also determined. To our knowledge, the present investigation is the first quantitative determination of atomic diffusion coefficients exclusively based on the results of SAXS experiments.

ACKNOWLEDGMENT

The authors thank Edgar D. Zanotto for his helpful suggestions for sample preparation. This work was supported by LNLS, PRONEX, CNPq, and FAPESP.

*Author to whom correspondence should be addressed. Permanent address: Laboratório Nacional de Luz Síncrotron, C.P. 6192, 13084-971 Campinas SP, Brazil. Email address: keller@lnls.br

[1] F. Gonella and P. Mazzoldi, *Handbook of Nanostructured Materials and Nanotechnology* (Academic, New York, 2000).

[2] G. Kellermann and A.F. Craievich, Phys. Rev. B **65**, 134204 (2002).

[3] G. Kellermann, A.F. Craievich, R. Neuenschwander, and T.S. Plivelic, Nucl. Instrum. Methods Phys. Res. B **199**, 112 (2003).

[4] G. Kellermann, F. Vicentin, E. Tamura, M. Rocha, H. Tolentino, A. Barbosa, A.F. Craievich, and I.L. Torriani, J. Appl. Crystallogr. **30**, 880 (1997).

[5] D. Orthaber, A. Bergmann, and O. Glatter, J. Appl. Crystallogr. **33**, 218 (2000).

[6] I.M. Lifshitz and V.V. Slyozov, J. Phys. Chem. Solids **19**, 35 (1961).

[7] C. Wagner, Z. Elektrochem. **4**, 581 (1961).

[8] J. Schmelzer, I. Gutzow, and R. Pascova, J. Cryst. Growth **104**, 505 (1990).

[9] A. J. Ardell, in *Proceedings of the International Conference on Mechanism of Phase Transformation in Crystalline Solids, London, 1969*, Report No. 33 (The Institute of Metals, London, 1969), p. 111.

[10] O. Glatter and O. Kratky, *Small Angle X-ray Scattering* (Academic, London, 1982).